Report No. SAIC-TN-99030

Trapped Radiation Model Uncertainties:

Model – Data and Model – Model Comparisons

Prepared by

T. W. Armstrong and B. L. Colborn

Science Applications International Corporation (SAIC)

Prepared for

NASA Marshall Space Flight Center
Space Environments and Effects (SEE) Program Office
Huntsville, Alabama

Contract No. NAS8 - 40294

Draft Report September 1999
Final Report February 2000

Science Applications International Corporation
1706 Prospect Road • Prospect, Tennessee • 38477
Tel: (931) 468 - 2603 • Fax: (931) 468 - 2676

Table of Contents

Table of Contents (cont'd)

1. Introduction

Under a study sponsored by the NASA Space Environments and Effects (SEE) program, the standard AP8 and AE8 models for predicting trapped proton and electron environments have been compared with several sets of flight data to evaluate model uncertainties. A summary of this work is given in ref. [1-1]. The purpose here is to document some of the detailed results generated in preparing the summary report.

Table 1-1 gives an overview of the flight data used in the model–data comparisons. In two cases, DMSP and LDEF, we have used the results of model–data comparisons reported in the literature, as discussed in [1-1]. For the APEX, CRRES, and NOAA measurements, we have used software programs containing the flight data bases to generate orbit-average data for circular orbits of various altitudes and inclinations for model comparison purposes, as discussed here in Secs. 4, 5, and 6.

Dose predictions based on AP8 and AE8 fluxes have been made and compared with thermoluminescent dosimeter (TLD) measurements on several low-altitude Russian spacecraft (Sec. 2). This data was assimilated as part of the present SEE study, and is reported in [1-2]. We have also made predictions to compare with the TLD measurements made on some 60 Shuttle flights (Sec. 3). These Russian and Shuttle measurements are for flight times typically of about one week, whereas the AP8 and AE8 models are really applicable only for predicting long-term average fluxes (over six months, or so). Thus, model comparisons with these data are useful in quantifying model–data differences for short flights, but the results are limited in assessing model uncertainties for longer missions.

In addition to model–data comparisons, the standard AP8 and AE8 models have been compared with the European Space Agency versions of AP8 and AE8 and with Russian trapped radiation models. These model–model comparisons are given in Sec. 7.

References

[1-1] T. W. Armstrong and B. L. Colborn, "Evaluation of Trapped Radiation Model Uncertainties for Spacecraft Design", Science Applications International Corporation, Contractor Report for NASA/MSFC, SAIC-TN-99020, September 1999.

[1-2]. E. R. Benton and E. V. Benton, "A Survey of Radiation Measurements Made Aboard Russian Spacecraft in Low-Earth Orbit", NASA/CR-1999-209056, March 1999.

Table 1-1. Overview of flight data used in evaluating uncertainties in AP8 and AE8 trapped radiation models.

Spacecraft	Data Compared With	Applicablility of Data: Altitudes (km)	Applicablility of Data: Inclinations (deg)
APEX	Electron Dose (Si)	300 - 2500	all
	Proton Dose (Si)	300 - 2500	all
CRRES	Electron Dose (Si)	> 800	< 30 (magnetic)
	Proton Dose (Si)	> 800	all
	Electron Flux, Spectra	outer zone	most
	Proton Flux, Spectra	> 2500	all
DMSP	Proton Dose (Si)	840	polar
LDEF	TLD Dose	350-500	28.5
	Material Activation	350-500	28.5
NOAA	Proton Flux, Spectra	< 850	all
"Russian"	TLD Dose	(limited)	
Shuttle	TLD Dose	(limited)	

Spacecraft acronyms:

APEX:	Advanced Photovoltaic and Electronics Experiment satellite
CRRES:	Combined Release and Radiation Effects Satellite
DMSP:	Defense Meteorological Support Program F7 satellite
LDEF:	Long Duration Exposure Facility satellite
NOAA:	National Oceanic and Atmospheric Administration weather satellite
"Russian":	Photon-8, Cosmos-1887, Cosmos-2044, Mir Space Station

2. Evaluation of AE8 Model Uncertainties for Low-Altitude Dose Predictions

2-1. Introduction

As part of the effort to evaluate uncertainties in trapped radiation models for spacecraft design applications, work on determining the uncertainties associated with the AE8 trapped electron flux model for low-earth orbit radiation dose predictions has been performed. Model predictions are compared here with available flight data from thinly shielded (less than about 1 g/cm^2) thermoluminescent detector (TLD) dose measurements, with emphasis on data from Russian (and former Soviet Union) missions. Such space experiments have been reported for some ten Russian missions over the past two decades [e.g., ref. 2-1]. Under NASA's Space Environments and Effects (SEE) Program, Eril Research, Inc., under subcontract from SAIC, has assimilated dose data and measurement details from Russian missions [2-2], and the Russian flight data compared with here is from this compilation.

The Russian measurements use a "waffle iron" type dosimeter container, located outside the spacecraft, in which the open faces of the container contain stacks of TLDs. The thickness of the outer TLDs for the more recent missions are typically about 100 μm [2-2], although thinner TLDs (about 50 μm) have sometimes been deployed [2-3]. The waffle iron container is closed for reentry. An advantage of these types of measurements for model comparisons is that the exposure geometry can be adequately modeled as a simple 1-D plane shield with thick (effectively infinite) backing. This is in contrast to dose measurements made inside the Russian spacecraft where the dosimetry shielding is generally not reported, preventing definitive comparisons with model predictions. In addition to model comparisons with data from Russian missions, we have made comparisons with the thin shielding dose data from two U.S. missions: Shuttle flight STS-46 and the Long Duration Exposure Facility (LDEF) satellite.

The data sources are summarized in Sec. 2-2, the models used are discussed in Sec. 2-3, and the model-data comparisons are given in Sec. 2-4. The emphasis of the comparisons is on extracting approximate "uncertainty factors" that can be applied to AE8 model dose predictions, which are discussed in Secs. 2-5 and 2-6.

An important factor limiting the model-data accuracy attainable is that, except for LDEF, the data have been taken over time periods typically of a few weeks, whereas AE8 is a static model most accurate for predicting the trapped electron environment over relatively long (six months or so) periods. Also, the electron dose for high inclination flights is influenced by the variability of outer zone electrons from geomagnetic disturbances, and AE8 does not take into account fluctuations due to magnet activity. These limitations are discussed in Sec. 2-7.

2-2. Flight Data

Model comparisons have been made with the thin shielding TLD dose data from the missions listed in Table 2-1. Mission times during the solar cycle (in terms of the F10.7

Table 2-1. Flight parameters for thin shielding dose measurements compared with.

	Russian Missions				U. S. Missions	
	Photon 8	Mir Space Station	Cosmos 2044	Cosmos 1887	Shuttle STS-46	LDEF
Inclination (deg)	62.8	51.65	82.3	62.8	28.5	28.5
Perigee (km)	220	400	216	224	420	479-319
Apogee (km)	359	400	294	406	520	479-319
Mission Start Date	10/8/92	6/24/91	9/15/89	9/29/87	7/31/92	4/7/84
Mission End Date	10/23/92	7/28/91	9/29/89	10/12/87	8/7/92	1/20/90
TLD Exposure (days)	15.6	34	14	13	8	2105
Solar Cycle	Max-Min	Max	Max	Max	Max-Min	Max-Min

solar flux) are indicated in Fig. 2-1, and the altitude-inclination coverage of the missions is shown in Fig. 2-2. The data used here are all from the compilation and assessments made by Eril Research [2-2] with two exceptions: For comparisons with measurements on the Mir space station, we have also included the Russian and German dosimetry data reported by Akatov, et al. [2-3]. We have also made comparisons with measurements on LDEF (not included in the Eril compilation); the LDEF data compared with are from the measurements of Blake and Imamoto [2-4] and Bourrieau [2-5].

Model comparisons have not been made with all of the data compiled [2-2] from Soviet /Russian missions for several reasons. For example, data from the early Cosmos 936 and Cosmos 1129 missions (carried out in 1977 and 1979, respectively) were from thick (1 g/cm^2) TLDs, and these results are not as definitive for the thin shielding model comparisons of interest here. On some flights (e.g., Cosmos 1514, Cosmos 1760, and Cosmos 1781) the data from different measurement groups using different types of TLD materials and measurement, analysis, and calibration techniques show substantial variability (see [2-2]) and have not been included here. Details on the measurement methodologies used and references for the individual data sources are given in [2-2].

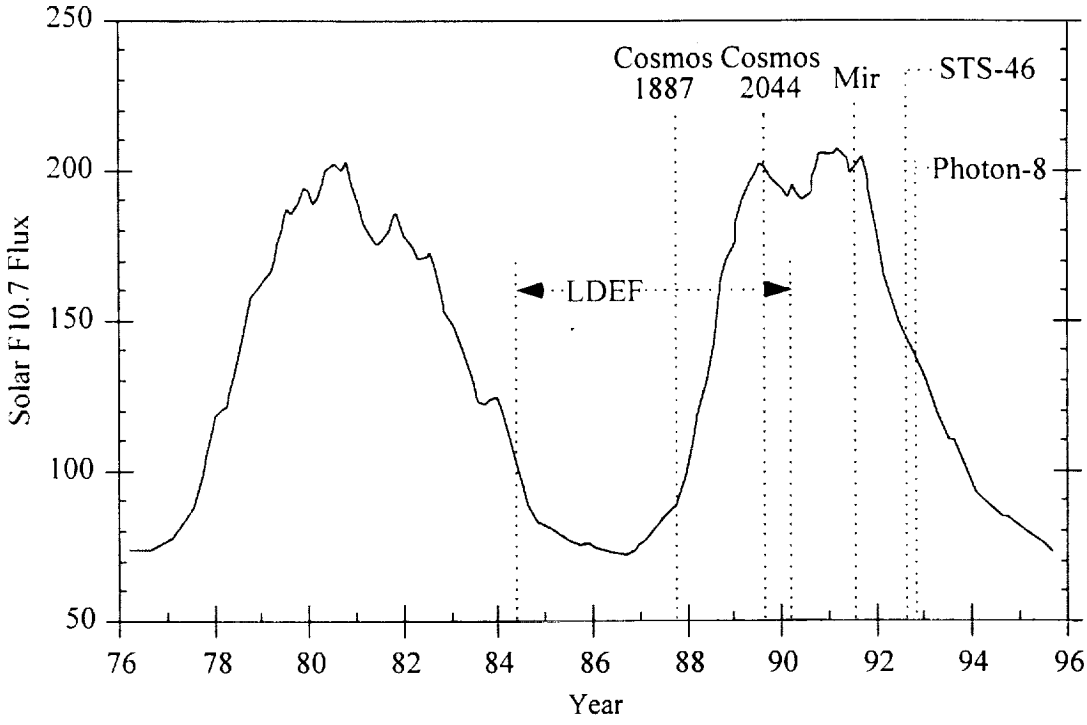

Fig. 2-1. Mission times for thin shielding measurements relative to solar cycle variation.

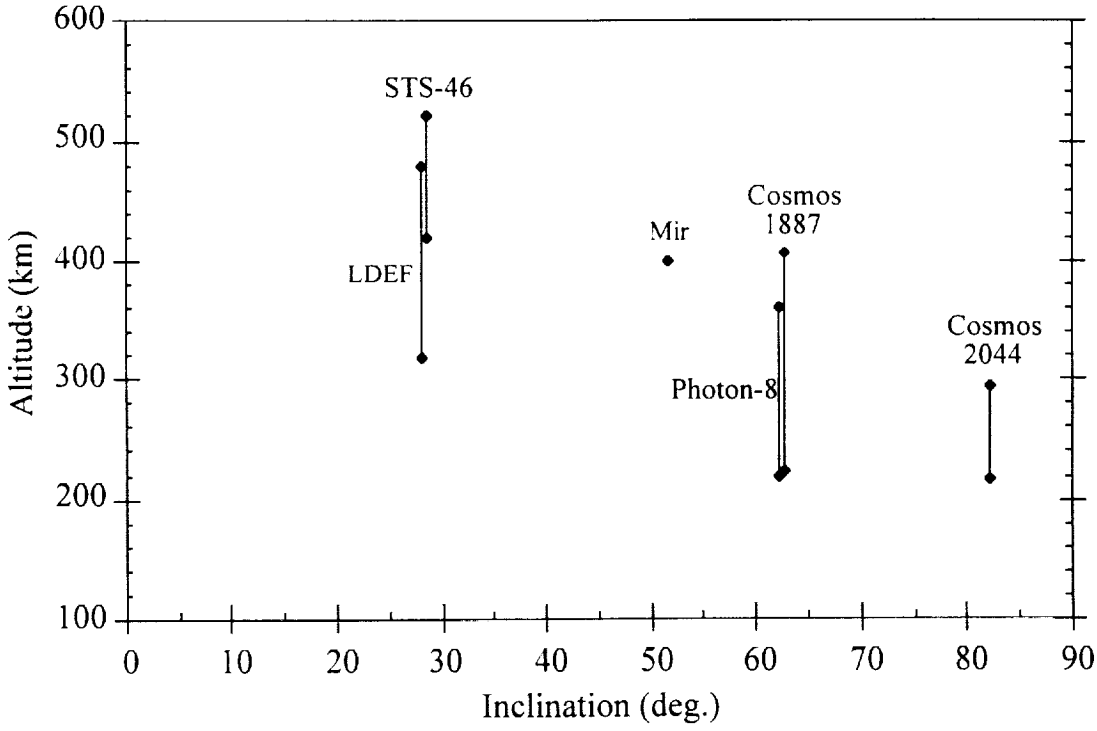

Fig. 2-2. Altitude-inclination coverage for thin shielding measurements compared with.

2-3. Models

The models and codes used in the dose predictions are summarized in Table 2-2. The trapped radiation flux models for electrons and protons, AE8 and AP8, and related

Table 2-2. Models and codes used.

• Trapped Radiation Dose Calculations		References
Orbit Trajectory	MSFC Orbit Code	[2-6]
Magnetic Field Code	ALLMAG	[2-7]
Magnetic Field Model	Solar Max: 1964 epoch, IGRF 1965 coefficients	[2-8]
	Solar Min: 1970 epoch, USC&GS 1970 coefficients	[2-9]
Trapped Electron Flux	AE8MAX, AE8MIN	[2-10]
Trapped Proton Flux	AP8MAX, AP8MIN	[2-11]
Transport/Dose Calculation	SHIELDOSE-2	[2-12]
Shielding Model	1-D Plane, Infinite Backing	
• Galactic Comic Ray Dose Calculations		
Flux Spectra (Z=1-28)	CREME96	[2-13]
Geomagnetic Transmission	CREME96	[2-13]
Tissue Dose	SPAR Code Stopping Powers	[2-14]
Shielding Model	1-D Solid Sphere	

magnetic field models, are standard versions in use at NASA/MSFC that have been applied, for example, in International Space Station radiation assessments. For the trapped radiation calculations here, the earth's magnetic field moment (used in extracting flux spectra from the model data bases) is calculated from the field models rather than using a fixed value. For the galactic cosmic ray (GCR) dose predictions, the CREME96 code was used to calculate the particle spectra of Z = 1 through 28 ions at the center of spherical aluminum shielding, and these spectra were folded with stopping powers from the SPAR code to obtain tissue dose. This assumed GCR shielding geometry is a more approximate representation of the measurement geometry than for the trapped radiation, but the primary interest here is for thin shielding where the GCR contribution is small.

For the trapped radiation, calculations were made at either solar minimum or solar maximum according to the mission times indicated in Fig. 2-1. For the Photon-8 and STS-46 missions, which took place about midway between solar minimum and solar maximum, a simple average of the trapped code calculations at solar minimum and solar maximum was used. For the LDEF mission, which occurred over 5.8 years covering both solar minimum and solar maximum, code results at solar minimum and solar maximum were weighted according to the

F10.7 solar flux during the mission (using the procedure described in ref. 2-15) to obtain mission-average trapped spectra. For the GCR dose, spectra at the time of the mission were calculated using the GCR time dependence contained in the CREME 96 code.

The calculations have been made with aluminum as the shielding material. Since the stopping power of aluminum is within ± 10% of LiF (the most commonly used TLD composition) for both electrons and protons over the energy range of interest, the attenuation in aluminum is a good approximation for LiF. The dose is calculated as absorbed energy in tissue since the measurements are reported as tissue dose. (The silicon dose appropriate for electronics dose estimates would be about 25% lower than the dose shown for tissue.)

2-4. Model-Data Comparisons

The more recent thin shielding dose data available is from the Russian Photon-8 mission at 62.8° inclination. Predictions for the dose rate at shielding depths above about 0.1 g/cm^2 (corresponding to the penetration of electrons > 300 keV) are in excellent agreement with the TLD measurements (Fig. 2-3). The model-data agreement becomes progressively worse for decreasing shielding below 0.1 g/cm^2.

Figure 2-4 compares dose rate predictions with measurements on the Russian Mir space station made using U.S., Russian, and German dosimeters. Here the predictions substantially underestimate the measurements (by factors ranging from 3 to 9, depending on shielding depth and data set). This large disagreement is attributed primarily to the enhanced radiation belts produced by the large geomagnetic storm and concurrent solar particle event which occurred in March 1991, about three months before the measurements; such transient events are not included in the models.

Figure 2-5 compares measurements and predictions for the high inclination (82.3°) Cosmos 2044 mission. The comparison here is similar to the Photon-8 mission with good agreement for depths above 0.1 g/cm^2 but substantial underprediction for thinner shielding.

Figure 2-6 shows a comparison of predictions with two sets of measurements on Cosmos 1887, data from the Univ. of San Francisco (USF) group using ^{7}LiF TLDs and data from the Institute of Biomedical Problems (IBMP) in Moscow using alumophosphate (Al-P) glass TLDs. Calculations to compare with these data have been made previously by Watts [2-16] using essentially the same models as here. The model predictions in this case agree with the data within a factor of about two over the whole depth range.

The predicted vs. measured comparison for dose rate on the low-inclination (28.5°) STS-46 flight is shown in Fig. 2-7. The near-surface (0.01 g/cm^2) dose rate here is overpredicted, in contrast to previous comparisons for mid- and high-inclination missions where the near-surface

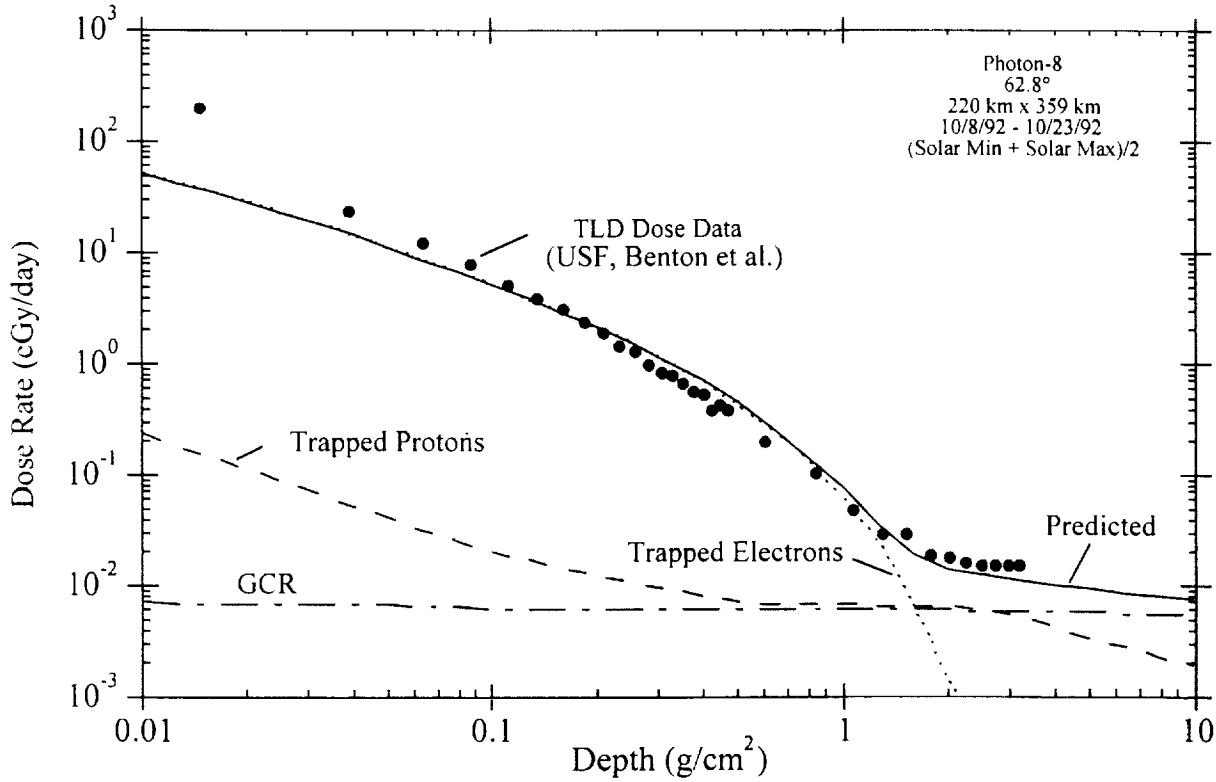

Fig. 2- 3. Predicted vs. measured dose rate on Photon-8 satellite.

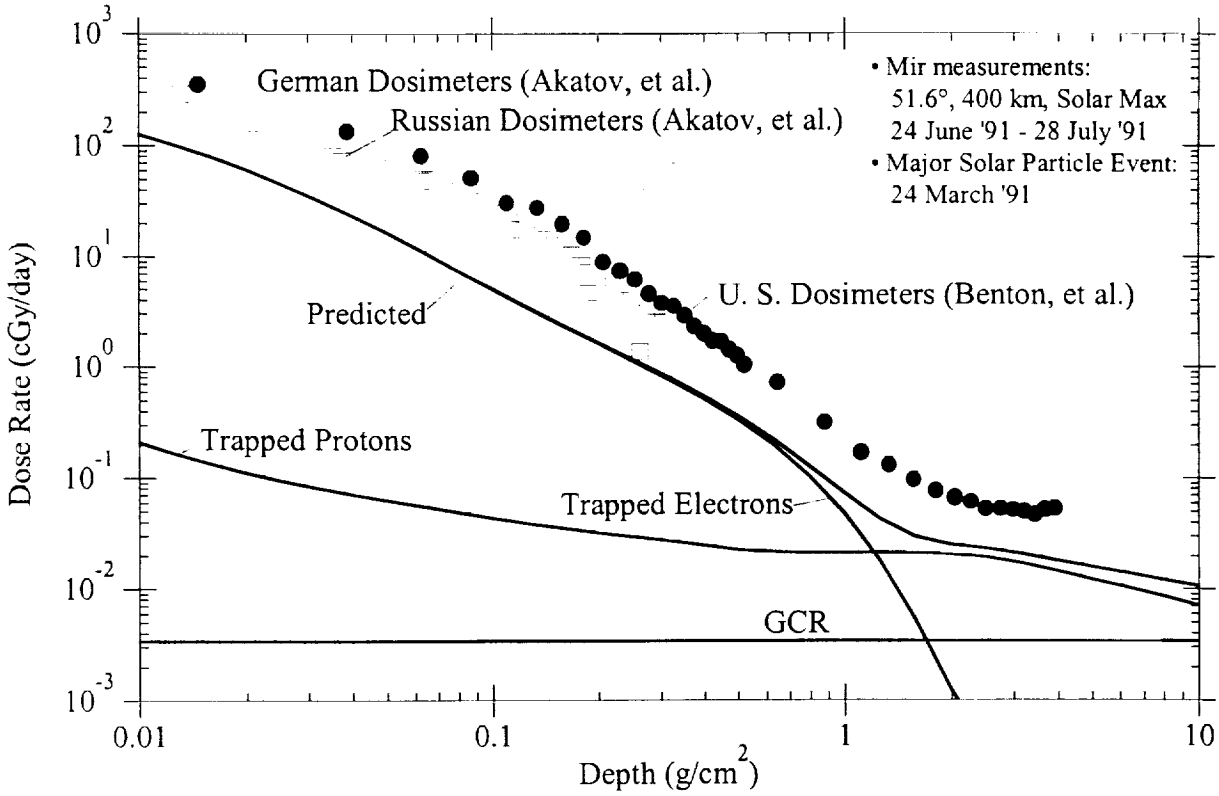

Fig. 2- 4. Predicted vs. measured dose rate on Mir space station.

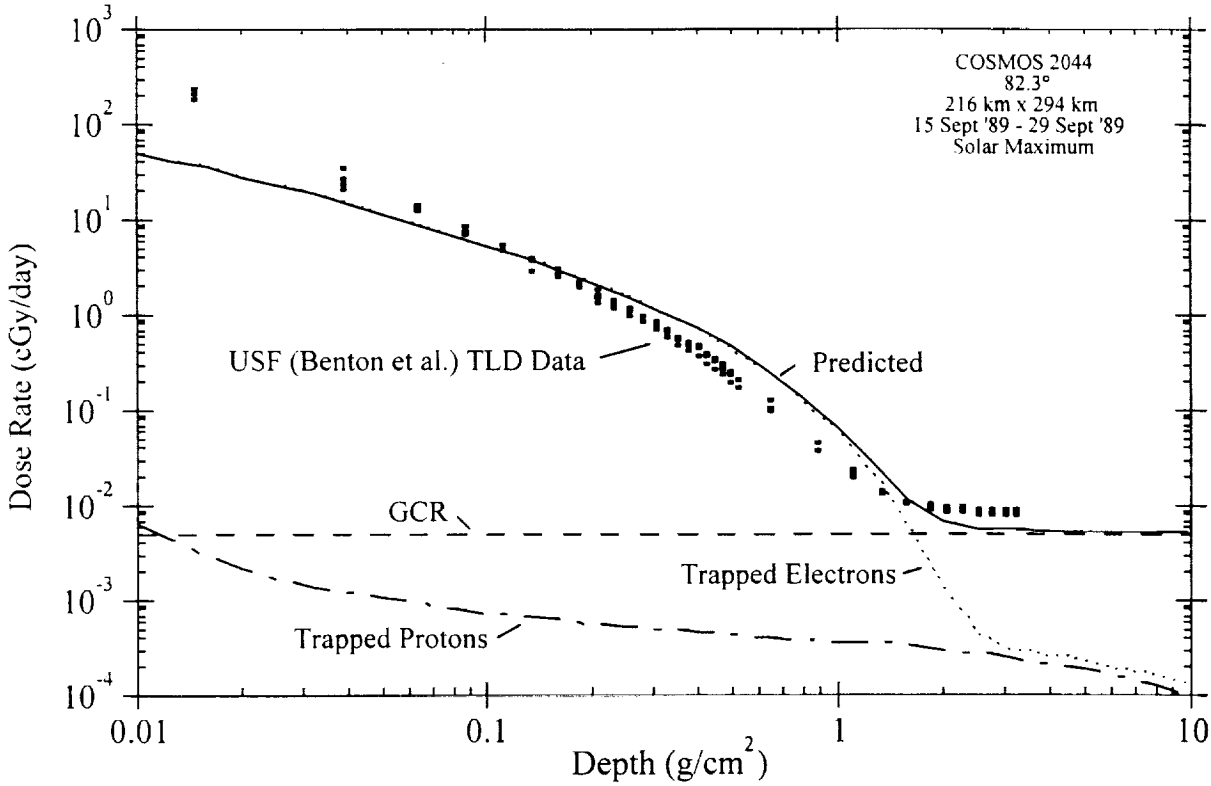

Fig. 2- 5. Predicted vs. measured dose rate on Cosmos 2044.

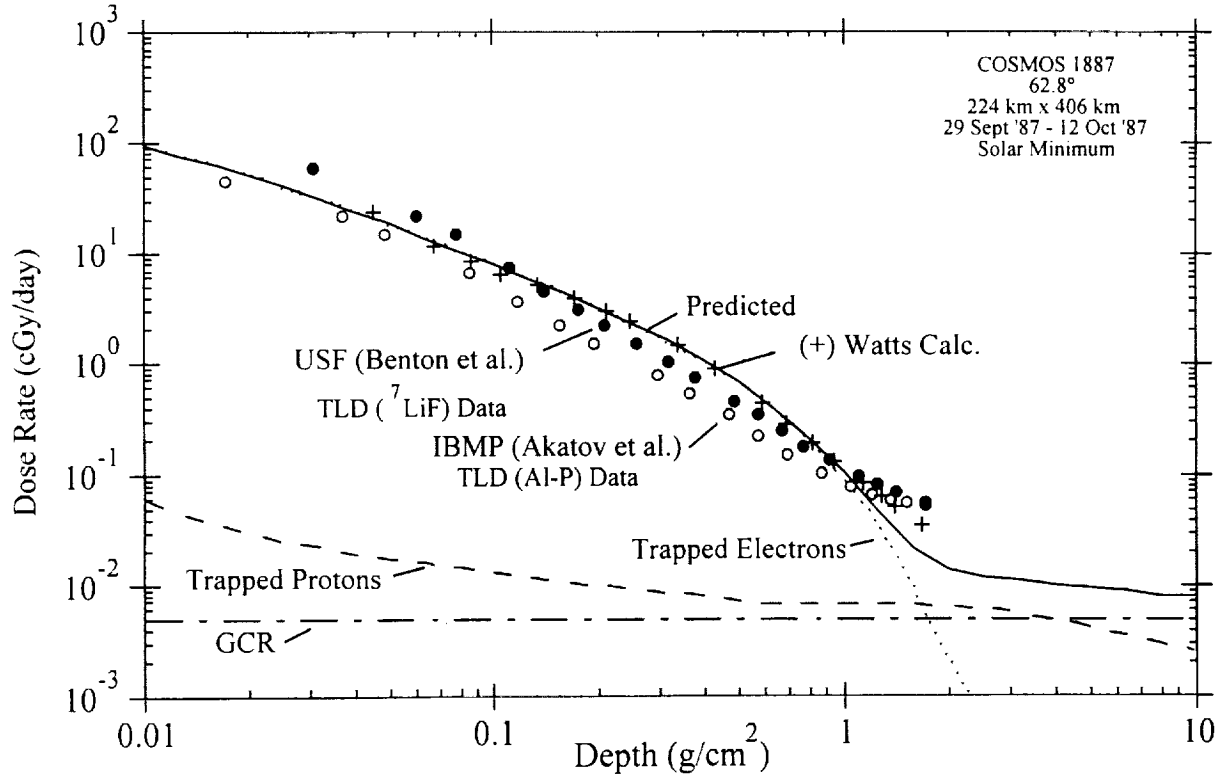

Fig. 2- 6. Predicted vs. measured dose rate on Cosmos 1887.

dose rate is substantially underestimated. There is a large difference in predicted vs. measured dose rate in this case at depths where trapped protons dominate. This may be due in part to orbit approximation; an elliptical 420 km x 520 km orbit was used for the calculations rather than actual trajectory data. (Additional predictions to compare with Shuttle dose data from dosimeters inside the spacecraft are given in Sec. 3.)

Fig. 2-8 shows predicted dose rates compared with thin shielding dose measurements on the 28.5° inclination LDEF mission. The agreement is good, within a factor of two at all depths. The over prediction near 0.01 g/cm^2 is similar to the STS-46 comparison.

Summary comparisons of the measured and predicted dose rates are shown in Figs. 2-9 and 2-10, respectively.

2-5. Discussion

We now quantify the predicted vs. measured dose rates for the above missions to extract uncertainty factors for the AE8 trapped electron model in predicting dose. The dose rate from trapped electrons is important at shielding depths less than about 0.8 g/cm^2 (100 mils of aluminum) for low-inclination (28.5°) orbits and at shielding depths less than about 2 g/cm^2 (350 mils) for high-inclination orbits, as shown in Fig. 2-11. For larger shielding depths, the dose from trapped protons and/or GCR particles dominate.

Although the availability of low-inclination data is limited to only two flights, the model-data comparisons seem to indicate a basic difference in agreement for near-surface shielding (0.01 g/cm^2, or 1.5 mils of aluminum) for low-inclination orbits compared to mid-and high-inclination orbits. For the two 28.5° inclination cases, the near-surface dose rates are over predicted (by a factor of about two), whereas for the higher-inclination missions the near-surface dose rates are underpredicted (by factors of 3 to 10). This is likely due to exposure of the high inclination flights to the "horns" of the outer zone electrons at high latitudes, and because the outer zone electrons can have large fluctuations due to geomagnetic activity which are not taken into account by the static AE8 model.

The depth-dependence of the predicted-to-measured dose rate ratios for the 28.5 deg. missions are plotted in Fig. 2-12. For electronics dose estimates, the minimum shielding of practical interest is about 30 mils of aluminum -- e.g., the thinnest electronics boxes deployed external to the International Space Station have this thickness. Thus, the "box" indicated on Fig. 2-12 represents the predicted-to-measured dose rate ratio variation relevant to estimating the electronics dose from trapped electrons. Also indicated at the top of Fig. 2-12 are the electron kinetic energies that can contribute at the shielding depths where the predicted-to-measured dose rate ratios are calculated.

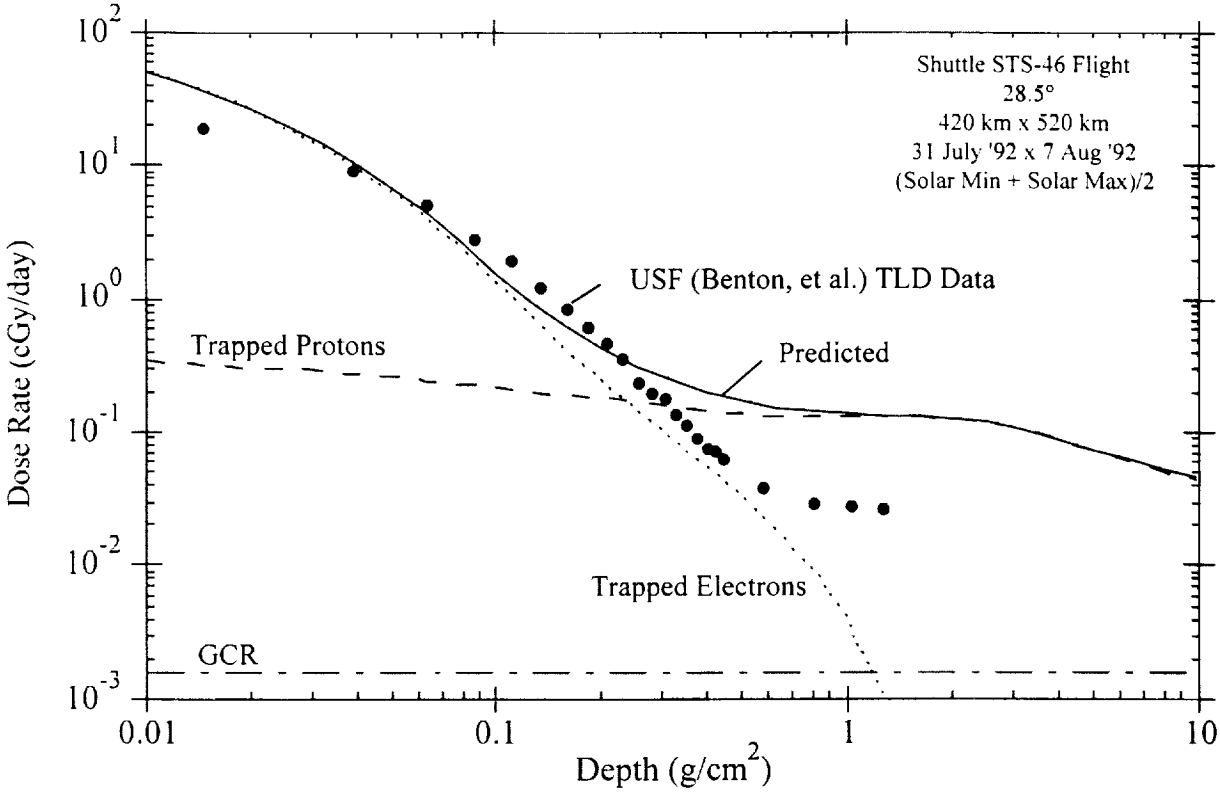

Fig. 2- 7. Predicted vs. measured dose rate on Shuttle Flight STS-46.

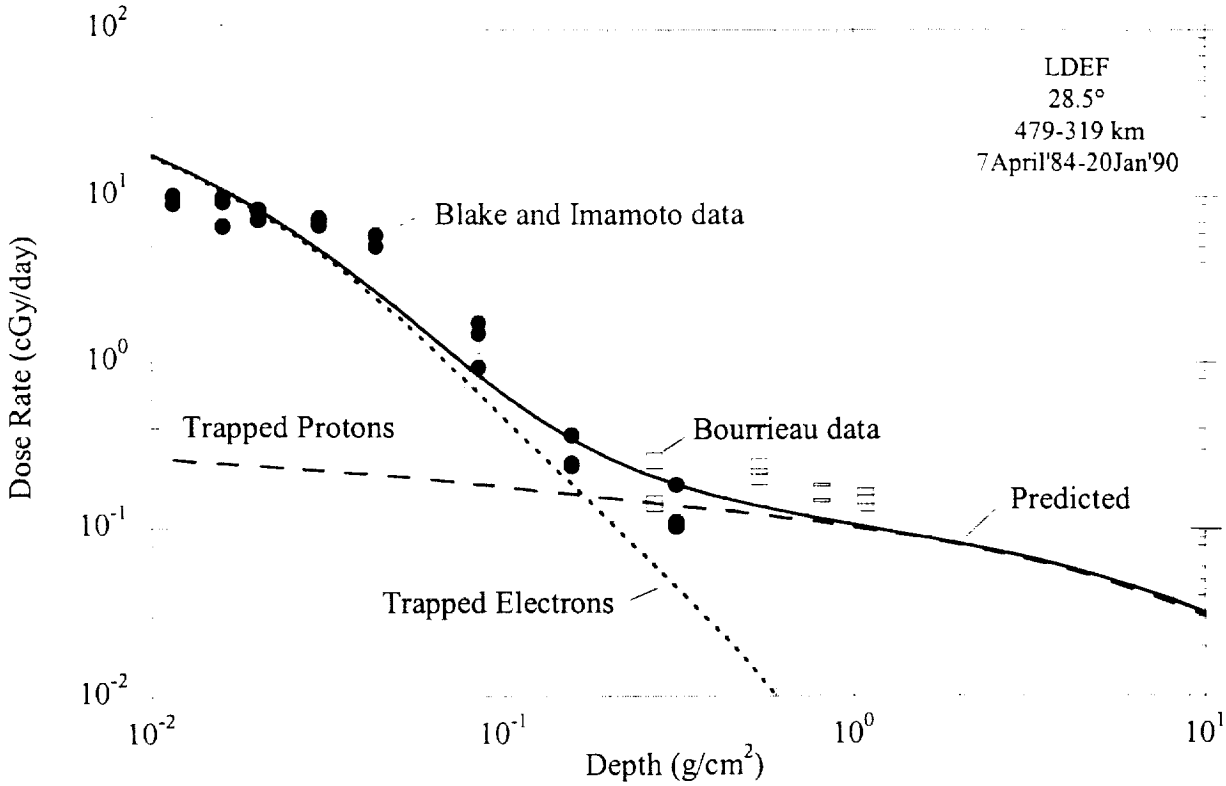

Fig. 2- 8. Predicted vs. measured dose rate on LDEF satellite.

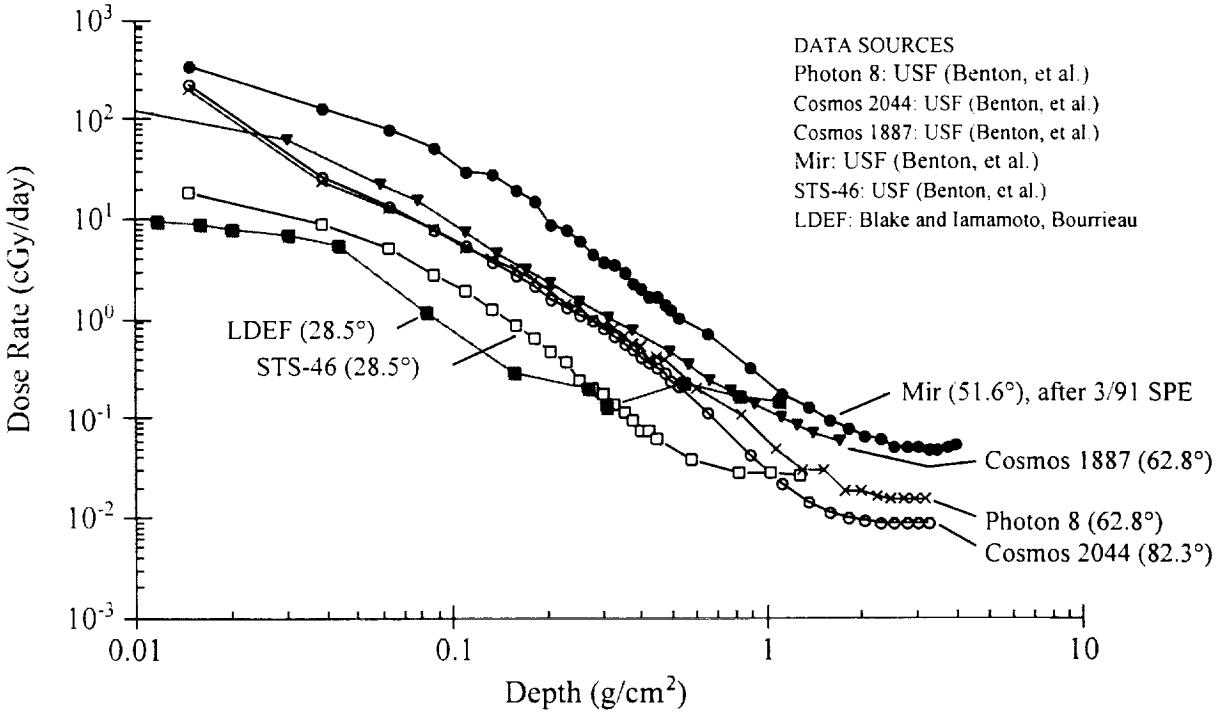

Fig. 2- 9. Comparison of measured dose rates.

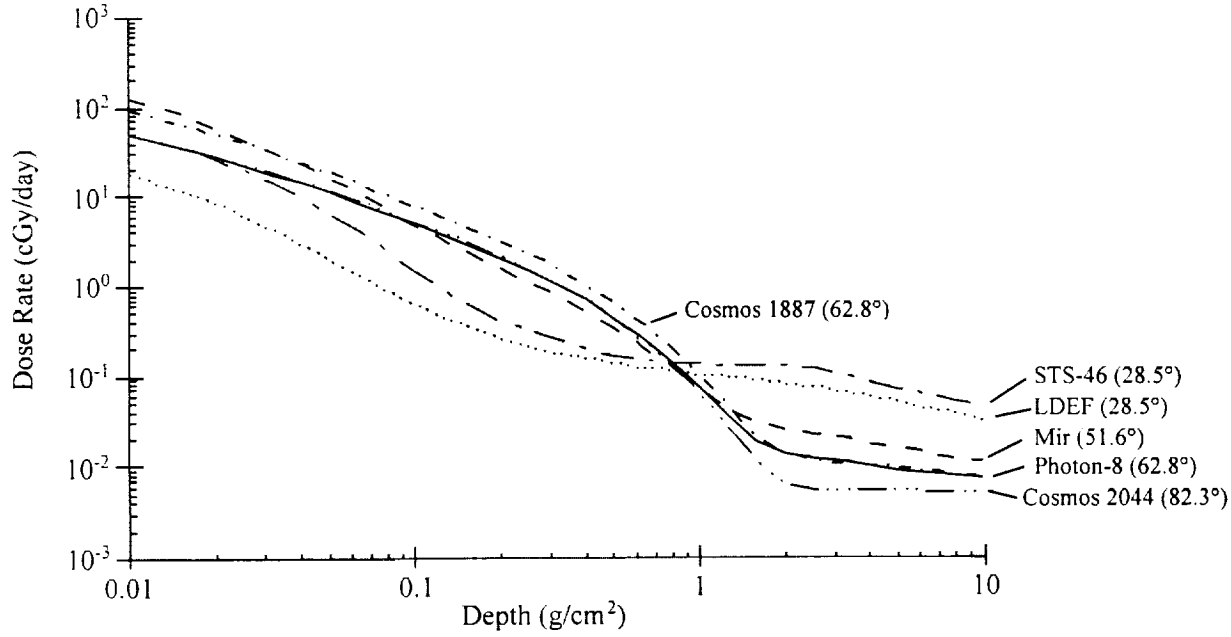

Fig. 2-10. Comparison of predicted dose rates.

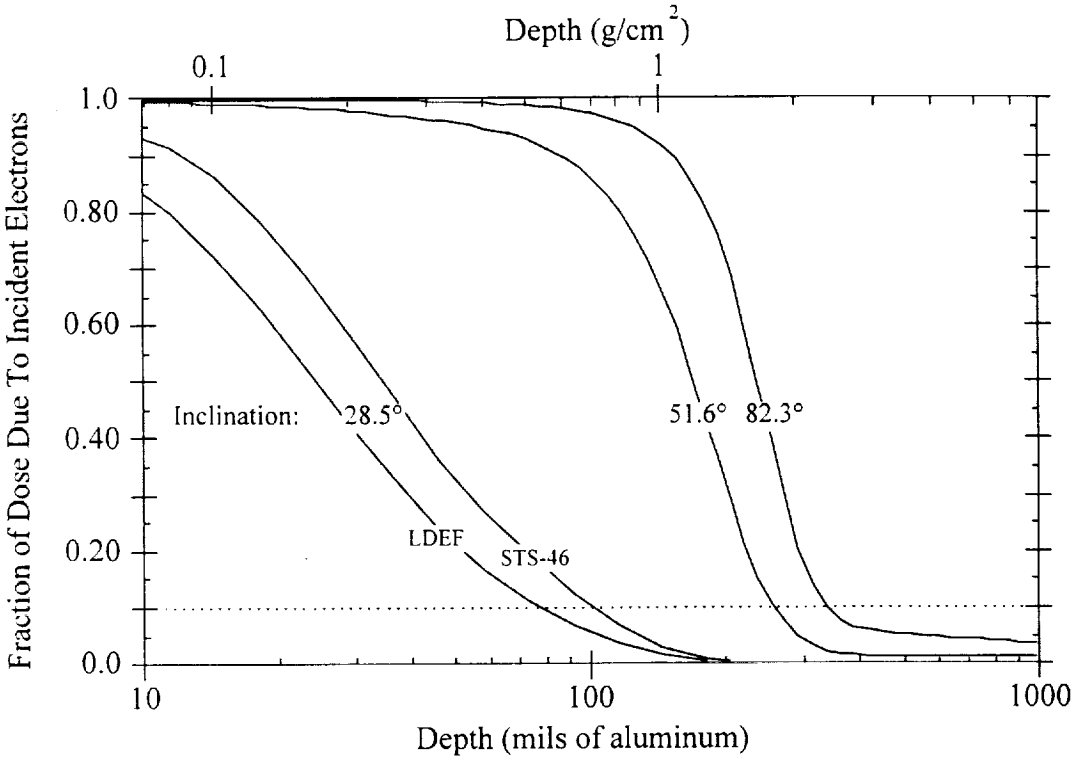

Fig. 2- 11. Predicted trapped electron contribution to dose rate.

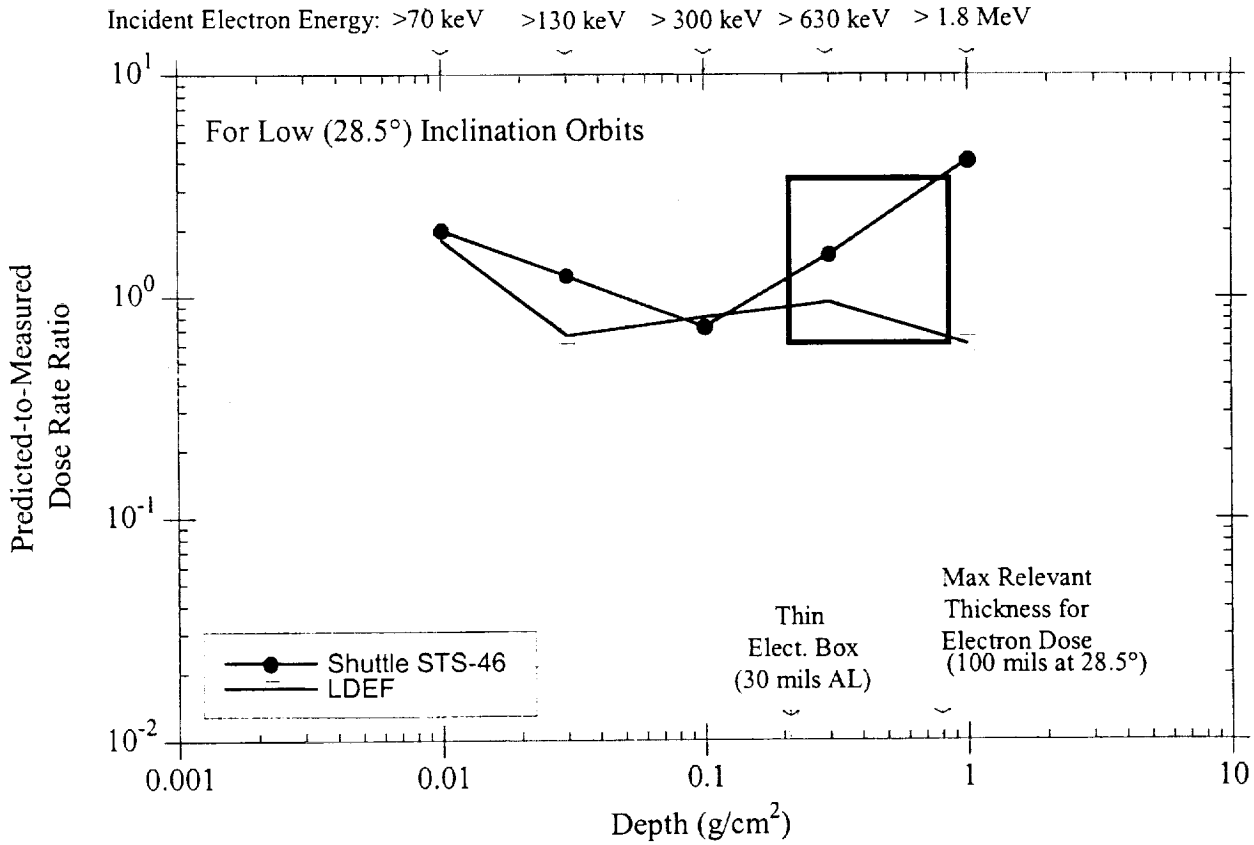

Fig. 2- 12. Ratio of predicted-to-measured dose rates for low inclination (28.5°) orbits.

Depth dependent predicted-to-measured dose rate ratios for the higher inclination missions are shown in Fig. 2-13. Again, the solid-line box indicates the relevant data range for electronics dose from electrons. In quantifying the AE8 model uncertainties, we consider only geomagnetically quiet conditions (represented by points in Fig. 2-13 contained in the dotted boxes). The Mir comparison, for measurements a few months after the unusually large geomagnetic storm and solar particle event of March 1991, gives some indication of the magnitude of the underestimate predicted by the models following "stormy" magnetic activity conditions.

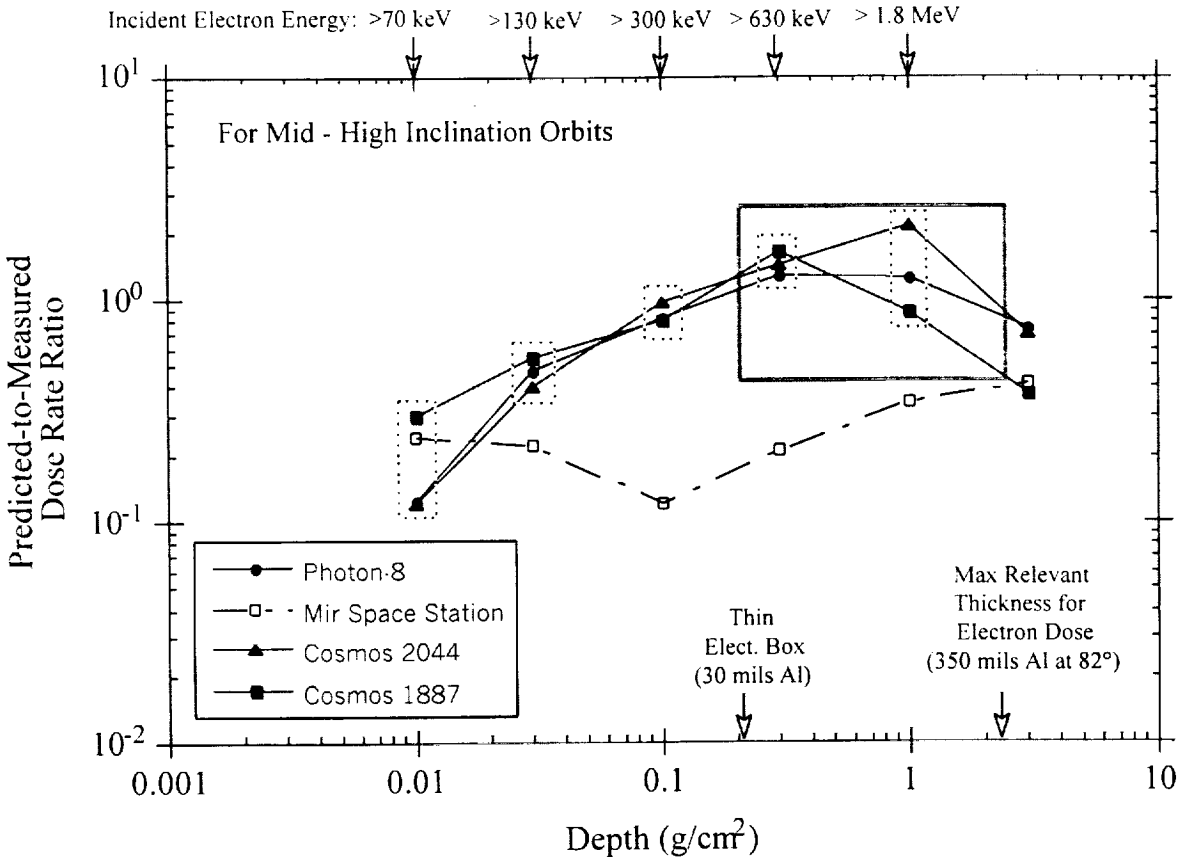

Fig. 2- 13. Ratio of predicted-to-measured dose rates for mid and high inclination orbits.

2-6. Uncertainty Factors

Uncertainty factors for the AE8 model in predicting dose rates for low-altitude orbits based on the flight data considered are summarized in Table 2-3. These values are from the predicted-to-measured ratios of Figs. 2-12 and 2-13 and the depth-dependence of the dose contribution by electrons shown in Fig. 2-11. These values do not consider the Mir data, which are influenced by high fluxes due to the after effects of a large geomagnetic disturbance.

Table 2-3. Uncertainty factors for AE8 model predictions of electron dose in low altitude orbits (for geomagnetically quite conditions).

	Ratio of Measured-to-Predicted Dose Rates		
Shielding	Low Inclination (28.5°)	Mid Inclinations (50°-65°)	High Inclinations (80°-90°)
Near Surface (1.5 mils Al)	0.5	3-10	10
30-100 mils (Al)	0.3-2	0.5-1	0.5-1
100-250 mils (Al)	NA	0.5-2	0.5-2
250-350 mils (Al)	NA	NA	1
> 350 mils (Al)	NA	NA	NA

NA = Not Applicable (dose rate at these depths dominated by trapped protons and/or GCR particles, not trapped electrons)

2-7. Conclusions

As evident from Table 2-3, the ratios of measured-to-predicted dose rate are relatively large and vary substantially, particularly for the thinnest shielding at mid- and high-inclinations. This may be expected since the conditions for the measurements generally do not correspond to conditions where the AE8 model is considered to be most accurate – namely: (a) The models are applicable for predicting average fluxes over relatively long times (six months or so) and do not account for short-term fluctuations, whereas, except for LDEF, the measurement times are for only 1– 4 weeks (Table 2-1); (b) the high-inclination flights receive exposure from outer zone electrons that enter low altitudes at high latitudes, and these electrons are subject to large

fluctuations due to geomagnetic disturbances, but the models neglect such flux variations; and, (c) the models are available only for solar minimum and solar maximum conditions, whereas some of the flights are at neither.

A more definitive flight data set (although for only a single shielding depth) for evaluating AE8 model uncertainties for thin shielding dose estimates at low altitudes is from APEX satellite measurements (discussed in Sec. 4). The APEX data is based on long term measurements and is available as a function of magnetic activity level. A comparison of the results here with data/model ratios determined using APEX data is given in [2-17].

2-8. References

[2-1]. E. V. Benton and T. A. Parnell, "Space Radiation Dosimetry on U.S. and Soviet Manned Missions", in Proc. NATO Advanced Study Institute on Terrestrial Space Radiation and It's Biological Effects (1987: Corfu, Greece), Plenum Press, New York, 1988.

[2-2]. E. R. Benton and E. V. Benton, "A Survey of Radiation Measurements Made Aboard Russian Spacecraft in Low-Earth Orbit", NASA/CR-1999-209056, March 1999.

[2-3]. Yu. A. Akatov, V. A. Shursha Koiv, P. Schmidt, H. Schtroibel, T. Han, and H. Hartman, "Analysis of the Absorbed Dose Measurements Outside the Mir Space Station in June-July, 1991" preprint of paper accepted for publication in Nucl. Meas.

[2-4]. J. B. Blake and S. S. Imamoto, "A Measurement of the Radiation Dose to Passive Dosimetry", Proc. Second LDEF Post-Retrieval Symposium, NASA CP 3194 (Part 1), 1993.

[2-5]. J. Bourrieau, "LDEF Dosimetric Measurement Results (AO 138-7 Experiment)" Proc. Second LDEF Post-Retrieval Symposium, NASA CP 3194 (Part 1), 1993.

[2-6]. M. O. Burrell and J. J. Wright, "Orbital Calculations and Trapped Radiation Mapping", NASA Marshall Space Flight Center, NASA TM X-53406, 8 March 1966.

[2-7]. E. G. Stassinopoulos and G. D. Mead, "ALLMAG, GDALMG, LINTRA: Computer Programs for Geomagnetic Field and Field-line Calculations", National Space Science Data Center, NASA Goddard Space Flight Center, NSSDC 72-12, 1972.

[2-8]. IAGA Commission 2 Working Group 4, "Analysis of the Geomagnetic Field, International Geomagnetic Reference Field 1965.0", J. Geophys. Res. 74, 4407 (1969).

[2-9]. Louis Hurwitz, "Mathematical Model of the 1970 Geomagnetic Field", ESSA Coast and Geodetic Survey, 4 May 1970.

[2-10]. James I. Vette, "The AE-8 Trapped Electron Model Environment", National Space Science Data Center, Goddard Space Flight Center, NSSDC/WDC-A-R&S 91-24, Nov. 1991.

[2-11]. Donald W. Sawyer and James I. Vette, "AP-8 Trapped Proton Environment for Solar Maximum and Solar Minimum", National Science Data Center, Goddard Space Flight Center, NSSDC/WDC-A-R&S 76-06, 1976.

[2-12]. Stephen M. Seltzer, "Updated Calculations for Routine Space-Shielding Radiation Dose Estimates: SHIELDOSE-2", National Institute of Standards and Technology, NISTIR-5477, Dec. 1994.

[2-13]. Allan J. Tylka, et al., CREME96 (beta version), Naval Research Laboratory (1996).

[2-14.] T. W. Armstrong and K. C. Chandler, "Stopping Powers and Ranges for Muons, Charged Pions, Protons, and Heavy Ions", Nucl. Instr. Meth. 113, 313 (1973).

[2-15]. J. W. Watts, Jr., T. W. Armstrong and B. L. Colborn, "Predictions of LDEF Exposure to the Ionizing Radiation Environment", Radiat. Meas. 26(6), 893 (1996).

[2-16]. Yu. A. Akatov, V. E. Dudkin, E. E. Kovalev, E. V. Benton, A. L. Frank, J. W. Watts, Jr., and T. A. Parnell, "Depth Distribution of Absorbed Dose on the External Surface of Cosmos 1887 Biosatellite", Nucl. Tracks Radiat. Meas. 17 (2), 105 (1990).

[2-17]. T. W. Armstrong and B. L. Colborn, "Evaluation of Trapped Radiation Model Uncertainties for Spacecraft Design ", Science Applications International Corporation, Contractor Report for NASA/MSFC, SAIC-TN-99020, September 1999.

3. Evaluation of AP8 Model Uncertainties Using Space Shuttle Dose Data

3-1. Introduction

Radiation dose measurements using passive thermoluminescent dosimeters (TLDs) have been made on all Space Shuttle flights. Locations in the Shuttle for two of the measurement positions, designated as DLOC#1 and DLOC#2, are shown in Fig. 3-1, and the TLD shielding distributions (from ref. [3-1]) are shown in Fig. 3-2 The minimum shielding is 1.25 g/cm^2, so the dose from the trapped electron environment is negligible, and, as shown later, the dose from galactic cosmic-rays is small except at the lowest Shuttle flight altitudes. Thus, the Shuttle TLD measurements provide a rather large trapped proton dose data set that can be utilized in investigating the accuracy of the AP8 trapped proton model for low altitude dose predictions.

A summary of the evaluation of AP8 model uncertainty based on Shuttle and other flight data is given in [3-2]; the purpose here is to give some of the details of the Shuttle model-data comparisons used in this summary.

The results here quantify the difference between trapped proton predictions using the AP8 model and Shuttle dose measurements over a range of altitudes, inclinations, and solar minimum and maximum conditions. However, it is important to note that, for the reasons discussed in Sec. 3-5, we conclude that the Shuttle model-data differences determined here cannot be interpreted as AP8 model uncertainties having general applicability for other missions.

3.2 Flight Data

Tables 3-1 and 3-2 list the Shuttle TLD dose data (from refs. [3-1] and [3-3]) for the 63 flights that we have made model comparisons with. Figure 3-3 shows the altitude dependence of measurements at the DLOC#1 and DLOC#2 locations. Figure 3-4 shows the altitude dependence of the DLOC#2 measurements for different orbit inclinations. Almost all of the data fall within a factor of two of an exponential altitude dependence having an e-folding altitude of 90 km.

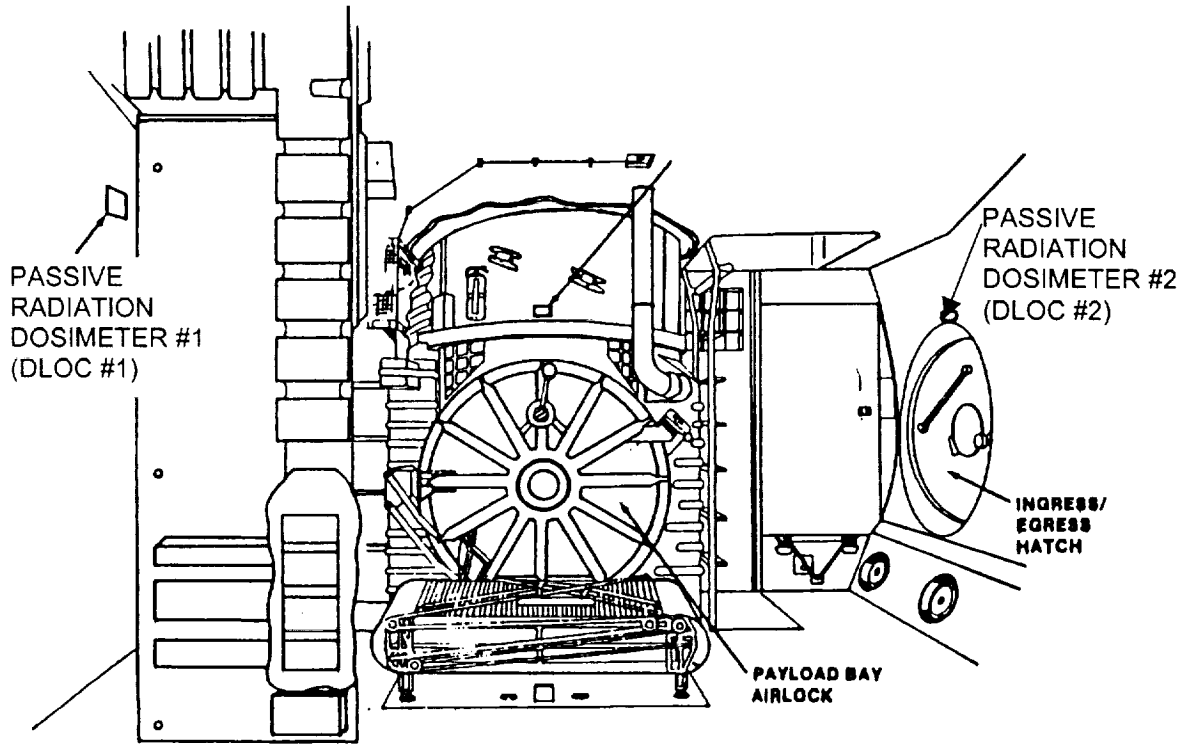

Fig. 3-1. Passive radiation dosimeters (TLDs) at locations DLOC #1 and DLOC #2 in aft mid-deck of Space Shuttle.

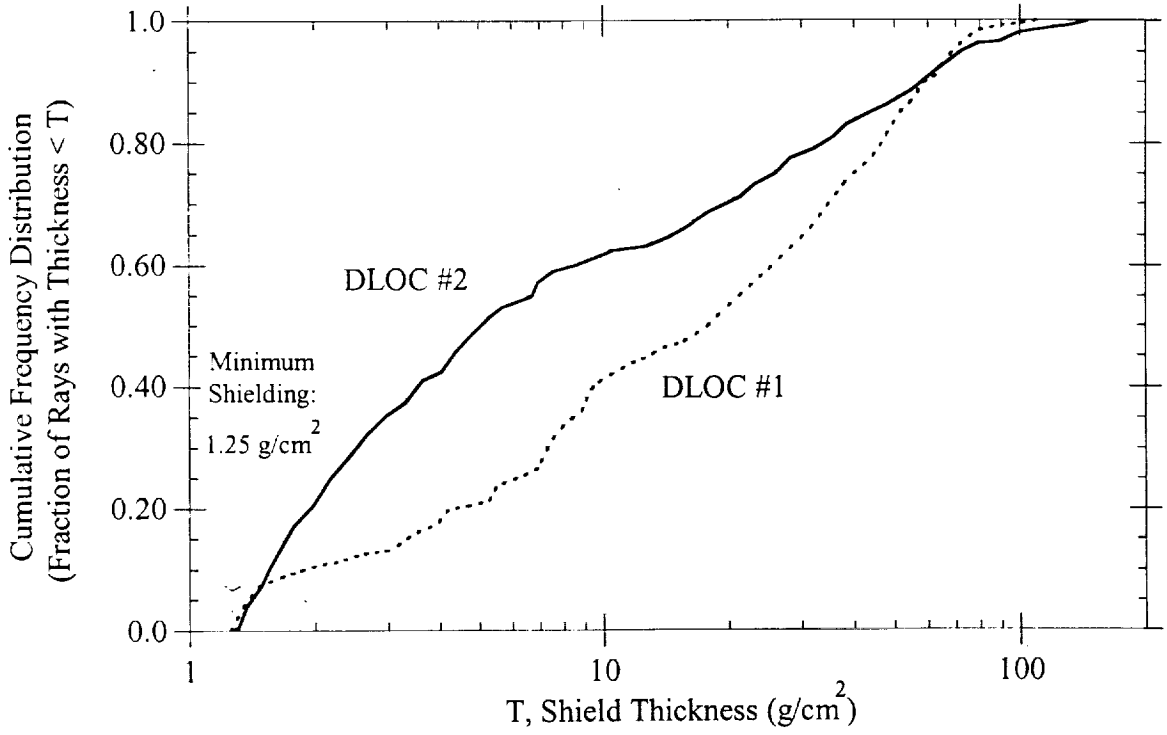

Fig. 3-2. Shielding distributions for TLD dose measurements at locations DLOC #1 and DLOC #2 on Space Shuttle.

Table 3-1. Shuttle dose measurements for low-inclination (28.5 deg.) flights.

Mission	Date	Duration (hr)	Inclination (deg)	Altitude (km)	Dose Rate (mrad-tissue/day)	
					DLOC#1	DLOC#2
STS-4	6/27/82	169.2	28.5	296	0.94	1.06
STS-5	11/11/82	122.2	28.5	283	1.2	1.5
STS-6	4/4/83	120.4	28.5	293	6.6	6.9
STS-7	6/18/83	146.4	28.5	296	7.9	8.0
STS-8	8/30/83	145.1	28.5	287	6.2	6.5
STS-41-B	2/3/84	191.3	28.5	296	6.7	7.0
STS-41-C	4/6/84	167.7	28.5	498	64.4	141.7
STS-41-D	8/30/84	144.9	28.5	315	8.7	10.5
STS-51-A	11/8/84	191.7	28.5	352	13.2	24.6
STS-51-C	1/24/85	73.6	28.5	333	12.5	14.2
STS-51-D	4/12/85	168	28.5	454	47.0	100.7
STS-51-G	6/17/85	169.7	28.5	370	16.4	26.2
STS-51-I	8/27/85	170.3	28.5	343	13.1	19.0
STS-51-J	10/3/85	97.8	28.5	509	94.7	186.0
STS-61-B	11/26/85	165.1	28.5	380	18.9	35.3
STS-61-C	1/12/86	146.1	28.5	324	11.2	15.1
STS-26	9/29/88	97	28.5	311	8.3	9.2
STS-29	3/13/89	119.7	28.5	317	8.3	11.4
STS-30	5/4/89	97	28.5	311	7.0	9.4
STS-33	11/22/89	120.1	28.5	537	101.5	190.4
STS-32	1/9/90	261	28.5	333	7.9	10.1
STS-31	4/24/90	121.3	28.5	617	170.2	356.1
STS-41	10/6/90	98.1	28.5	291	4.6	3.7
STS-38	11/15/90	117.9	28.5	215	5.0	4.5
STS-35	12/2/90	215.1	28.5	352	9.8	10.9
STS-37	4/5/91	143.6	28.5	450	25.1	58.8
STS-43	8/2/91	213.4	28.5	296	4.6	5.0
STS-44	11/24/91	166.8	28.5	361	8.9	8.8
STS-49	5/7/92	213.3	28.5	339	7.7	10.5
STS-50	6/25/92	331.5	28.5	298	5.9	5.8
STS-52	10/22/92	237	28.5	296	5.8	5.9
STS-54	1/13/93	143.7	28.5	304	5.8	6.6
STS-55	4/26/93	239.8	28.5	302	5.9	6.5
STS-57	6/21/93	239.8	28.5	470	40.0	77.4
STS-51	9/12/93	238.2	28.5	296	5.8	7.7
STS-61	12/2/93	260	28.5	594	141.6	257.9
STS-65	7/9/94	353.9	28.5	306	6.6	6.8
STS-67	3/2/95	399.2	28.5	352	14.7	29.1
STS-70	7/13/95	214.3	28.5	296	9.0	13.8
STS-69	9/7/95	260.5	28.5	370	20.1	50.8
STS-72	1/11/96	214	28.5	463	17.8	44.9
STS-75	2/22/96	377.7	28.5	296	8.6	12.9

Table 3-2. Shuttle dose measurements for mid-inclination (51.6, 57 deg.) flights.

Mission	Date	Duration (hr)	Inclination (deg)	Altitude (km)	Dose Rate (mrad-tissue/day)	
					DLOC#1	DLOC#2
STS-63	2/2/91	198	51.6	400	22.8	44.5
STS-71	6/26/91	235	51.6	400	24.0	54.0
STS-74	11/11/91	196	51.6	400	20.6	41.2
STS-41A	11/27/79	248	57	250	11.4	12.2
STS-41G	10/4/80	197	57	259	10.5	12.9
STS-51B	4/28/81	168	57	352	18.0	30.0
STS-61A	10/29/81	169	57	324	16.6	22.0
STS-27	12/1/84	105	57	459	33.0	66.4
STS-28	8/7/85	122	57	306	12.2	14.9
STS-39	4/27/87	199	57	263	8.3	12.0
STS-48	9/11/87	128	57	565	57.9	122.6
STS-42	1/21/88	193	57	304	9.3	11.2
STS-45	3/23/88	214	57	296	10.3	12.4
STS-47	9/11/88	190	57	306	11.5	14.8
STS-53	12/1/88	175	57	339	13.0	16.1
STS-56	4/7/89	222	57	302	11.2	14.3
STS-60	2/2/90	199	57	352	17.1	23.4
STS-59	4/8/90	270	57	222	11.3	13.4
STS-64	9/8/90	263	57	259	12.4	12.8
STS-68	9/29/90	270	57	222	12.5	10.9
STS-66	11/2/90	263	57	304	13.2	16.4

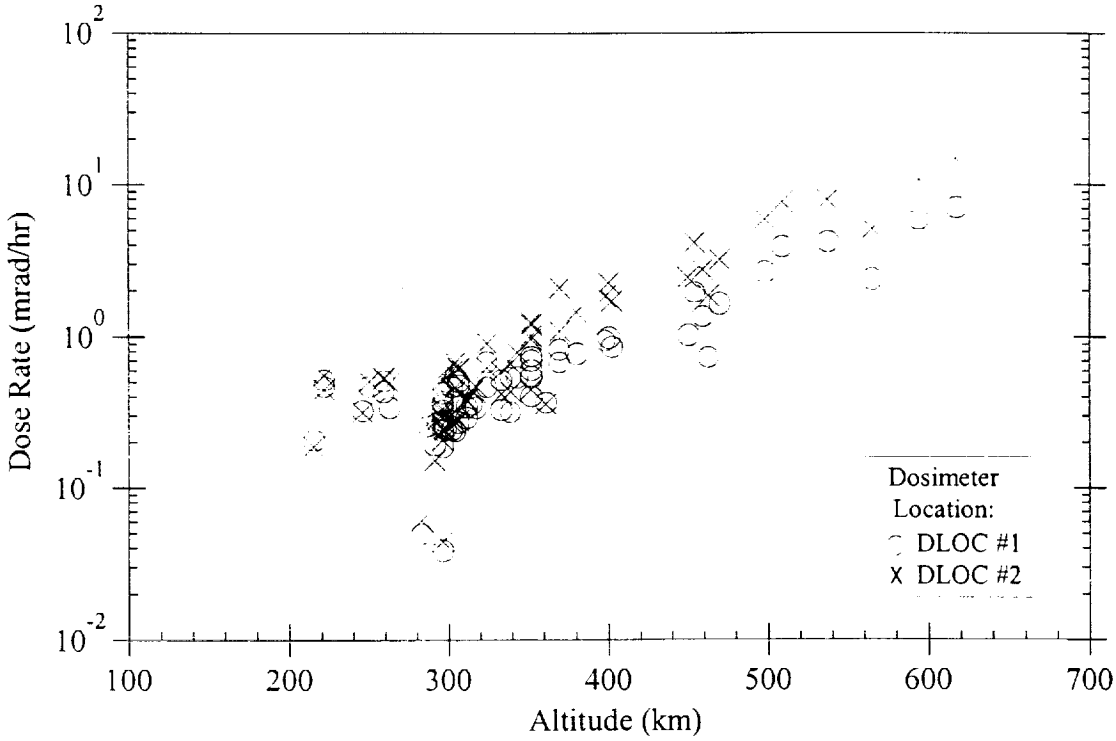

Fig. 3-3. Altitude dependence of Shuttle dose measurements.

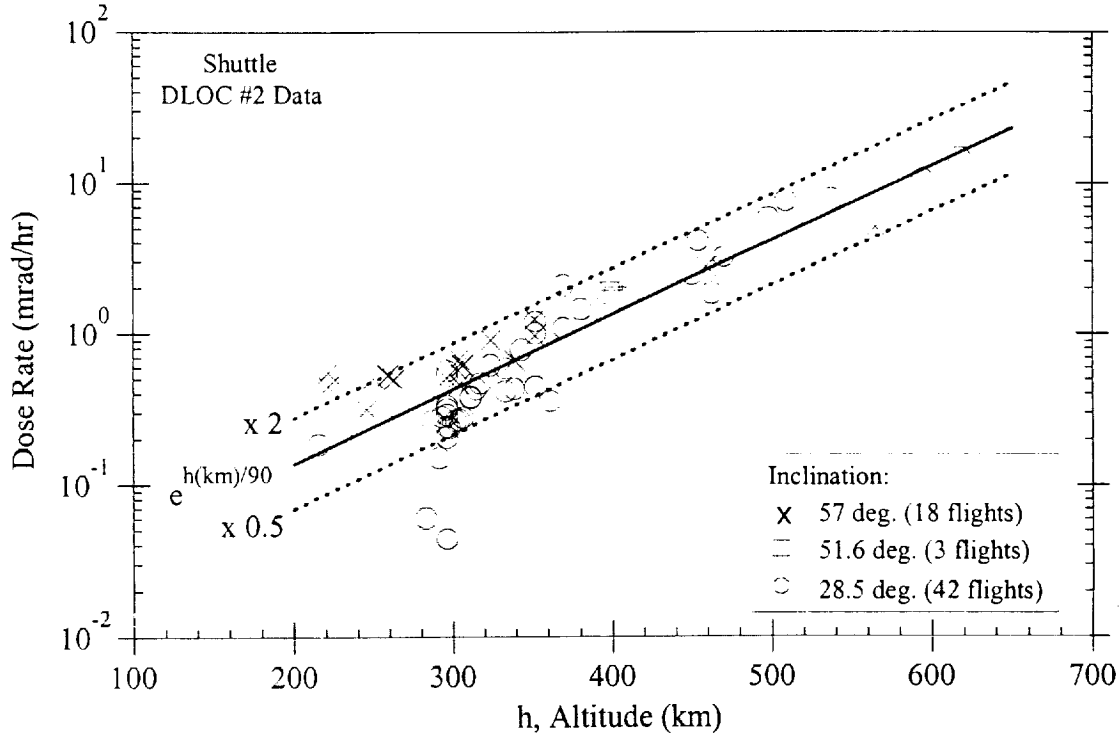

Fig. 3-4. Dose measurements on Shuttle flights – TLD data at location DLOC #2. The solid line is an exponential fit to the data, the dotted lines are a factor of two higher and lower than the fit.

3-3. Prediction Models and Methods

The models and codes used in predicting the dose for Shuttle flights are summarized in Table 3-3. The basic procedure consists of applying the AP8 model to calculate orbit-average flux spectra for the trapped proton environment (for various altitudes and inclinations at solar minimum and solar maximum), performing one-dimensional transport calculations (spherical geometry, aluminum shielding) using the SHIELDOSE-2 code to determine dose vs. shielding thickness for these spectra incident isotropically over the sphere surface, and then using the solid angle sectoring approximation to apply these 1-D dose results, together with the 3-D shielding distribution about the detector, to estimate the dose at the detector locations. This was done numerically by first fitting the cumulative shielding distribution for shielding thickness T (given in Fig. 3-2) by a polynomial lnT:

$$F(\leq T) = \sum_{i=o}^{n} m_i (\ln T)^i$$

with n = 6. The differential shielding distribution is then

$$f(T) = \frac{dF}{dT} = \frac{1}{T} \sum_{i=1}^{n} i \cdot m_i (\ln T)^{i-1}$$

and the detector dose, D_d, is

$$D_d = \int_{T_{min}}^{T_{max}} D_s(T) f(T) dT$$

where T_{min} = 1.25 g/cm^2 (from Fig. 3-3), T_{max} was taken to be 100 g/cm^2, and $D_s(T)$ is the 1-D dose at the center of a solid spherical shield (taken to be aluminum) of radius T due to isotropic incident trapped proton flux over the sphere surface. Example results for $D_s(T)$, from SHIELDOSE-2 code output, are shown in Fig 3-5.

Since the trapped proton dose decreases rapidly with decreasing altitude, the galactic cosmic-ray (GCR) dose becomes significant for the lowest altitude flights. The GCR dose was calculated using the CREME96 code to obtain GCR spectra (Z = 1 through Z = 28 ions) outside the magnetosphere, the orbit-average geomagnetic transmission, and then the orbit-average spectra at the altitude and inclination of interest. Spectra were then calculated as a function of shielding for a 1-D spherical shield of aluminum and folded with energy-dependent tissue

Table 3-3. Models and codes used in predictions.

		References
•Trapped Radiation Dose Calculations		
Orbit Trajectory :	MSFC Orbit Code	[3-4]
Trapped Proton Flux :	AP8MAX, AP8MIN	[3-5]
Magnetic Field Code :	ALLMAG	[3-6]
Magnetic Field Model :	Solar Max: 1964 epoch,	
	IGRF 1965 coefficients	[3-7]
	Solar Min: 1970 epoch,	
	USC&GS 1970 coefficients	[3-8]
Magnetic Moment :	Calculated from field coeff.	
Trapped Proton Anisotropy :	neglected	
Transport/Dose Calculation :	SHIELDOSE-2	[3-9]
Shielding Model :	3-D (solid angle sectoring)	
Shielding Distributions :	from NASA/JSC	[3-1]
•Galactic Comic-Ray Dose Calculations		
Flux Spectra (Z=1-28) :	CREME96	[3-10]
Geomagnetic Transmission :	CREME96	[3-10]
Tissue Dose :	SPAR Code Stopping Powers	[3-11]
Shielding Model :	1-D Solid Sphere, aluminum	

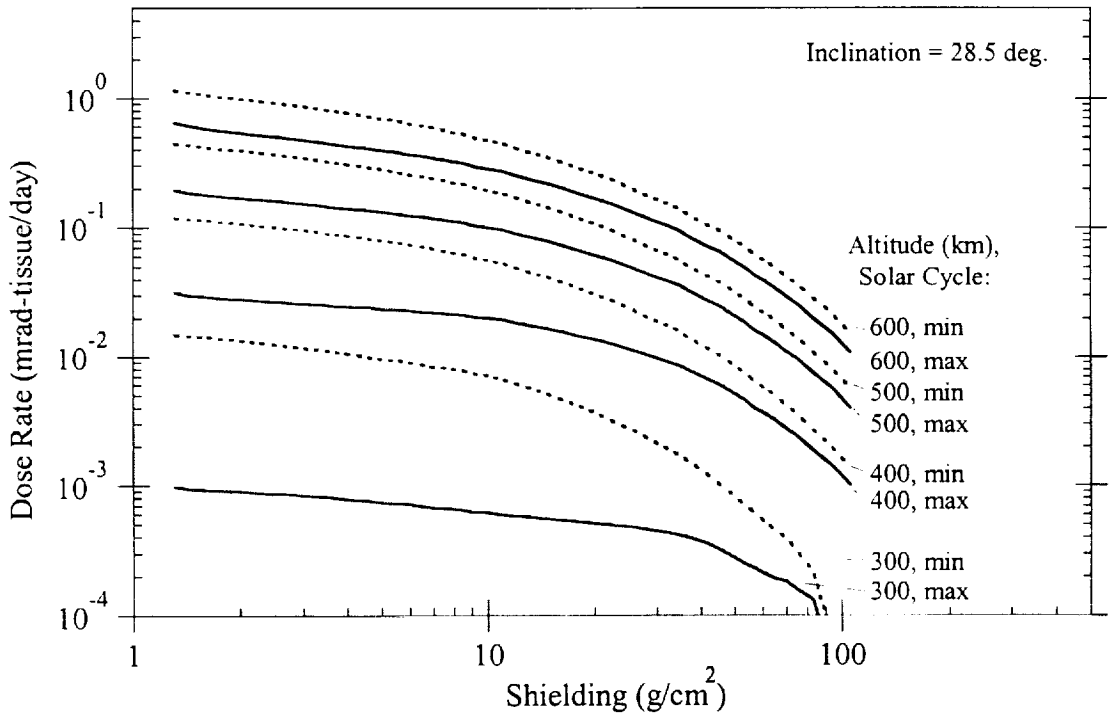

Fig. 3-5. Example results from 1-D shielding calculations, used as input in estimating dose at detector behind 3-D Shuttle shielding distribution.

stopping powers from the SPAR code to obtain tissue dose vs. shielding. The GCR dose contribution for detector location DLOC#2 is given in Table 3-4.

Since Shuttle flights have taken place throughout the solar cycle, but we only have versions of AP8 applicable for solar minimum and solar maximum, the variation of the solar F10.7 flux over the Shuttle launch dates was used in relating the flight dates to the solar cycle. This resulted in assigning flights during 1979-1983 and 1988.5-1992 to solar maximum and flights during 1984.5-1988 and 1994-1997 to solar minimum for comparison with AP8MAX and AP8MIN model predictions.

For orbits of interest here, the trapped proton dose is dominated by exposure during passes through the high-flux South Atlantic Anomaly region where the flux is anisotropic, as shown, for example, by LDEF satellite measurements [3-12]. To take into account this anisotropy in predicting Shuttle dose measurements, the time-dependence of the Shuttle orientation during the mission is needed. This information is not available to us, so the influence of trapped proton anisotropy has not been taken into account in the dose predictions

3-4 Model-Data Comparisons

Figures 3-6 and 3-7 compare the predicted and measured doses at DLOC#2 for low-inclination and mid-inclination Shuttle flights, respectively. The ratio of predicted-to-measured dose rates are plotted in Figs. 3-8 and 3-9 for TLD locations DLOC#1 and DLOC#2, respectively, and tabulated in Tables 3-5 and 3-6.

These comparisons show that for low-inclination (28.5°) orbits the predicted/measured dose ratio for DLOC#1 shielding is about 1-2 at solar minimum and 0.5-2 at solar maximum. For DLOC#2 shielding the ratio is 1.0 at solar minimum and 0.6-0.8 at solar maximum. For mid-inclination orbits (comparisons with 51.6° and 57° data), the predicted/measured dose ratio (for both solar minimum and solar maximum) is 2-3 for DLOC#1 and about 2 for DLOC#2. Thus, for altitudes in the 300-600 km range and low inclinations, the AP8 model overpredicts the measured Shuttle dose rates (up to a factor of 2) or underpredicts (up to a factor of 2), depending on shielding, solar cycle conditions, and altitude. For mid-inclinations, AP8 overpredicts by a factor of 1.5-3.

Table 3-4. Predicted dose contribution of galactic cosmic-rays at DLOC #2.

Inclination (deg)	Altitude (km)	Solar Cycle	Dose Rate (mrad/hr)			Ratio: GCR/Total
			Trapped Protons	GCR	Total	
28.5	300	Max	0.027	0.051	0.078	65%
28.5	400	Max	0.82	0.054	0.88	6.2%
28.5	500	Max	4.63	0.058	4.68	1.2%
28.5	600	Max	14.3	0.062	14.4	0.43%
28.5	300	Min	0.34	0.060	0.40	15%
28.5	400	Min	2.79	0.064	2.85	2.3%
28.5	500	Min	10.1	0.069	10.2	0.68%
28.5	600	Min	25.4	0.074	25.5	0.29%
57	250	Max	0.96	0.14	1.10	13%
57	300	Max	1.20	0.14	1.35	11%
57	400	Max	2.62	0.15	2.77	5.5%
57	500	Max	6.04	0.16	6.20	2.6%
57	600	Max	12.5	0.17	12.7	1.3%
57	250	Min	0.62	0.26	0.88	30%
57	300	Min	1.08	0.27	1.35	20%
57	400	Min	3.41	0.29	3.70	8%
57	500	Min	8.50	0.30	8.80	3.4%
57	600	Min	17.5	0.32	17.9	1.8%

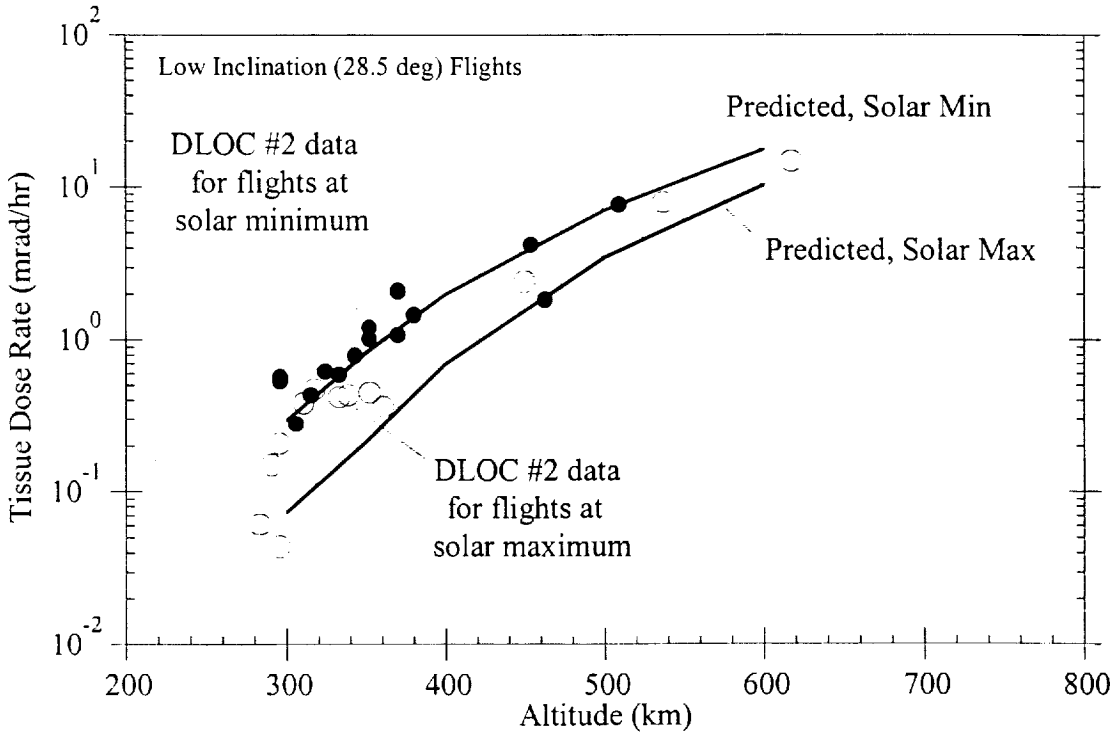

Fig. 3-6. Comparison of predicted and measured dose rates for low-inclination Shuttle flights.

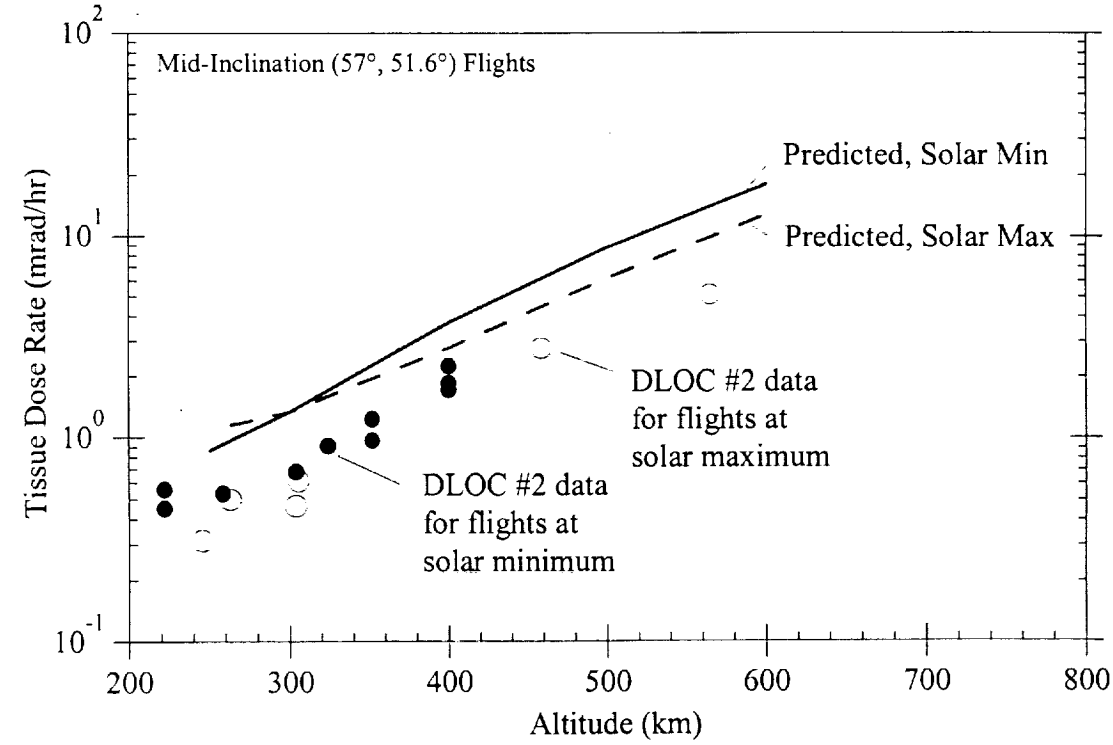

Fig. 3-7. Comparison of predicted and measured dose rates for mid-inclination Shuttle flights.

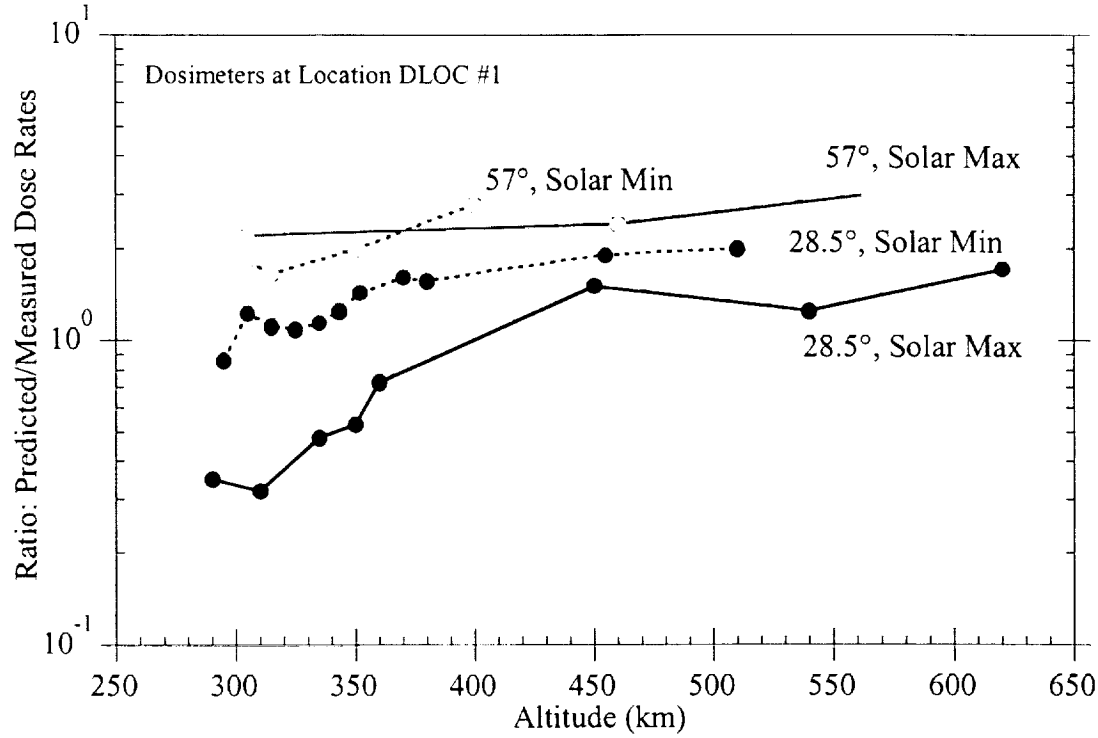

Fig. 3-8. Predicted-to-measured dose rates for dosimeters at location DLOC #1.

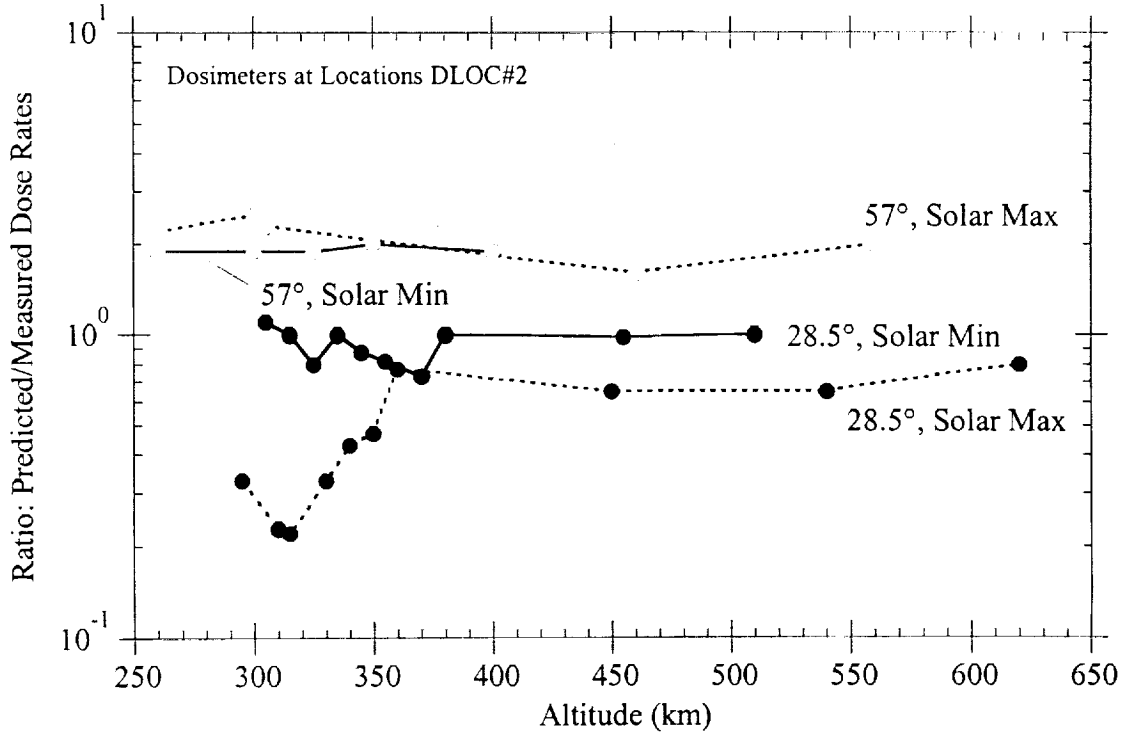

Fig. 3-9. Predicted-to-measured dose rates for dosimeters at location DLOC #2.

Table. 3-5. Tabulation of predicted-to-measured dose rates for dosimeters at DLOC #1.

	Ratio of Predicted-to-Measured Dose Rate (DLOC #1)			
	Low Inclination (28.5°)		Mid Inclination (57°)	
Altitude (km)	Solar Min	Solar Max	Solar Min	Solar Max
300	1.0	NA	1.6	2.1
350	1.4	0.6	2.0	2.2
400	1.6	1.0	2.6	2.3
450	1.9	1.3		2.4
500	2.0	1.5		2.6
550		1.6		2.8
600		1.8		3.0

NA = Not Applicable (GCR dose dominates over trapped proton dose)

Table. 3-6. Tabulation of predicted-to-measured dose rates for dosimeters at DLOC #2.

	Ratio of Predicted-to-Measured Dose Rate (DLOC #2)			
	Low Inclination (28.5°)		Mid Inclination (57°)	
Altitude (km)	Solar Min	Solar Max	Solar Min	Solar Max
300	1.1	NA	1.9	2.3
350	0.85	0.55	2.0	2.0
400	1.0	0.70	1.9	1.9
450	1.0	0.65		1.7
500	1.0	0.65		1.8
550		0.68		2.0
600		0.75		

NA = Not Applicable (GCR dose dominates over trapped proton dose)

3-5. Conclusions

The dominant feature of the comparisons made here of predicted trapped proton dose rates based on the AP8 model and dose rates measured on Shuttle flights is the variablility obtained – i.e., the predicted-to-measured ratios vary from about 0.5 to 2. While this result is consistent with the often quoted ± 2 accuracy factor for the AP8 model, the results here are not consistent AP8 comparisons with other flight data shown in [3-2]. Figures 3-10 and 3-11 compare the Shuttle results with other model comparisons with flight data discussed in [3-2]. This shows that AP8 consistently underpredicts the non-Shuttle flight data by about a factor of about 2, but that AP8 may either underpredict or overpredict the Shuttle measurement by a factor of 2.

The large variablility found for the Shuttle model-data comparisons may be due to several factors. First, the AP8 model is really not applicable for Shuttle predictions in that the AP8 model describes long-term average fluxes (for periods of 6 months or so), whereas Shuttle flights are typically of about one-week duration. There are short-term temporal flux variations which AP8 is incapable of taking into account. Secondly, some of the model-data variation may be due to the lack of detail included in the simulations, such as the neglect of altitude variation during the Shuttle flights. Also, according to LDEF satellite measurements (28.5° inclination, ≈ 450 km, three-axis stablized) the trapped proton anisotropy can cause a factor of 2 or more variation in observed dose on the West vs. East side of the spacecraft. This anisotropy effect is difficult to estimate for the Shuttle because typically the spacecraft orientation varies throughout the mission.

Therefore, we conclude that the difference between AP8 model predictions and Shuttle measurements has very limited applicability for other missions – i.e., the model uncertainty derived from short duration Shuttle measurements does not apply to AP8 model dose predictions for long-term missions.

We also note that the model-data comparisons and conclusions here differ from the results of previous AP8 model comparisons with Shuttle dose data that have been reported (e.g., [3-1], [3-13], [3-14]) in which AP8 is said to overpredict by a factor of 2, whereas we find that the model can either overpredict or underpredict Shuttle data by a factor of 2 or more.

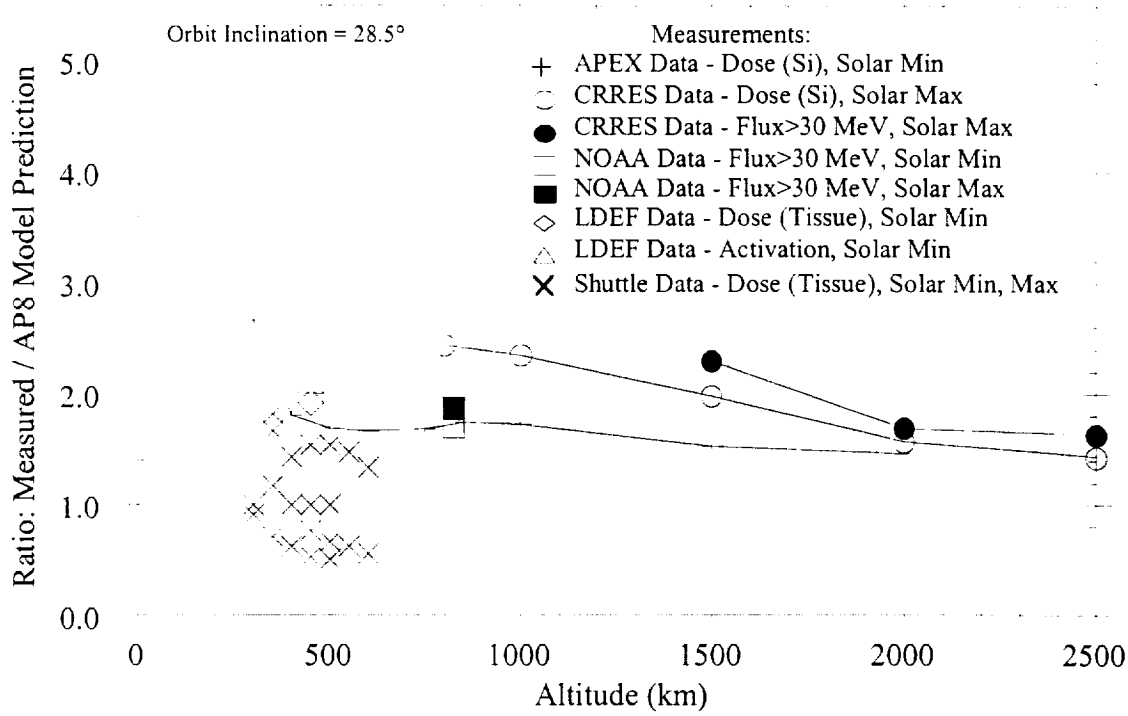

Fig. 3-10 Measured-to-predicted dose ratio calculated here based on Shuttle data compared with data-model ratios from ref. [3-2] using other flight data (all for circular, 28.5 deg. inclination orbits).

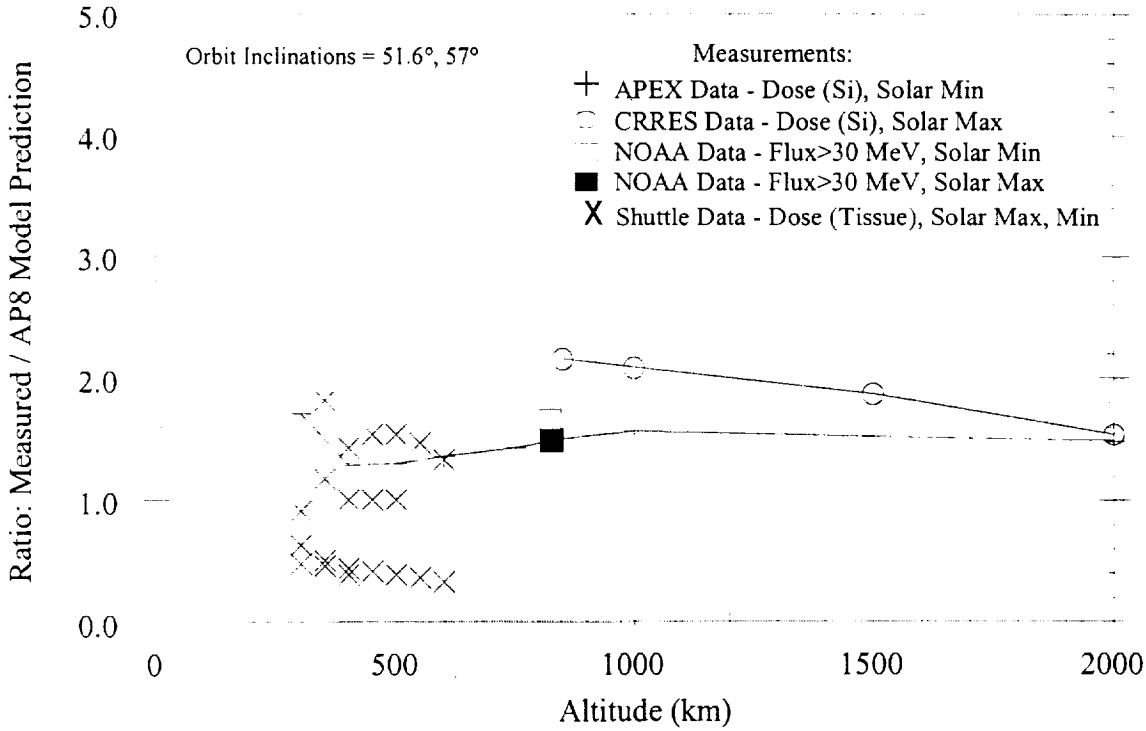

Fig. 3-11 Like Fig. 3-10 but for mid-inclination (51.6 or 57 deg.) orbits.

3-6. References

[3-1] William Atwell, "The Space Radiation Environment: An Overview for Mir and ISS Missions", Proc. 34th Aerospace Sciences Meeting, American Inst. Aeronautics and Astronautics, 15-18 Jan. 1996, Reno, NV, AIAA 96-0928 (1996).

[3-2] T. W. Armstrong and B. L. Colborn, "Evaluation of Trapped Radiation Model Uncertainties for Spacecraft Design", Science Applications International Corporation, Contractor Report for NASA/MSFC, SAIC-TN-99020, September 1999.

[3-3] William Atwell, NASA/JSC, pri. comm., 1996.

[3-4] M. O. Burrell and J. J. Wright, "Orbital Calculations and Trapped Radiation Mapping", NASA Marshall Space Flight Center, NASA TM X-53406, March 1966.

[3-5] Donald W. Sawyer and James I. Vette, "AP-8 Trapped Proton Environment for Solar Maximum and Solar Minimum", National Space Science Data Center, NASA Goddard Space Flight Center, NSSDC/WDC-A-R&S 76-06, 1976.

[3-6] E. G. Stassinopoulos and G. D. Mead, "ALLMAG, GDALMG, LINTRA: Computer Programs for Geomagnetic Field and Field-line Calculations", National Space Science Data Center, NASA Goddard Space Flight Center, NSSDC 72-12, 1972.

[3-7] IAGA Commission 2 Working Group 4, "Analysis of the Geomagnetic Field, International Geomagnetic Reference Field 1965.0", J. Geophys. Res. 74, 4407 (1969).

[3-8] Louis Hurwitz, "Mathematical Model of the 1970 Geomagnetic Field", ESSA Coast and Geodetic Survey, preprint, 4 May 1970.

[3-9] Stephen M. Seltzer, "Updated Calculations for Routine Space Shielding Radiation Dose Estimates: SHIELDOSE-2", National Institute of Standards and Technology, NISTIR-5477, Dec. 1994.

[3-10] A. J. Tylka, et al., "CREME96: A Revision of the Cosmic Ray Effects on Micro-Electronics Code", IEEE Trans. Nucl. Sci. 44(6), 2150 (1997).

[3-11] T. W. Armstrong and K. C. Chandler, "Stopping Powers and Ranges for Muons, Charged Pions, Protons, and Heavy Ions", Nucl. Instr. Meth. 113, 313 (1973).

[3-12] T. W. Armstrong, B. L. Colborn, and E. V. Benton, "Model Calculations of the Radiation Dose and LET Spectra on LDEF and Comparisons with Flight Date", Radiat. Meas. 26 (6), 751 (1996).

[3-13] G. D. Badhwar, et al., "Intercomparison of Measurements on STS-63", Radiat. Meas. 26(6), 901 (1997).

[3-14] G. D. Badhwar, et al., "In-flight Radiation Measurements on STS-60", Radiat. Meas. 26(1), 17 (1996).

4. Model Comparisons with APEX Satellite Data

4-1. Introduction

Radiation dose measurements were made on the Advanced Photovoltaic and Electronics Experiment (APEX) satellite from August 1994 to June 1996 [4-1]. In [4-2] we give a summary of dose predictions based on the AE8 trapped electron model and the AP8 trapped proton model compared with APEX dose measurements. The purpose here is to document some of the detailed results generated in preparing the summary comparisons.

4-2. Flight Data

The APEX satellite flew in a 362 km x 2544 km orbit at 70° inclination for 21 months near solar minimum. Four radiation dosimeters consisting of planar silicon semiconductor detectors under different thicknesses of aluminum shielding were on board; features of these dosimeters (from [4-1]) are summarized in Table 4-1. Data were binned for low LET and high LET dose contributions covering the electron and proton energy ranges indicated in Table 4-1.

As described in [4-3], the APEX data were organized into L shell and B/B_o bins, where L is the McIwain L parameter and B/B_o is the ratio of the magnetic field magnitude divided by the minimum value on the same field line. The APEX dose data bases in L and B/B_o coordinates, together with orbit and magnetic field model routines, have been incorporated by Hanscom AFB Phillips Laboratory into a software package called APEXRAD [4-3], which has the capability of generating orbit-average doses for specified orbit parameters. APEXRAD is considered to be most accurate for orbits between 300 and 2500 km, inclinations below 60°, and for times corresponding to solar minimum [4-3], but has been applied (and seems to give reasonable results) for inclinations up to 90° [4-1].

At high latitudes electrons in the "horns" of the outer belt electrons reach low altitudes. Thus, for high-inclination (above about 40°), low-altitude (below roughly 750 km) orbits and thin (< 1 g/cm^2) shielding, the dose is dominated by these horn electrons. Since the outer belt electron population can have high variability depending on geomagnetic activity, the APEX dose has been binned according to the magnetic activity index Ap_{15}, a 15-day running average (offset by one day) of the Ap magnetic activity index. (Ap is a 3-hour average index of magnetic

Table 4-1. Features of APEX radiation dose detectors.

	Detector Shielding		Shielding	Dose Contributions		
				Low LET		High LET
Detector	mils Al	g/cm^2 Al	Geometry	electrons	protons	protons
D1	4.29	0.029	slab	> 0.15 MeV	> 80 MeV	5-80 MeV
D2	82.5	0.57	hemisphere	> 1.0 MeV	> 115 MeV	20-115 MeV
D3	232.5	1.59	hemisphere	> 2.5 MeV	> 120 MeV	32-120 MeV
D4	457.5	3.14	hemisphere	> 5 MeV	> 125 MeV	52-125 MeV

Table 4-2. Frequency distribution of magnetic activity during APEX mission.

Ap_{15} Range	APEX Mission
5 - 7.5	14%
7.5 - 10	27%
10 - 15	35%
15 - 20	12%
20 - 25	7%

activity based on measurements at ground magnetometer stations worldwide.) The frequency distribution of magnetic activity during the APEX mission [4-1] is shown in Table 4-2.

For the model-data comparisons here, we have used the APEXRAD software to generate orbit-average doses based on APEX data for circular orbits in the 300 to 2000 km altitude range for various inclinations from 0° to 90°. Two day orbit averages were used with the following initial orbit parameters: argument of perigee = 180°, right ascension of ascending node = 280°, and mean anomaly = 180°.

APEXRAD dose results for the thinnest shielding (4.29 mils of aluminum) are plotted as a function of inclination and altitude in Figs. 4-1 and 4-2, respectively. For this shielding the dose is essentially all due to electrons (i.e., the high LET dose component is negligible). These results are for the APEX mission-average magnetic activity – i.e., for the Ap_{15} frequency distribution of Table 4-2. As an indication of the sensitivity of these dose results to magnetic activity, we have compared this mission average dose to the highest activity level dose (i.e., assuming the whole mission took place for Ap_{15} in the 20-25 range). This comparison (Table 4-3) shows that the major magnetic activity influence is for inclinations above about 40° and altitudes below about 750 km.

APEXRAD results for the thickest shielding (457 mils of aluminum) vs. inclination are shown in Fig. 4-3 and vs. altitude in Fig. 4-4. The dose for this shield thickness is dominated by protons. The very low doses for the lowest inclinations and lowest altitudes where the orbits are underneath the proton belt and do not intersect the South Atlantic Anomaly are probably not very accurate. In the APEX data analysis, the GCR dose contribution, determined as the dose measured in the lowest dose regions, has been subtracted [4-1], so the resulting doses calculated from APEXRAD are for trapped particles only. Table 4-4 gives a tabulated summary of the results plotted in Figs. 4-1 through 4-4.

4-3. Model Predictions

Model predictions to compare with the APEX dose measurements have been made using the AP8MIN trapped proton model at solar minimum and the AE8MIN trapped electron model at solar minimum to predict orbit-average trapped spectra. These spectra were then used as input to

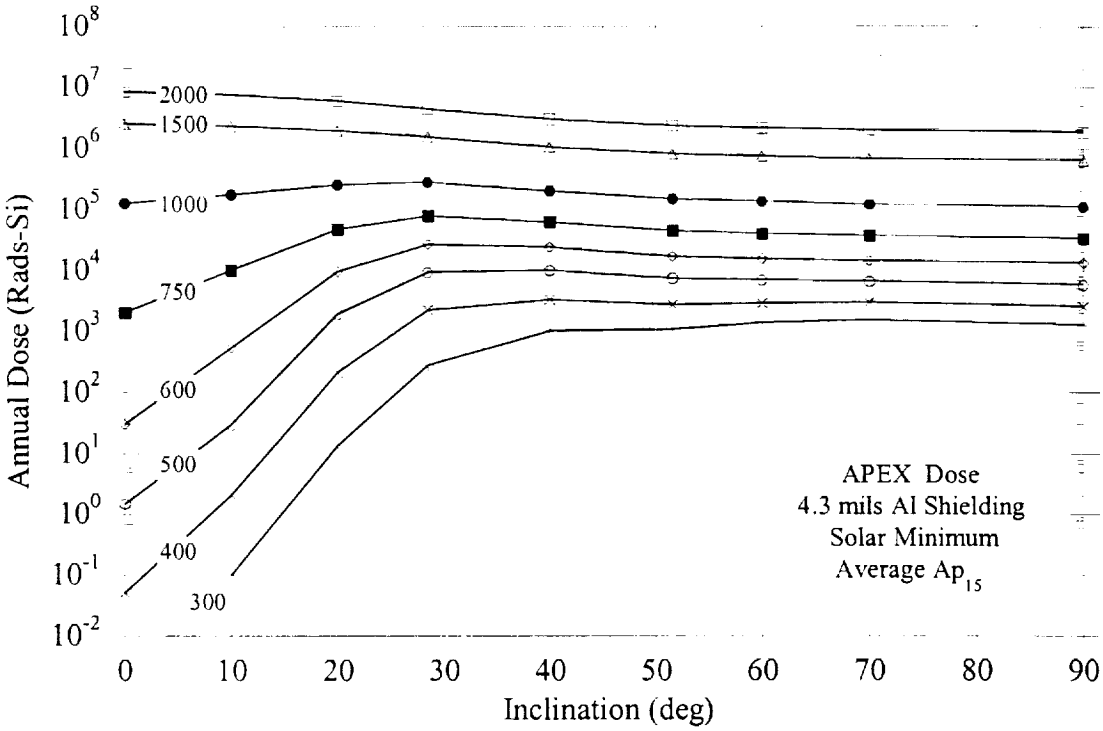

Fig. 4-1. Orbit-average dose behind 4.29 mils of aluminum shielding vs. orbit inclination – based on APEX satellite measurements.

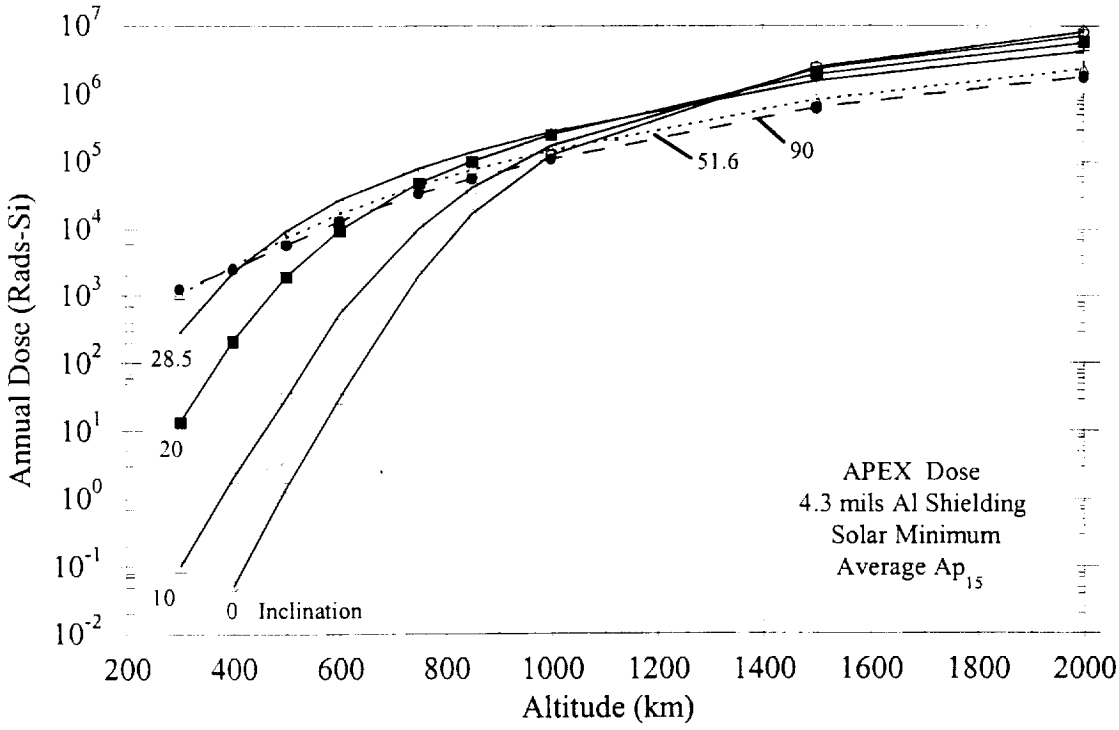

Fig. 4-2. Orbit-average dose behind 4.29 mils of aluminum shielding vs. orbit altitude – based on APEX satellite measurements.

Table 4-3. Influence of magnetic activity on electron dose.

(a) APEX dose (rads-Si/yr) for high activity (Ap_{15} = 20-25), 4.29 mils shielding

	Altitude (km)						
Inclination (deg)	300	400	500	750	1000	1500	2000
0			2.65E+00	4.10E+03	2.04E+05	3.48E+06	1.13E+07
10			6.94E+01	1.01E+04	2.71E+05	3.14E+06	9.80E+06
20	2.62E+01	3.85E+02	3.25E+03	7.32E+04	3.60E+05	2.62E+06	7.78E+06
28.5	4.61E+02	3.20E+03	1.30E+04	1.08E+05	3.82E+05	2.08E+06	5.70E+06
40	2.10E+03	5.06E+03	1.32E+04	8.18E+04	2.75E+05	1.45E+06	3.94E+06
51.6	4.55E+03	7.28E+03	1.41E+04	6.77E+04	2.20E+05	1.16E+06	3.17E+06
60	6.57E+03	9.55E+03	1.56E+04	6.46E+04	2.01E+05	1.06E+06	2.88E+06
70	6.36E+03	9.17E+03	1.48E+04	6.05E+04	1.83E+05	9.68E+05	2.63E+06
90	4.93E+03	7.25E+03	1.23E+04	5.26E+04	1.67E+05	8.97E+05	2.45E+06

(b) APEX dose (rads-Si/yr) for mission average activity, 4.29 mils shielding

	Altitude (km)						
Inclination (deg)	300	400	500	750	1000	1500	2000
0			1.46E+00	2.03E+03	1.27E+05	2.49E+06	8.29E+06
10			3.02E+01	1.02E+04	1.74E+05	2.31E+06	7.38E+06
20	1.35E+01	2.13E+02	1.91E+03	4.77E+04	2.56E+05	1.92E+06	5.86E+06
28.5	2.79E+02	2.22E+03	9.34E+03	7.89E+04	2.81E+05	1.54E+06	4.33E+06
40	1.04E+03	3.31E+03	1.00E+04	6.30E+04	2.01E+05	1.06E+06	2.99E+06
51.6	1.07E+03	2.73E+03	7.36E+03	4.49E+04	1.50E+05	8.33E+05	2.37E+06
60	1.39E+03	2.90E+03	6.96E+03	4.01E+04	1.35E+05	7.44E+05	2.12E+06
70	1.52E+03	2.94E+03	6.47E+03	3.69E+04	1.21E+05	6.81E+05	1.95E+06
90	1.26E+03	2.52E+03	5.85E+03	3.36E+04	1.12E+05	6.36E+05	1.82E+06

(c) Ratio: (high magnetic activity) / (mission average magnetic activity)

	Altitude (km)						
Inclination (deg)	300	400	500	750	1000	1500	2000
0			1.82	2.02	1.61	1.40	1.36
10			2.30	0.99	1.56	1.36	1.33
20	1.94	1.81	1.70	1.53	1.41	1.36	1.33
28.5	1.65	1.44	1.39	1.37	1.36	1.35	1.32
40	2.02	1.53	1.31	1.30	1.37	1.37	1.32
51.6	4.27	2.66	1.92	1.51	1.47	1.39	1.34
60	4.74	3.29	2.24	1.61	1.49	1.42	1.36
70	4.19	3.12	2.29	1.64	1.51	1.42	1.35
90	3.92	2.88	2.10	1.57	1.49	1.41	1.35

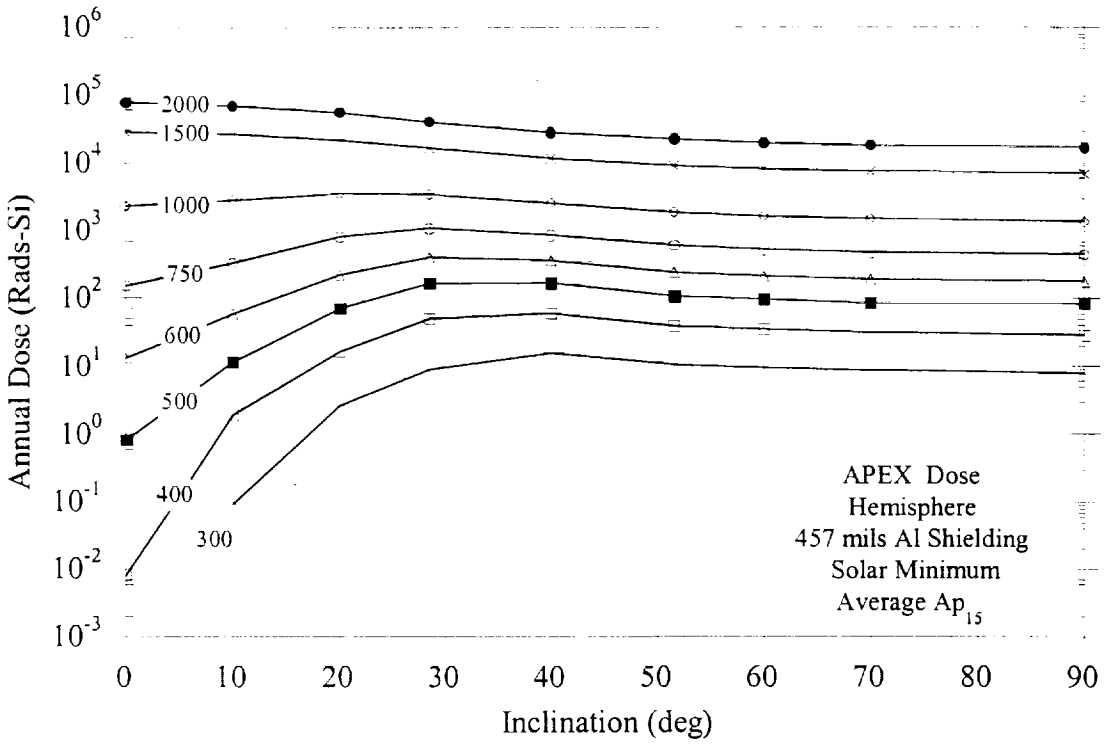

Fig. 4-3. Orbit-average dose behind 457 mils of aluminum shielding vs. orbit inclination – based on APEX satellite measurements.

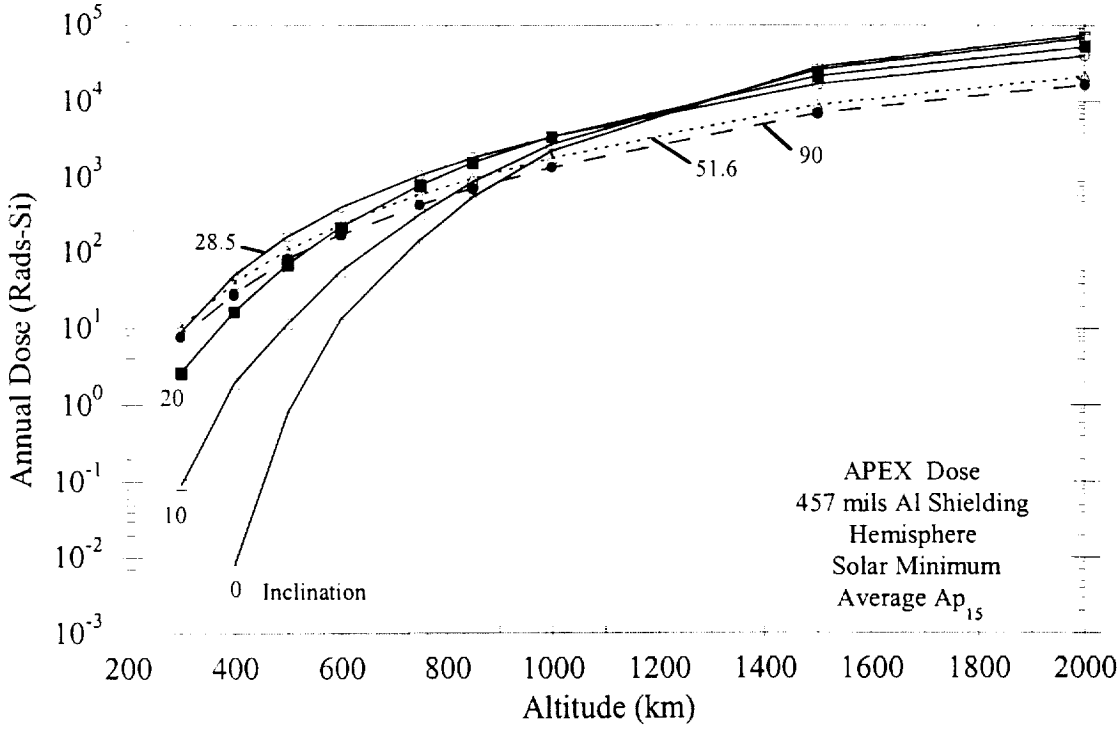

Fig. 4-4. Orbit-average dose behind 457 mils of aluminum shielding vs. orbit altitude – based on APEX satellite measurements.

Table 4-4. Orbit-average dose for circular orbits at various inclinations and altitudes based on APEX satellite measurements.

(a) Annual dose (rads-Si), 4.29 mils aluminum shielding, slab shielding.

Inclination	Altitude (km)								
(deg)	300	400	500	600	750	850	1000	1500	2000
0		0.051	1.46	30.4	2.03E+03	1.67E+04	1.27E+05	2.49E+06	8.29E+06
10	0.1	2.06	30.2	538	1.02E+04	4.08E+04	1.74E+05	2.31E+06	7.38E+06
20	13.6	213	1.91E+03	9.59E+03	4.77E+04	1.02E+05	2.56E+05	1.92E+06	5.86E+06
28.5	279	2.22E+03	9.34E+03	2.66E+04	7.89E+04	1.39E+05	2.81E+05	1.54E+06	4.33E+06
40	1.04E+03	3.31E+03	1.00E+04	2.40E+04	6.30E+04	1.05E+05	2.01E+05	1.06E+06	2.99E+06
51.6	1.07E+03	2.73E+03	7.36E+03	1.69E+04	4.49E+04	7.60E+04	1.50E+05	8.33E+05	2.37E+06
60	1.39E+03	2.90E+03	6.96E+03	1.55E+04	4.01E+04	6.68E+04	1.35E+05	7.44E+05	2.12E+06
70	1.52E+03	2.94E+03	6.47E+03	1.43E+04	3.69E+04	6.12E+04	1.21E+05	6.81E+05	1.95E+06
90	1.26E+03	2.52E+03	5.85E+03	1.31E+04	3.36E+04	5.61E+04	1.12E+05	6.36E+05	1.82E+06

(b) Annual dose (rads-Si), 457 mils aluminum shielding, 2π (hemisphere) shielding.

Inclination	Altitude (km)								
(deg)	300	400	500	600	750	850	1000	1500	2000
0			0.4	6.6	74.5	279	1148	1.41E+04	3.84E+04
10	0.046	0.96	5.79	28.9	167	442	1385	1.31E+04	3.49E+04
20	1.32	8.26	35	111	402	793	1744	1.07E+04	2.73E+04
28.5	4.45	24.8	83.2	205	545	917	1740	8350	2.03E+04
40	7.92	30.1	84.3	180	434	695	1270	5820	1.39E+04
51.6	5.31	19.6	53.8	121	302	495	927	4530	1.10E+04
60	4.73	17.2	47.4	105	263	430	815	4040	9800
70	4.29	15.5	41.9	93.9	239	389	737	3700	9000
90	3.88	14.2	42	88.1	221	362	689	3460	8400

the SHIELDOSE-2 code to calculate dose vs. shielding. The assumptions associated with the trapped model calculations are the same as described in [4-2].

4-4. Model-Data Comparisons

Model comparisons have been made with APEX data for the thinnest (4.29 mil) shielding and thickest (457 mil) shielding. Model dose calculations show that > 99% of the 4.29 mil detector dose is from trapped electrons, and > 99% of the 457 mil detector is from trapped protons, so these two detectors allow unambiguous checks on the accuracies of the AE8MIN and AP8MIN models, respectively, in predicting low-altitude doses.

Table 4-5 shows the APEX dose for 4.29 mils of aluminum (for APEX mission average Ap_{15}, same as shown earlier in Table 4-3(b)), dose predictions using the AE8MIN trapped electron model for solar minimum conditions, and the ratio of measured-to-AE8MIN doses. Considering the dose ratio table, the ratios obtained are large at the lowest inclinations and altitudes where the orbits do not pass through the high latitude electron horns or the inner belt; there are probably major uncertainties in both the data and model predictions in this low-flux region. These ratios are not considered meaningful and are not shown in the ratio table for some orbits. For orbits with inclinations above 40° and altitudes below 750 km, where the dose is dominated by exposure to outer zone electrons via the electron horns, the measured-to-modeled ratio is within a factor of ± 2. As pointed out earlier, the electron flux in this region is sensitive to magnetic activity, which is not accounted for by the AE8MIN model. Thus, the ratios in this region will vary from those shown depending on how different the activity level for a given mission is from the activity during the APEX mission (Table 4-2). For orbits passing through the inner belt, Table 4-5 shows that AE8MIN underpredicts the dose by factors in the range from about 1.3 – 2.

Table 4-6 gives the ratio of measured-to-predicted doses for the APEX heavily shielded (457 mil) detector for which the dose is essentially all from trapped protons. The calculated dose is for trapped protons incident over the surface of a sphere, designated as "4π sphere" in Table 4-6, so the APEX dose with hemispherical shielding has been multiplied by two for this comparison. We do not show ratios in Table 4-6 for the lowest inclinations and altitudes where the flux levels are very low and the accuracy of both the data and models are questionable.

Table 4-5. Comparison of AE8MIN electron model predictions with APEX measurements.

(a) Dose (rads-Si/yr) based on APEX satellite measurements for 4.29 mils shielding.

	Altitude (km)						
Inclination (deg)	300	400	500	750	1000	1500	2000
0				2.03E+03	1.27E+05	2.49E+06	8.29E+06
10			3.02E+01	1.02E+04	1.74E+05	2.31E+06	7.38E+06
20	1.36E+01	2.13E+02	1.91E+03	4.77E+04	2.56E+05	1.92E+06	5.86E+06
28.5	2.79E+02	2.22E+03	9.34E+03	7.89E+04	2.81E+05	1.54E+06	4.33E+06
40	1.04E+03	3.31E+03	1.00E+04	6.30E+04	2.01E+05	1.06E+06	2.99E+06
51.6	1.07E+03	2.73E+03	7.36E+03	4.49E+04	1.50E+05	8.33E+05	2.37E+06
60	1.39E+03	2.90E+03	6.96E+03	4.01E+04	1.35E+05	7.44E+05	2.12E+06
70	1.52E+03	2.94E+03	6.47E+03	3.69E+04	1.21E+05	6.81E+05	1.95E+06
90	1.26E+03	2.52E+03	5.85E+03	3.36E+04	1.12E+05	6.36E+05	1.82E+06

(b) Dose (rads-Si/yr) based on AE8MIN trapped proton model for 4.29 mils shielding.

	Altitude (km)						
Inclination (deg)	300	400	500	750	1000	1500	2000
0				2.59E+02	1.32E+04	1.03E+06	4.92E+06
10			8.02E+00	7.18E+02	2.35E+04	1.08E+06	4.80E+06
20	6.90E-01	1.37E+01	5.50E+01	7.35E+03	8.12E+04	1.06E+06	4.17E+06
28.5	7.94E+00	2.78E+02	1.88E+03	2.43E+04	1.24E+05	9.96E+05	3.39E+06
40	5.24E+02	2.33E+03	6.00E+03	3.27E+04	1.15E+05	7.41E+05	2.40E+06
51.6	9.39E+02	2.58E+03	5.93E+03	2.79E+04	9.01E+04	5.80E+05	1.88E+06
60	2.46E+03	4.34E+03	7.71E+03	2.77E+04	8.26E+04	5.17E+05	1.67E+06
70	3.38E+03	5.58E+03	9.36E+03	2.95E+04	8.05E+04	4.78E+05	1.53E+06
90	2.64E+03	4.53E+03	7.65E+03	2.44E+04	7.02E+04	4.37E+05	1.42E+06

(c) Dose ratio: measured / AE8MIN model

	Altitude (km)						
Inclination (deg)	300	400	500	750	1000	1500	2000
0				7.9	9.6	2.4	1.7
10			3.8	14	7.4	2.1	1.5
20	20	16	35	6.5	3.2	1.8	1.4
28.5	35	8.0	5.0	3.2	2.3	1.5	1.3
40	2.0	1.4	1.7	1.9	1.7	1.4	1.2
51.6	1.1	1.1	1.2	1.6	1.7	1.4	1.3
60	0.6	0.7	0.9	1.4	1.6	1.4	1.3
70	0.4	0.5	0.7	1.3	1.5	1.4	1.3
90	0.5	0.6	0.8	1.4	1.6	1.5	1.3

Fig. 4-6. Comparison of AP8MIN proton model dose predictions with APEX measurements.

(a) Dose (rads-Si/yr) based on APEX satellite measurements for 457 mils shielding (4π sphere).

	Altitude (km)						
Inclination (deg)	300	400	500	750	1000	1500	2000
0		8.00E-03	8.00E-01	1.49E+02	2.30E+03	2.82E+04	7.68E+04
10	9.20E-02	1.92E+00	1.16E+01	3.34E+02	2.77E+03	2.62E+04	6.98E+04
20	2.64E+00	1.65E+01	7.00E+01	8.04E+02	3.49E+03	2.14E+04	5.46E+04
28.5	8.90E+00	4.95E+01	1.66E+02	1.09E+03	3.48E+03	1.67E+04	4.06E+04
40	1.58E+01	6.01E+01	1.69E+02	8.68E+02	2.54E+03	1.16E+04	2.78E+04
51.6	1.06E+01	3.92E+01	1.08E+02	6.04E+02	1.85E+03	9.06E+03	2.20E+04
60	9.46E+00	3.44E+01	9.48E+01	5.26E+02	1.63E+03	8.08E+03	1.96E+04
70	8.58E+00	3.10E+01	8.38E+01	4.78E+02	1.47E+03	7.40E+03	1.80E+04
90	7.76E+00	2.84E+01	8.40E+01	4.42E+02	1.38E+03	6.92E+03	1.68E+04

(b) Dose (rads-Si/yr) based on AP8MIN trapped proton model for 457 mils shielding (4π sphere).

	Altitude (km)						
Inclination (deg)	300	400	500	750	1000	1500	2000
0				9.86E+01	1.34E+03	1.44E+04	4.44E+04
10			1.64E+00	2.21E+02	1.50E+03	1.44E+04	4.27E+04
20		4.68E+00	3.70E+01	4.76E+02	1.96E+03	1.30E+04	3.52E+04
28.5	3.34E+00	2.74E+01	9.88E+01	6.48E+02	2.02E+03	1.09E+04	2.78E+04
40	1.09E+01	4.94E+01	1.30E+02	6.17E+02	1.67E+03	7.88E+03	1.92E+04
51.6	6.22E+00	3.04E+01	8.28E+01	4.23E+02	1.19E+03	5.96E+03	1.48E+04
60	5.18E+00	2.50E+01	6.84E+01	3.57E+02	1.02E+03	5.26E+03	1.32E+04
70	4.60E+00	2.22E+01	6.04E+01	3.18E+02	9.18E+02	4.78E+03	1.20E+04
90	4.16E+00	1.95E+01	5.54E+01	2.86E+02	8.54E+02	4.46E+03	1.12E+04

(c) Dose ratio: measured / AP8MIN model

	Altitude (km)						
Inclination (deg)	300	400	500	750	1000	1500	2000
0				1.5	1.7	2.0	1.7
10			7	1.5	1.9	1.8	1.6
20		3.5	1.9	1.7	1.8	1.6	1.5
28.5	2.7	1.8	1.7	1.7	1.7	1.5	1.5
40	1.5	1.2	1.3	1.4	1.5	1.5	1.4
51.6	1.7	1.3	1.3	1.4	1.6	1.5	1.5
60	1.8	1.4	1.4	1.5	1.6	1.5	1.5
70	1.9	1.4	1.4	1.5	1.6	1.5	1.5
90	1.9	1.5	1.5	1.5	1.6	1.6	1.5

These results show that the AP8MIN model underpredicts the dose at all of the altitudes and inclinations covered, with the underprediction being about a factor of 1.5 – 2 outside of the low-flux region.

4-5. Conclusions

Dose data from APEX satellite measurements provide a definitive data set for evaluating uncertainties in the AE8 trapped electron model and the AP8 trapped proton model for predicting low-altitude doses at solar minimum. While the data do not appear to be reliable at the lowest altitudes and lowest inclinations where the trapped flux levels are very low, this is not generally of practical consequence because the dose in this region is dominated by galactic cosmic-rays (with perhaps some contribution from albedo protons and electrons), so trapped radiation model accuracy in this region is generally not an issue.

For the dose due to trapped electrons, the model-data comparisons here indicate that for orbits where the main exposure is to outer belt electrons via the belt "horns" that reach low altitudes at high latitudes (i.e., for orbits having inclinations above about 40° and altitudes below about 750 km), the predicted dose based on AE8MIN model fluxes is within a factor of ± 2 of the measurements. Since the actual fluxes in this region are sensitive to fluctuations due to magnetic activity, and since AE8MIN does not account for such fluctuations, this finding of ± 2 uncertainty applies for the average activity during the APEX mission.

For orbits where the electron dose is due to inner belt electrons, the predicted AE8MIN doses are less than measured by factors ranging from about 1.3 to 2 (Table 4-5(c)).

Doses predicted using the AP8MIN model are lower than measured for all of the altitude (300 – 2000 km) and inclination (0° - 90°) ranges considered. Except for the low-flux region (i.e., for orbits that are underneath the inner belt and do not pass through the South Atlantic Anomaly) where both the model and data accuracy is questionable, the AP8MIN model underpredicts the measured doses by factors ranging from about 1.3 to 2 (Table 4-6 (c)).

These model uncertainties based on APEX dose data are compared with uncertainties based on other flight data in [4-2].

4-6. References

[4-1] M. S. Gussenhoven, E. G. Mullen, J. T. Bell, D. Madden, and E. Holman, "APEXRAD: Low Altitude Orbit Dose as a Function of Inclination, Magnetic Activity, and Solar Cycle", IEEE Trans. Nucl. Sci. 44 (6), 2161 (1997).

[4-2] T. W. Armstrong and B. L. Colborn, "Evaluation of Trapped Radiation Model Uncertainties for Spacecraft Design", Science Applications International Corporation, Contractor Report for NASA/MSFC, SAIC-TN-99020, September 1999.

[4-3] J. T. Bell and M. S. Gussenhoven, "APEXRAD Documentation", Phillips Laboratory, Geophysics Directorate, Hanscom AFB, PL-TR-97-2117, September 1997.

5. Model Comparisons with CRRES Satellite Data

5-1. Introduction

Trapped radiation measurements were made by the Combined Release and Radiation Effects Satellite (CRRES) from July 1990 to October 1991 in a 327 km x 33,575 km orbit at 18.2° inclination during the maximum of solar Cycle 22 [5-1, 5-2]. In [5-3] we give a summary comparison of CRRES data with predictions based on the AP8MAX and AE8MAX trapped proton and electron models, respectively, for solar maximum conditions. The purpose here is to document some of the detailed results generated in preparing the summary comparisons reported in [5-3].

5-2. Flight Data

The CRRES satellite carried several radiation detectors which measured dose, electron flux, and proton flux, as summarized in Table 5-1. A unique feature of the CRRES data is that an extremely large geomagnetic storm and solar particle event occurred during the mission, greatly enhancing the radiation belt fluxes. Thus, CRRES dose and flux data are available as averages over the 8 month prior to the storm, denoted as "low activity" or "quiet" period, and as an average over a 6-month period of enhanced flux levels after the storm, denoted as "high activity" period.

As with the APEX data described in Sec. 4, the CRRES data have been binned in L and B/B_0 coordinates, and these data bases have been incorporated in software programs so that orbit-average estimates for specified orbits can be obtained. These utility codes, CRRESRAD [5-4], CRRESELE [5-5], and CRRESPRO [5-6], for dose, HEEF electron detector, and PROTEL proton detector measurements, respectively, have been used here to generate data for circular orbits at various altitudes. The energy range of the CRRES MEA detector electron measurements in the 90 keV-1.7 MeV energy range have been extended by Vampola to cover 40 keV-7 MeV using OVI-19 satellite data [5-7], and the data base has been incorporated into the RADMODLS code [5-8] so that orbit-average spectra can be generated for arbitrary orbit trajectories passing through the outer zone electrons.

Table 5-1. Radiation detectors on CRRES satellite.

Detector	Measured	Applicability	Comments
Space Radiation Dosimeters	Dose behind hemispherical shields of aluminum for four different thicknesses	> 800 km	Data for quiet and active magnetic activity levels, low and high LET
PROTEL	proton flux 1-100 MeV 24 energy intervals	> 2500 km	Data for quiet and active magnetic activity levels
HEEF	electron flux 0.5-6.6 MeV 10 energy intervals	outer zone electrons	Data binned in Ap_{15} magnetic activity levels
MEA	electron flux 90 keV-1.7 MeV 17 energy intervals	outer zone electrons	Mission average data available

Table 5-2. Features of dose detectors on CRRES satellite.

				Dose Contributions		
	Detector Shielding		Shielding	Low LET		High LET
Detector	mils Al	g/cm^2 Al	Geometry	electrons	protons	protons
D1	82.5	0.57	hemisphere	> 1.0 MeV	> 130MeV	20-30 MeV
D2	232.5	1.59	hemisphere	> 2.5 MeV	> 135 MeV	35-135 MeV
D3	457.5	3.14	hemisphere	> 5 MeV	> 140 MeV	51-140 MeV
D4	886.5	6.08	hemisphere	> 10 MeV	> 150 MeV	75-155 MeV

5-3. Model-Data Comparisons

As for all of the model predictions here, we have used the NASA/MSFC implementation [5-9] of the Vette, et al. AP8 and AE8 models [5-10, 5-11, 5-12] for predicting the trapped radiation environments and the SHIELDOSE-2 code [5-13] for dose calculations.

All of the model-data comparisons shown here are in terms of orbit-average dose or flux for circular orbits at various altitudes and 28.5° inclinations. Some comparisons for other inclinations are given in [5-3].

5-3.1. Electron Dose Comparisons

Features of the dose detectors on CRRES are summarized in Table 5-2. Figure 5-1 shows the orbit-average dose for the least shielded (0.57 g/cm^2) dosimeter on CRRES as a function of altitude for circular orbits at 28.5° inclination. These results demonstrate that the low-LET data for the least shielded detector represents the dose predominately from electrons. Therefore, we use the low LET data from this detector to compare with electron dose predicted using the AE8MAX model.

A tabulation of the low-LET dose from all of the CRRES dose detectors is given in Table 5-3. Table 5-4 compares the AE8MAX predicted dose with the low-LET CRRES dose for 0.57 g/cm^2 shielding for both low and high magnetic activity levels. A plot comparing the predicted and measured electron doses (values from Table 5-4) is shown as Fig. 5-2. (In comparing the CRRES data for hemispherical shielding with the model dose for omnidirectional fluxes over 4π steradians, the CRRES data have been multiplied by a factor of two; these results are labeled "4π" in the tables and figures.)

As indicated by Fig. 5-2 and the measured/predicted ratios tabulated in Table 5-4, the AE8MAX model substantially overpredicts the electron dose in both the inner and outer belts. During quiet magnetic activity periods, AE8MAX overpredicts the inner belt electron dose by about a factor of 3, overpredicts in the slot region between the two belts by about a factor of 3-50, overpredicts in the peak flux region of the outer belt by about a factor of 5-10, and overpredicts by a factor of 10-100 at the outer edge of the outer belt. For high-activity conditions, the AE8MAX still substantially overestimates the electron dose over most altitudes (Fig. 5-2, Table 5-4).

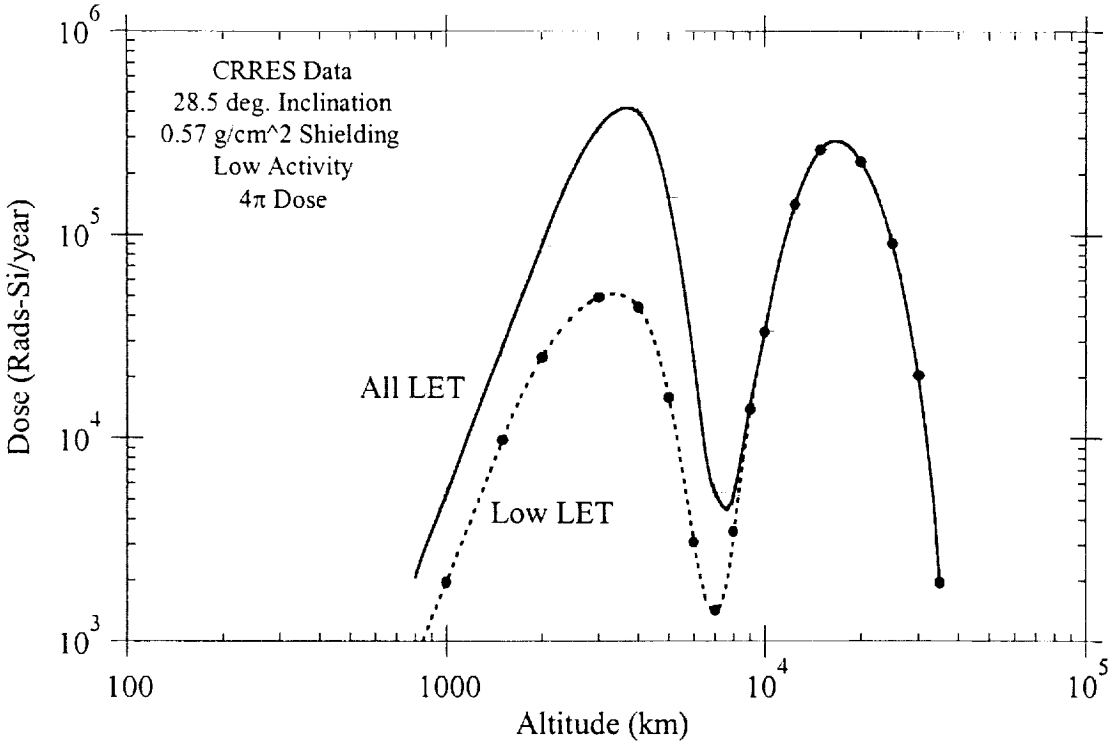

Fig. 5-1. Altitude dependence of low LET and total LET dose measured by thinnest shielded (0.57 g/cm^2) dosimeter on CRRES satellite.

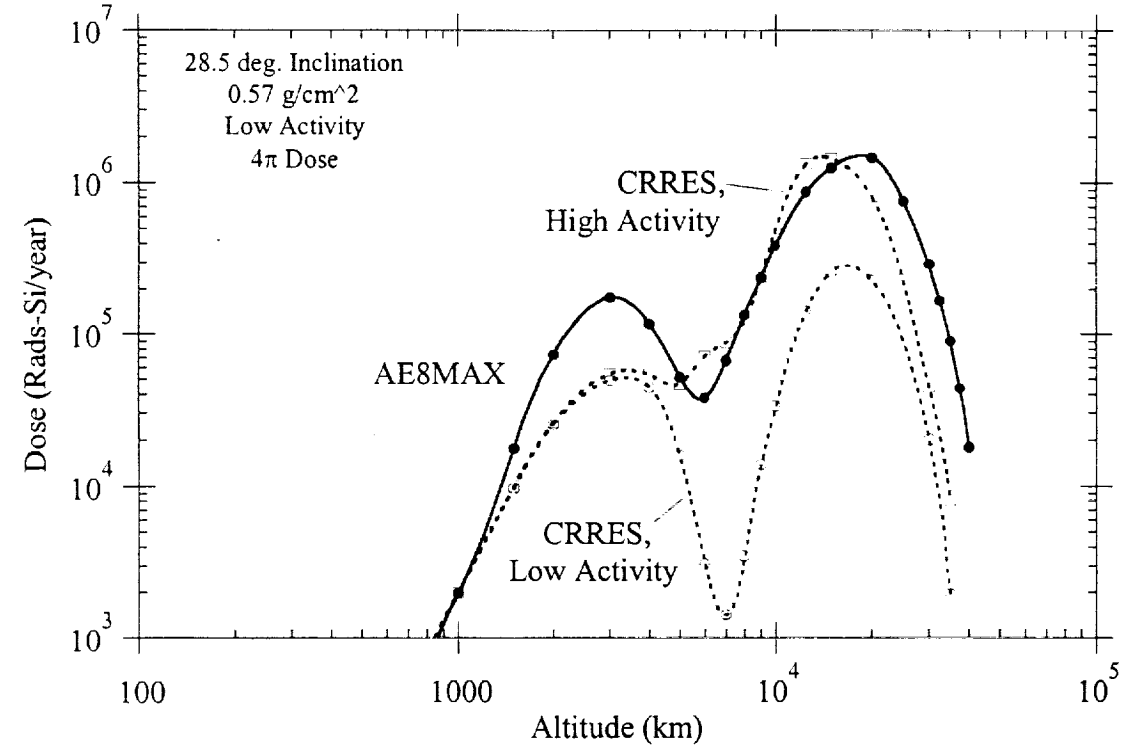

Fig. 5-2. Comparison of electron dose predicted using AE8MAX model with dose based on CRRES satellite measurements during periods of high and low geomagnetic activity.

Table 5-3. CRRES dose vs. altitude for 28.5 deg. orbits, low and high magnetic activity, low LET, and hemispherical shielding.

Detector:	1	2	3	4	1	2	3	4
Shielding, mils:	82.5	232.5	457.5	886.5	82.5	232.5	457.5	886.5
Shielding, g/cm^2:	0.57	1.59	3.14	6.08	0.57	1.59	3.14	6.08
Magnetic Activity:	**Low**	**Low**	**Low**	**Low**	**High**	**High**	**High**	**High**
LET Range:	Low	Low	Low	Low	Low	Low	Low	Low
Altitude (km)	Annual Dose (rads - Si)	Annual Dose (rads - Si)	Annual Dose (rads - Si)	Annual Dose (rads - Si)	Annual Dose (rads - Si)	Annual Dose (rads - Si)	Annual Dose (rads - Si)	Annual Dose (rads - Si)
800	3.95E+02	2.58E+02	2.48E+02	1.86E+02	3.96E+02	2.53E+02	2.48E+02	2.04E+02
1000	9.82E+02	6.29E+02	6.06E+02	4.44E+02	9.94E+02	6.14E+02	6.02E+02	4.86E+02
1500	4.89E+03	3.04E+03	2.94E+03	2.04E+03	5.02E+03	3.05E+03	3.01E+03	2.29E+03
2000	1.26E+04	7.22E+03	6.96E+03	4.61E+03	1.31E+04	7.32E+03	7.17E+03	5.20E+03
3000	2.47E+04	9.22E+03	8.55E+03	5.22E+03	2.72E+04	1.00E+04	9.49E+03	6.27E+03
4000	2.23E+04	5.22E+03	4.45E+03	2.48E+03	2.69E+04	8.71E+03	8.34E+03	5.29E+03
5000	8.01E+03	1.67E+03	1.39E+03	6.79E+02	2.33E+04	1.52E+04	1.64E+04	1.05E+04
6000	1.55E+03	4.39E+02	3.90E+02	1.34E+02	3.58E+04	3.08E+04	3.39E+04	1.86E+04
7000	7.11E+02	2.78E+02	2.36E+02	6.30E+01	4.38E+04	3.49E+04	3.67E+04	1.73E+04
8000	1.75E+03	3.08E+02	1.58E+02	3.60E+01	6.24E+04	2.90E+04	2.48E+04	1.00E+04
9000	6.99E+03	5.15E+02	1.15E+02	2.60E+01	1.21E+05	2.58E+04	1.20E+04	3.70E+03
10000	1.68E+04	9.26E+02	1.01E+02	2.80E+01	2.53E+05	3.11E+04	5.98E+03	1.19E+03
12500	7.11E+04	2.20E+03	1.38E+02	7.30E+01	6.71E+05	3.01E+04	2.12E+03	6.21E+02
15000	1.32E+05	2.13E+03	2.13E+02	1.31E+02	7.21E+05	1.70E+04	1.37E+03	5.94E+02
20000	1.15E+05	9.95E+02	2.39E+02	1.37E+02	4.10E+05	6.07E+03	8.21E+02	3.51E+02
25000	4.56E+04	2.95E+02	1.29E+02	6.80E+01	1.16E+05	1.24E+03	2.64E+02	1.04E+02
30000	1.02E+04	6.40E-01	4.10E+01	2.20E+01	2.25E+04	1.98E+02	6.70E+01	2.60E+01
35000	9.82E+02	7.00E+00	5.00E+00	4.00E+00	4.04E+03	3.50E+01	1.40E+01	7.00E+00

Table 5-4. CRRES/AE8MAX dose ratio for 0.57 g/cm^2 shielding, low and high magnetic activity levels, and circular, 28.5 deg. inclination orbits.

		Low Activity, Low LET		High Activity, Low LET	
Altitude (km)	AE8MAX (rads-Si/yr, 4π)	CRRES (rads-Si/yr, 4π)	Dose Ratio: CRRES/AE8MAX	CRRES (rads-Si/yr, 4π)	Dose Ratio: CRRES/AE8MAX
800	6.30E+02	7.90E+02	1.25	7.92E+02	1.26
1000	1.98E+03	1.96E+03	0.99	1.99E+03	1.00
1500	1.78E+04	9.78E+03	0.55	1.00E+04	0.57
2000	7.38E+04	2.53E+04	0.34	2.62E+04	0.35
3000	1.75E+05	4.94E+04	0.28	5.45E+04	0.31
4000	1.17E+05	4.46E+04	0.38	5.38E+04	0.46
5000	5.22E+04	1.60E+04	0.31	4.66E+04	0.89
6000	3.79E+04	3.09E+03	0.082	7.17E+04	1.89
7000	6.74E+04	1.42E+03	0.021	8.75E+04	1.30
8000	1.34E+05	3.50E+03	0.026	1.25E+05	0.93
9000	2.40E+05	1.40E+04	0.058	2.42E+05	1.01
10000	3.91E+05	3.36E+04	0.086	5.05E+05	1.29
12500	8.77E+05	1.42E+05	0.16	1.34E+06	1.53
15000	1.26E+06	2.63E+05	0.21	1.44E+06	1.14
20000	1.47E+06	2.31E+05	0.16	8.20E+05	0.56
25000	7.67E+05	9.12E+04	0.12	2.32E+05	0.30
30000	2.92E+05	2.04E+04	0.070	4.50E+04	0.15
35000	8.99E+04	1.96E+03	0.022	8.08E+03	0.09

5-3.2. Proton Dose Comparison

In considering the appropriate CRRES dosimeter for comparing with trapped proton dose, Fig. 5-3 shows predicted doses vs. altitude for the shielding used on the four CRRES dosimeters, which indicates that either the 3.14 or 6.08 g/cm^2 shielding is sufficient to stop incident electrons. Figure 5-4 shows predicted dose from protons and from electrons for the dosimeter shielded by 3.14 g/cm^2. The electron dose is negligible over the inner proton belt except at the outer edge. (The local maximum in dose near 20,000 km for the 3.14 g/cm^2 shielding in Figs. 5-3 and 5-4 is due to bremsstrahlung production in the high electron flux region of the outer belt.) Therefore, we use the CRRES high-LET data for the dosimeter with 3.14 g/cm^2 shielding for comparisons with the predicted doses from trapped protons.

Figure 5-5 compares the predicted inner belt trapped proton dose with the CRRES-measured dose for low and high magnetic activity, and Fig. 5-6 shows the altitude dependence of the measured-to-predicted dose ratio. These results show that the AP8MAX underpredicts the dose by about a factor of two at the lowest altitude (800 km) where the CRRES dose data are applicable, with the data-model difference gradually decreasing with altitude until there is essentially no difference in the peak flux region. On the outer side of the belt, AP8MAX overpredicts during quiet times and significantly underpredicts during high activity at altitudes from about 6,000-10,000 km where the large geomagnetic storm and solar event during the CRRES mission created a second proton belt. Table 5-5 gives a tabulation of the results in Figs. 5-5 and 5-6.

5-3.3. Proton Flux Comparisons

Figure 5-7 compares the CRRES PROTEL instrument proton flux > 30 MeV with AP8MAX predictions. The model-data agreement is similar to the dose comparison of Fig. 5-5, but the flux difference in the altitude range from 1500 – 4000 km about the peak is higher for the flux comparison. As discussed in [5-14], corrections to the PROTEL data had to be applied to remove contamination by out-of-aperture protons, which may influence the comparison. The values in Fig. 5-7 and the measured/predicted flux ratios are given in Table 5-6.

Figure 5-8 compares measured and predicted proton energy spectra in the region of peak intensity (3,000 km). The agreement is quite good, but the AP8MAX model underpredicts in the 10 – 50 MeV range. This spectral comparison suggests that the energy of 30 MeV selected for

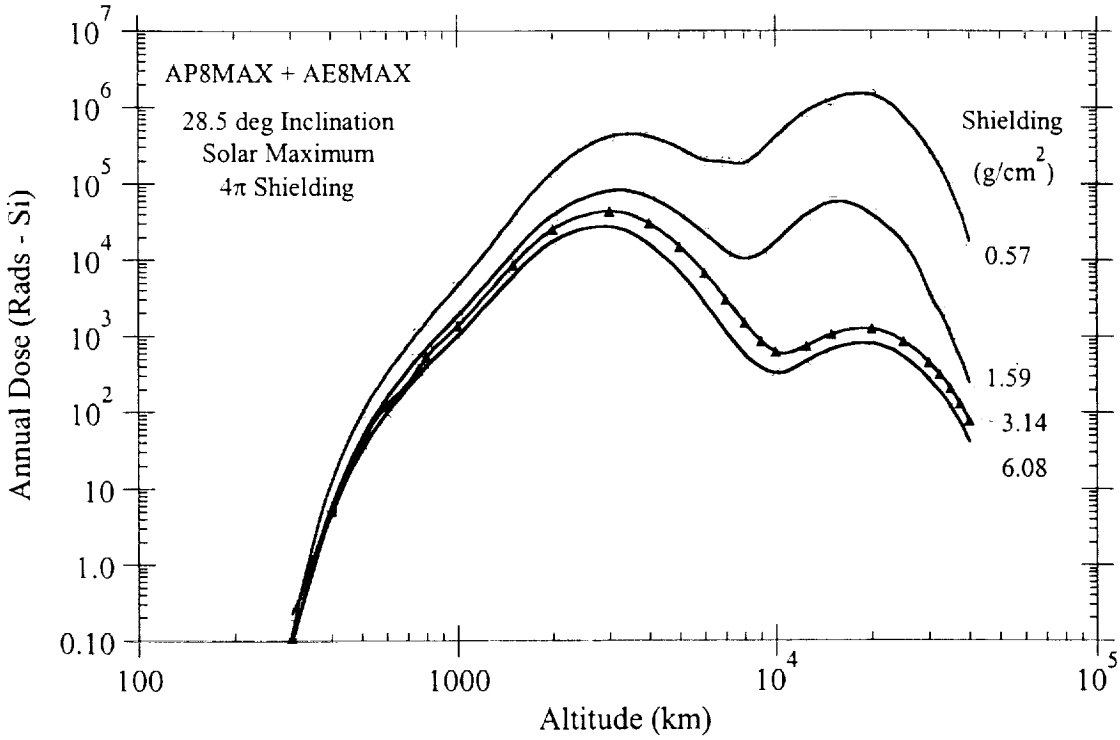

Fig. 5-3. Predicted altitude dependence of trapped radiation dose for CRRES dosimeter shielding thicknesses.

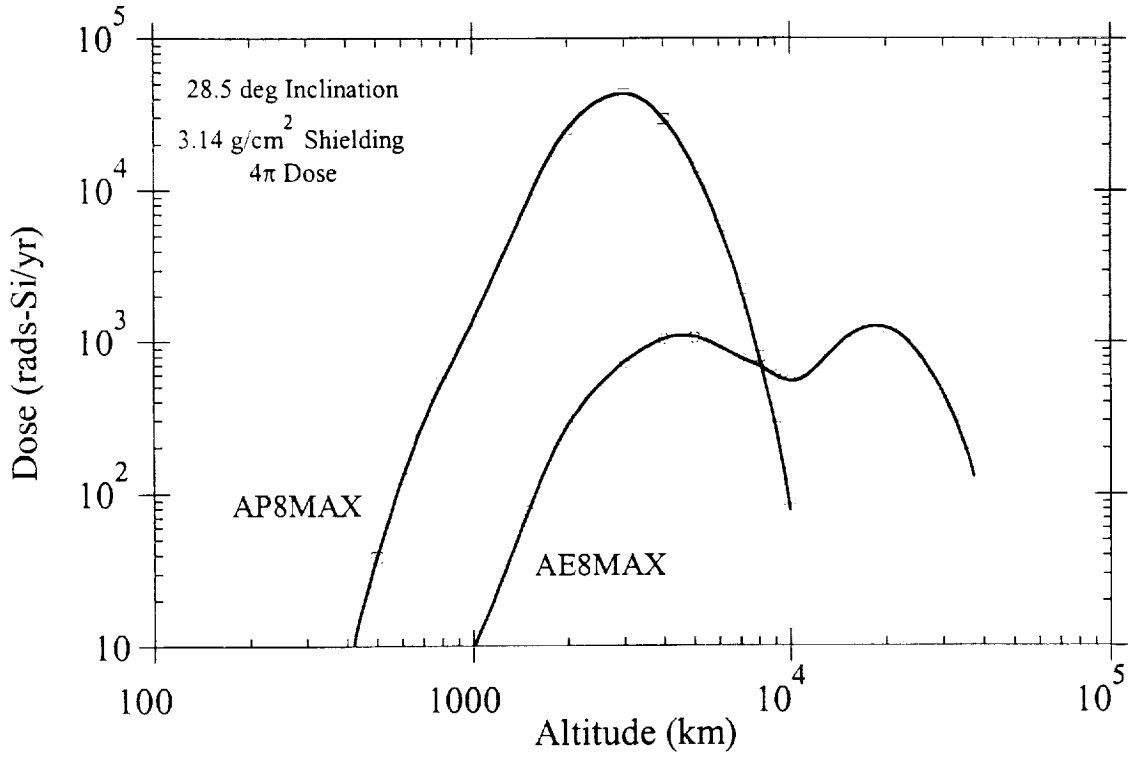

Fig. 5-4. Altitude dependence of radiation dose predicted using AP8MAX trapped proton model and AE8MAX trapped electron model.

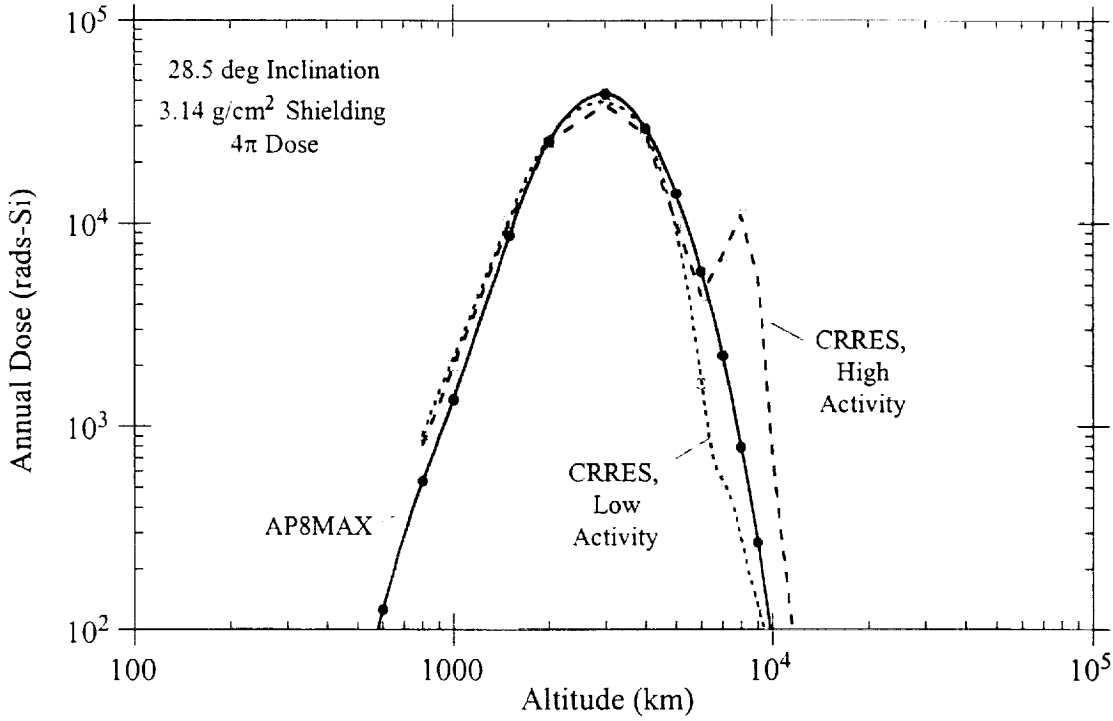

Fig. 5-5. Comparison of proton dose predicted using AP8MAX model and dose based on CRRES satellite measurements for low and high magnetic activity levels,

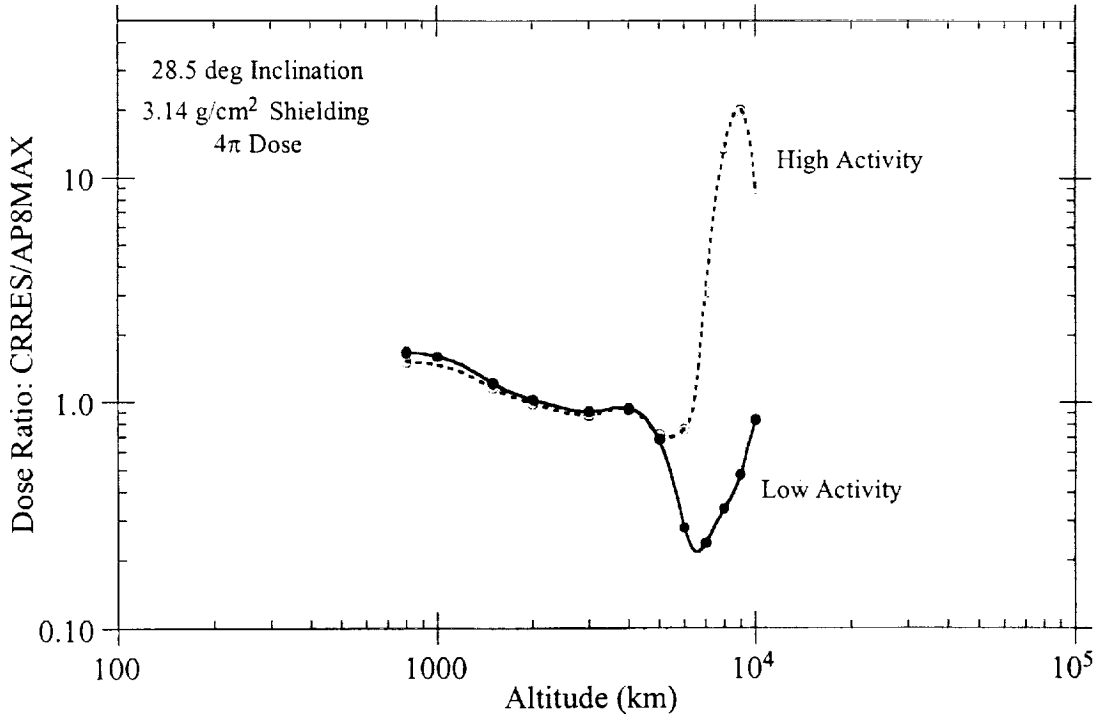

Fig. 5-6. Ratio of proton dose based on CRRES satellite measurements for low and high magnetic activity to dose predicted using AP8MAX trapped proton model.

Table 5-5. CRRES/AP8MAX dose ratio for 3.14 g/cm^2 shielding, low and high magnetic activity levels, and circular, 28.5 deg. inclination orbits.

		Low Activity, High LET		High Activity, High LET	
Altitude (km)	AP8MAX (rads-Si/yr, 4π)	CRRES (rads-Si/yr, 4π)	Dose Ratio: CRRES/AP8MAX	CRRES (rads-Si/yr, 4π)	Dose Ratio: CRRES/AP8MAX
800	5.38E+02	8.96E+02	1.67	8.16E+02	1.52
1000	1.37E+03	2.19E+03	1.60	2.01E+03	1.47
1500	8.69E+03	1.06E+04	1.22	1.01E+04	1.16
2000	2.54E+04	2.63E+04	1.03	2.51E+04	0.99
3000	4.34E+04	3.93E+04	0.91	3.84E+04	0.88
4000	2.94E+04	2.76E+04	0.94	2.72E+04	0.93
5000	1.40E+04	9.49E+03	0.68	1.02E+04	0.72
6000	5.83E+03	1.64E+03	0.28	4.45E+03	0.76
7000	2.23E+03	5.40E+02	0.24	6.97E+03	3.13
8000	7.96E+02	2.72E+02	0.34	1.09E+04	13.7
9000	2.70E+02	1.30E+02	0.48	5.44E+03	20.2
10000	7.89E+01	6.60E+01	0.84	7.14E+02	9.05

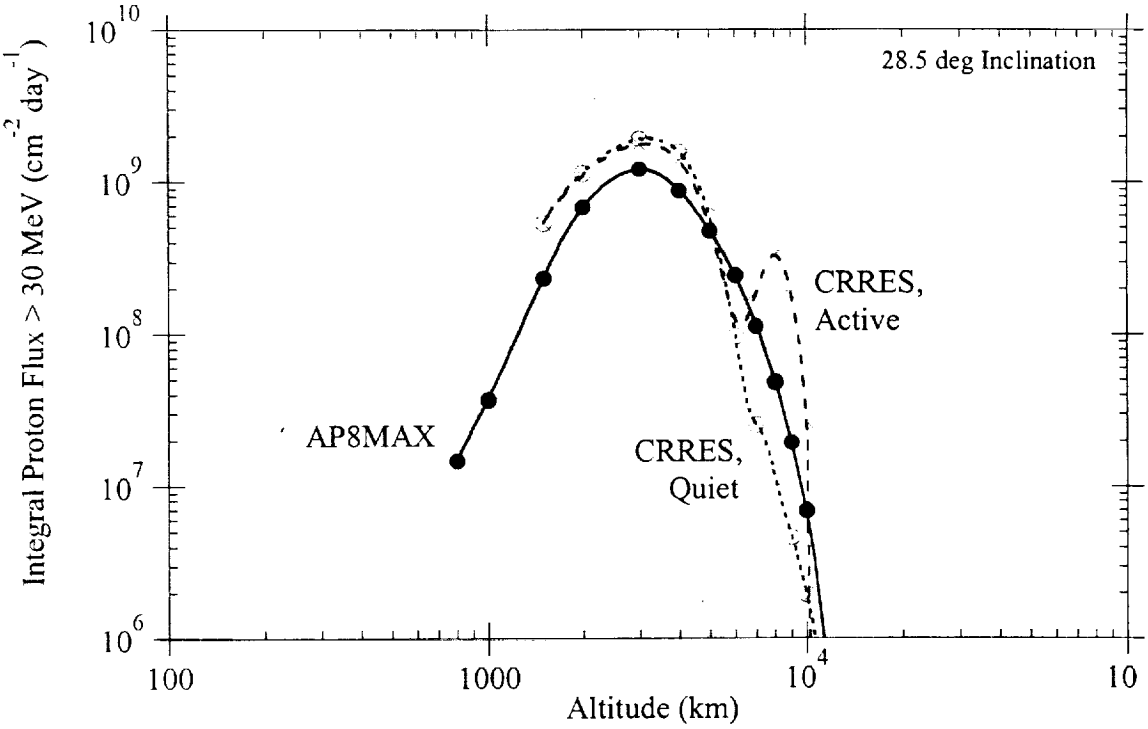

Fig. 5-7. Comparison of proton flux > 30 MeV based on CRRES satellite measurements for quiet and active geomagnetic activity conditions with AP8MAX trapped proton model predictions.

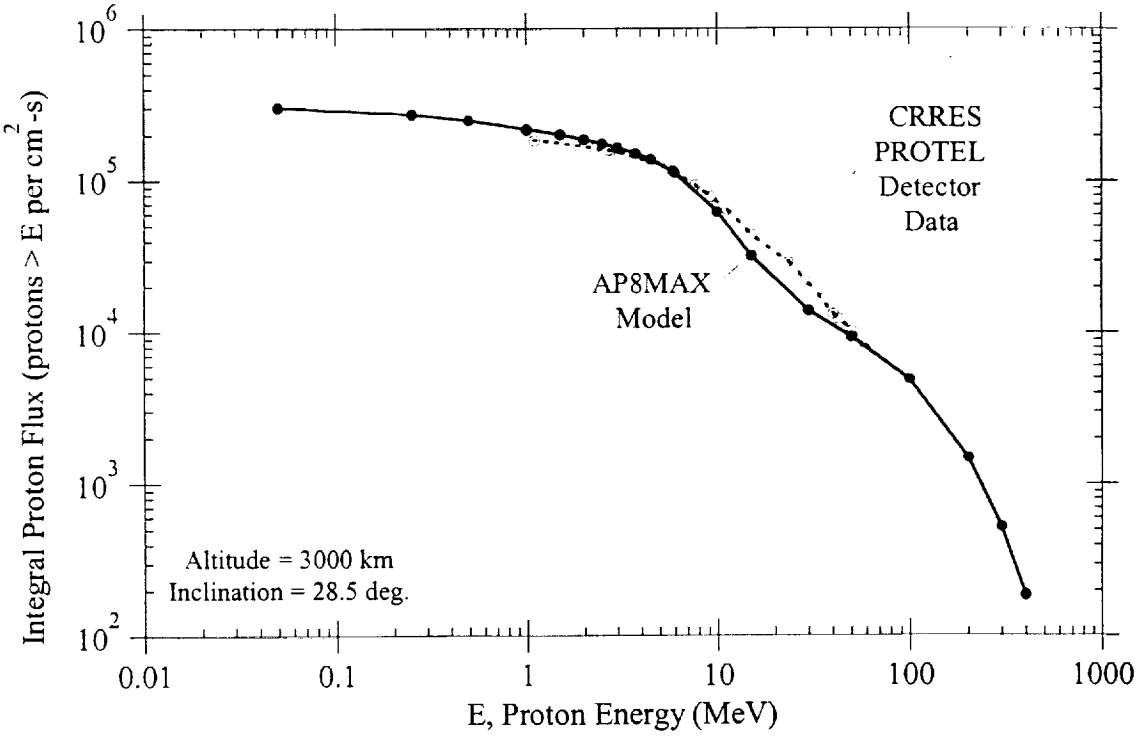

Fig. 5-8. Comparison of trapped proton spectrum based on CRRES satellite measurements with spectrum predicted using AP8MAX model.

Table 5-6. Comparison of proton flux at high altitudes form AP8MAX model predictions and based on PROTEL detector measurements on CRRES.

		Low Activity		High Activity	
Altitude (km)	AP8MAX Flux (a)	CRRES Flux (a)	Flux Ratio: CRRES/AP8MAX	CRRES Flux (a)	Flux Ratio: CRRES/AP8MAX
1500	2.35E+08	5.39E+08	2.30	5.37E+08	2.28
2000	6.85E+08	1.16E+09	1.69	1.11E+09	1.62
3000	1.21E+09	1.91E+09	1.58	1.77E+09	1.46
4000	8.79E+08	1.58E+09	1.80	1.39E+09	1.58
5000	4.76E+08	5.89E+08	1.24	5.01E+08	1.05
6000	2.44E+08	9.72E+07	0.40	1.25E+08	0.51
7000	1.13E+08	2.57E+07	0.23	1.88E+08	1.67
8000	4.87E+07	1.15E+07	0.24	3.29E+08	6.75
9000	1.94E+07	4.65E+06	0.24	1.79E+08	9.22
10000	6.95E+06	1.95E+06	0.28	2.68E+07	3.85
12500	1.93E+05	1.88E+05	0.97	6.38E+04	0.33

(a) Integral omnidirectional proton flux > 30 MeV per cm^2-day

the integral flux altitude comparison of Fig. 5-7 corresponds to the approximate energy of maximum difference between the measured and predicted spectra.

5-3.4. Electron Flux Comparison

Figure 5-9 compares AE8MAX – predicted electron flux vs. altitude with data from the HEEF instrument on CRRES for several different magnetic activity levels: "quiet", for measurements before the large March 1991 geomagnetic disturbance; "mission average", which includes the 6 month period after the March 1991 event when the outer zone electrons were greatly enhanced; and, for "high activity", where we have used results for the highest activity level (Ap_{15} = 25 – 55) for which CRRES data are available. These electron flux results are consistent with the electron dose comparisons shown earlier (Fig. 5-2), showing that AE8MAX model predictions substantially overestimate the electron population in the outer belt. AE8MAX predictions for the inner and central regions of the outer belt are comparable to measured doses for very high geomagnetic activity conditions, and the model predictions for the outer edge of the belt are substantial overestimates for all levels of magnetic activity.

Figure 5-10 compares orbit-average measured and predicted electron spectra for 28.5 deg. inclination and 20,000 km altitude, in the peak intensity region of the outer belt. Somewhat fortuitously, the mission average CRRES flux and the AE8MAX predicted flux are in excellent agreement (within 10%) for energies above 0.5 - 0.8 MeV – i.e., the spectra have not been normalized to each other. This spectral comparison suggests that the model-data comparison vs. altitude in Fig. 5-9 based on electron flux > 1.2 MeV would be better if a lower threshold energy had been selected and much worse for a higher energy comparison.

5-4. Conclusions

The CRRES satellite data, and the convenient availability of the data in PC programs, provide an important flight data set for quantitatively evaluating the accuracy of both the AP8 and AE8 trapped radiation models for solar maximum conditions. Furthermore, since the data include measurements during greatly enhanced belt fluxes due to a large geomagnetic storm, the CRRES data provide bounds on the model inaccuracies during storm conditions. Model-data differences based on the CRRES data are further quantified, and compared with other flight data, in [5-3].

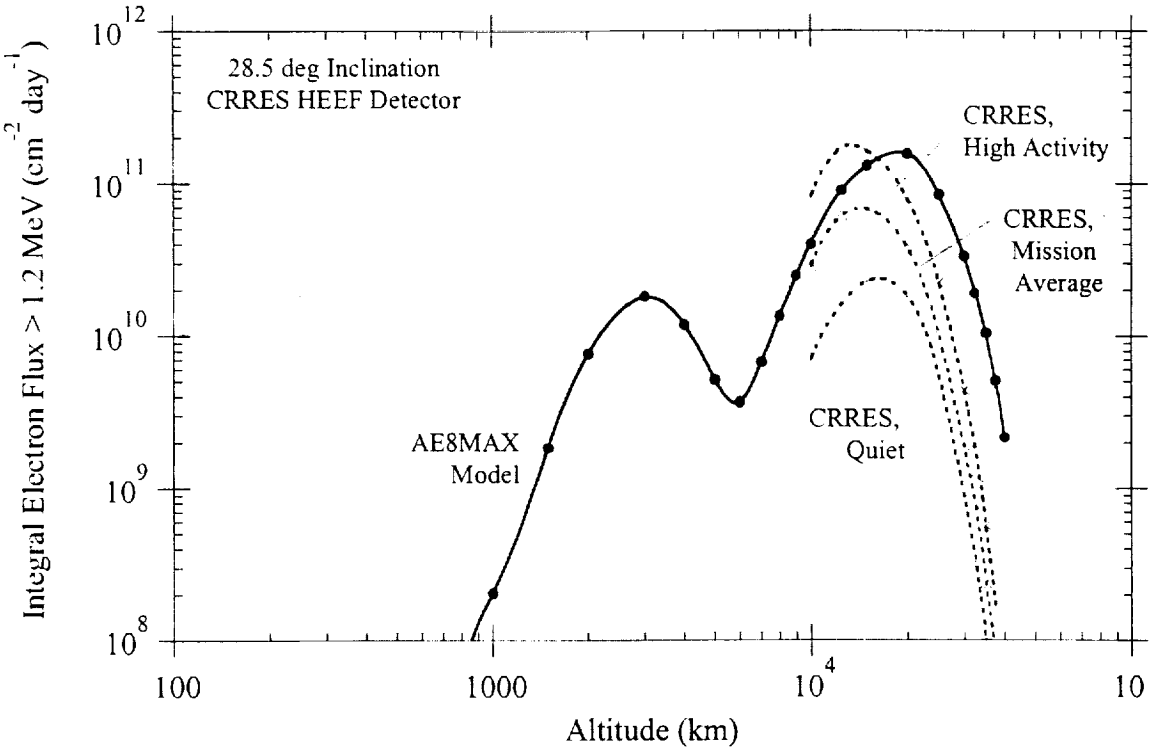

Fig. 5-9. Comparison of electron flux > 1.2 MeV based on CRRES satellite measurements for various geomagnetic activity conditions with AE8MAX trapped electron model predictions.

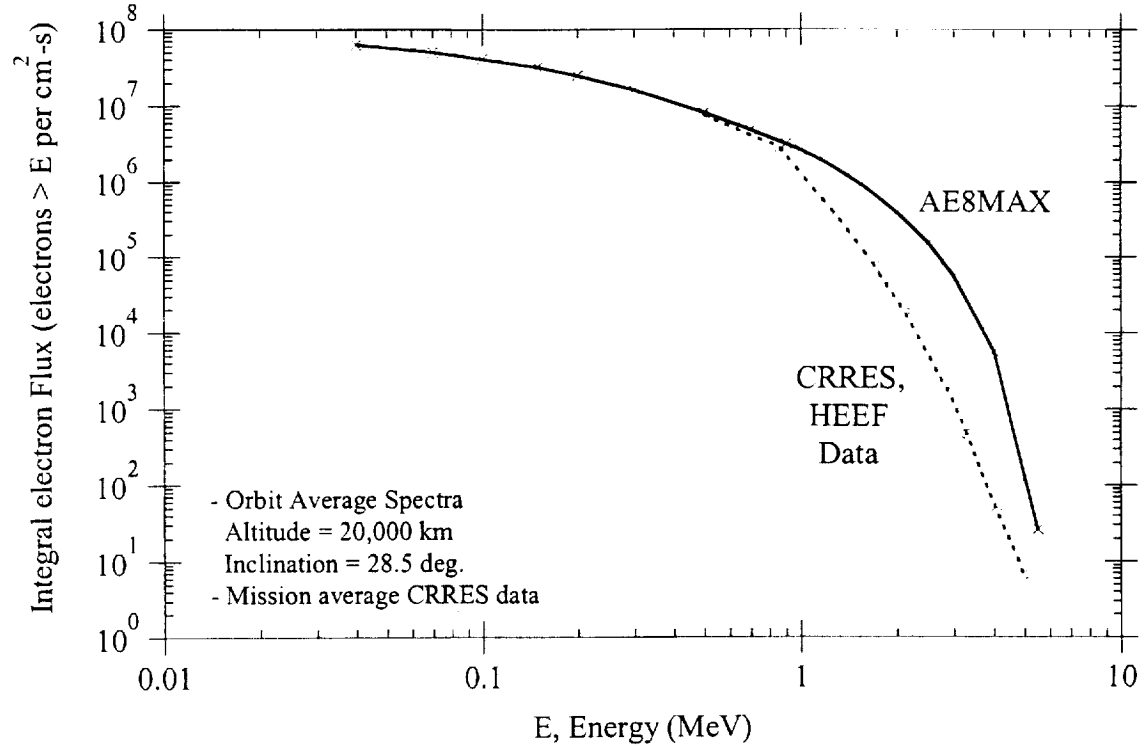

Fig. 5-10. Comparison of outer belt trapped electron spectrum based on CRRES satellite measurements with spectrum predicted using AE8MAX model.

5-5. References

[5-1] M. S. Gussenhoven and E. G. Mullen, "Space Radiation Effects Program: An Overview", IEEE Trans, Nucl. Sci. 40 (2), 221 (1993).

[5-2] M. S. Gussenhoven, E. G. Mullen, and D. H. Brautigam, "Improved Understanding of the Earth's Radiation Belts from the CRRES Satellite:, IEEE Trans. Nucl. Sci. 43 (2), 353 (1996).

[5-3] T. W. Armstrong and B. L. Colborn, "Evaluation of Trapped Radiation Model Uncertainties for Spacecraft Design", Science Applications International Corporation, Contractor Report for NASA/MSFC, SAIC-TN-99020, September 1999.

[5-4] K. J. Kerns and M. S. Gussenhoven, "CRRESRAD Documentation", Phillips Laboratory, Geophysics Directorate, Hanscom AFB, PL-TR-92-2202, August 1992.

[5-5] Donald H. Brautigam and Jabin T. Bell, "CRRESELE Documentation", Phillips Laboratory, Geophysics Directorate, Hanscom AFB, PL-TR-95-2128, July 1995.

[5-6] Jeralyn D. Meffert and M. S. Gussenhoven, "CRRESPRO Documentation", Phillips Laboratory, Geophysics Directorate, Hanscom AFB, PL-TR-94-2218, July 1994.

[5-7] A. L. Vampola, "ESA Update of AE-8 Using CRRES Data and a Neutral Network", in: Radiation Belts: Models and Standards (J. F. Lemaire, D. Heynderickx, and D. N. Baker, Eds.), Geophysical Monograph 97, American Geophysical Union (1996).

[5-8] A. L. Vampola, "Radiation Belt Model for the PC: RADMODLS", in: Radiation Belts: Models and Standards (J. F. Lemaire, D. Heynderickx, and D. N. Baker, Eds.), Geophysical Monograph 97, American Geophysical Union (1996).

[5-9] T. W. Armstrong and B. L. Colborn, "TRAP/SEE Code Users Manual for Predicting Trapped Radiation Environments", Science Applications International Corporation, Contractor Report for NASA/MSFC, SAIC-TN-99010, August 1999.

[5-10] Donald W. Sawyer and James I. Vette, "AP-8 Trapped Proton Environment for Solar Maximum and Solar Minimum", National Space Science Data Center, NASA Goddard Space Flight Center, NSSDC/WDC-A-R&S 76-06, 1976.

[5-11] M. J. Teague and J. I. Vette, "A Model of the Trapped Electron Population for Solar Minimum", National Space Science Data Center, NASA Goddard Space Flight Center, NSSDC 03-74, 1974.

[5-12] James I. Vette, "The AE-8 Trapped Electron Model Environment", National Space Science Data Center, Goddard Space Flight Center, NSSDC/WDC-A-R&S 91-24, Nov. 1991.

[5-13] Stephen M. Seltzer, "Updated Calculations for Routine Space Shielding Radiation Dose Estimates: SHIELDOSE-2", National Institute of Standards and Technology, NISTIR-5477, Dec. 1994.

[5-14] M. S. Gussenhoven, E. G. Mullen, M. D. Violet, C. Hein, J. Bass, and D. Madden, "CRRES High Energy Proton Flux Maps", IEEE Trans. Nucl. Sci. 40 (6), 1450 (1993).

6. Model Comparisons with NOAA Satellite Data

6-1. Introduction

The National Oceanic and Atmospheric Administration (NOAA) has flown radiation detectors of essentially the same design on its weather satellites (850 km, 99°) since 1978. One of the radiation sensors, the Medium Energy Proton and Electron Detector (MEPED), consists of planar silicon detectors behind hemispherical shields of different thicknesses to provide integral proton fluxes > 16, > 30, and > 80 MeV.

Huston and Pfitzer [6-1, 6-2] have recently analyzed the MEPED data from seven NOAA satellites covering the period from 1978 through 1995 (1.5 solar cycles). This data base has been incorporated into a model, NOAAPRO, with associated FORTRAN routines so that orbit-average integral fluxes for the above thresholds can be calculated (below 850 km) for an input ephemeris file. We have made calculations using NOAAPRO, with the ephemeris file generated using the MSFC Burrell orbit code [6-3], to compare with AP8MIN and AP8MAX model predictions.

6-2. Flight Data

The NOAAPRO code has been applied to generate orbit-average, omnidirectional integral proton fluxes for circular low-altitude orbits at various inclinations and altitudes in the 300-850 km range at solar minimum and solar maximum. Solar minimum fluxes were calculated based on F10.7 solar fluxes on day 1 of 1996 and solar maximum on day 1 of 1991. These results are summarized in Table 6-1.

6-3. Model – Data Comparisons

A comparison of integral proton fluxes based on NOAA satellite measurements with AP8MIN model predictions is given in Table 6-2 for the case of 850 km orbits at solar minimum, and measured/predicted ratios are plotted in Fig. 6-1.

6-4. Conclusions

These results show that for this altitude of 850 km the AP8MIN model underpredicts proton fluxes down to 16 MeV by factors of 1.5 – 2.5 over all inclinations at solar minimum; additional comparisons at this altitude for solar maximum give similar ratios. This AP8 comparison with NOAA satellite data is consistent with AP8 comparisons made with other low-altitude flight data, as shown in [6-4].

6-5. References

[6-1] S. L. Huston and K. A. Pfitzer, "A New Model for the Low Altitude Trapped Proton Environment", IEEE Trans. Nucl. Sci. 45 (6), 2972 (1998).

[6-2] S. L. Huston and K. A. Pfitzer, "Space Environment Effects: Low-Altitude Trapped Radiation Model", NASA/CR-1998-208593, August 1998.

[6-3] M. O. Burrell and J. J. Wright, "Orbital Calculations and Trapped Radiation Mapping", NASA TM X-53406, March 8, 1966.

[6-4] T. W. Armstrong and B. L. Colborn, "Evaluation of Trapped Radiation Model Uncertainties for Spacecraft Design", Science Applications International Corporation, Contractor Report for NASA/MSFC, SAIC-TN-99020, September 1999.

Table 6-1. Integral proton flux based on NOAA satellite data (orbit average, omnidirectional).

Orbit		Integral Proton Flux (cm^{-2}-s^{-1})					
Altitude	Inclination	Solar Minimum (1996)			Solar Maximum (1991)		
(km)	(deg)	>16MeV	>30MeV	>80MeV	>16MeV	>30MeV	>80MeV
300	0	-	-	-	-	-	-
	10	-	-	-	-	-	-
	20	0.97	0.68	0.49	0.11	0.10	0.07
	28.5	7.55	5.62	4.57	1.35	1.03	1.01
	40	17.4	11.9	9.88	4.09	3.10	2.82
	51.6	9.68	6.68	5.52	2.22	1.70	1.56
	60	7.94	5.49	4.55	1.79	1.37	1.27
	70	6.76	4.69	3.90	1.58	1.20	1.10
	90	6.45	4.46	3.66	1.44	1.10	1.01
400	0	-	-	-	-	-	-
	10	-	-	-	-	-	-
	20	10.4	7.46	4.88	1.65	1.38	1.10
	28.5	44.1	31.7	22.1	12.2	9.42	7.06
	40	58.8	41.0	28.8	21.8	15.3	11.1
	51.6	35.9	25.0	17.5	12.8	9.13	6.64
	60	30.4	21.2	14.8	10.8	7.68	5.58
	70	26.5	18.5	13.0	9.38	6.70	4.88
	90	24.5	17.1	11.9	8.51	6.06	4.44
500	0	-	-	-	-	-	-
	10	6.13	4.31	3.00	0.71	0.66	0.50
	20	49.8	36.3	24.0	13.1	10.8	7.85
	28.5	132	97.5	66.4	56.2	41.6	29.8
	40	133	96.2	64.5	65.8	46.0	31.4
	51.6	82.9	59.8	40.6	39.9	28.2	19.4
	60	71.7	51.9	34.9	34.0	24.1	16.5
	70	63.1	45.5	30.7	29.0	20.6	14.2
	90	58.3	42.3	28.5	27.5	19.5	13.4

(continued)

Table 6-1. (continued)

Orbit		Integral Proton Flux (cm^{-2}-s^{-1})					
Altitude	Inclination	Solar Minimum (1996)			Solar Maximum (1991)		
(km)	(deg)	>16MeV	>30MeV	>80MeV	>16MeV	>30MeV	>80MeV
600	0	3.49	2.36	1.79	0.43	0.34	0.26
	10	37.5	26.8	17.0	7.24	6.25	4.76
	20	158	119	80.0	62.5	49.5	36.7
	28.5	284	217	149	161	117	85.1
	40	244	181	123	149	103	72.1
	51.6	156	116	78.0	91.3	64.2	45.0
	60	132	98.2	66.3	76.8	54.2	38.2
	70	117	87.6	59.3	68.3	48.2	34.1
	90	109	81.6	55.1	63.2	44.7	31.6
750	0	108	77.1	48.3	21.4	18.2	13.8
	10	221	168	108	81.6	67.6	49.9
	20	496	396	270	297	229	169
	28.5	593	506	346	425	338	244
	40	486	390	262	353	266	185
	51.6	325	270	181	229	181	127
	60	278	233	157	201	156	109
	70	249	209	141	175	139	97.9
	90	232	187	126	157	125	87.4
850	0	376	280	176	127	105	74.5
	10	530	421	278	262	215	161
	20	678	558	385	471	364	267
	28.5	676	562	392	515	412	298
	40	516	425	283	426	338	231
	51.6	360	301	200	290	234	162
	60	344	283	188	252	209	144
	70	324	272	185	261	209	147
	90	276	225	151	229	175	123

Table 6-2. Comparison of integral proton fluxes based on NOAA satellite data with AP8MIN trapped proton model predictions for circular, 850 km orbits at solar minimum.

Orbit Inclination (deg)	Flux > 16MeV NOAA Flux (cm^{-2}-s^{-1})	Flux > 16MeV AP8MIN Flux (cm^{-2}-s^{-1})	Flux > 16MeV Ratio: NOAA/ AP8MIN	Flux > 30MeV NOAA Flux (cm^{-2}-s^{-1})	Flux > 30MeV AP8MIN Flux (cm^{-2}-s^{-1})	Flux > 30MeV Ratio: NOAA/ AP8MIN	Flux > 80MeV NOAA Flux (cm^{-2}-s^{-1})	Flux > 80MeV AP8MIN Flux (cm^{-2}-s^{-1})	Flux > 80MeV Ratio: NOAA/ AP8MIN
0	376	152	2.5	280	134	2.1	176	92	1.9
10	530	199	2.7	421	179	2.3	278	127	2.2
20	678	326	2.1	558	288	1.9	385	196	2.0
28.5	676	389	1.7	562	331	1.7	392	212	1.9
40	516	351	1.5	425	288	1.5	283	177	1.6
51.6	360	250	1.4	301	201	1.5	200	124	1.6
60	344	212	1.6	283	172	1.6	188	107	1.8
70	324	189	1.7	272	155	1.8	185	96	1.9
90	276	175	1.6	225	144	1.6	151	89	1.7

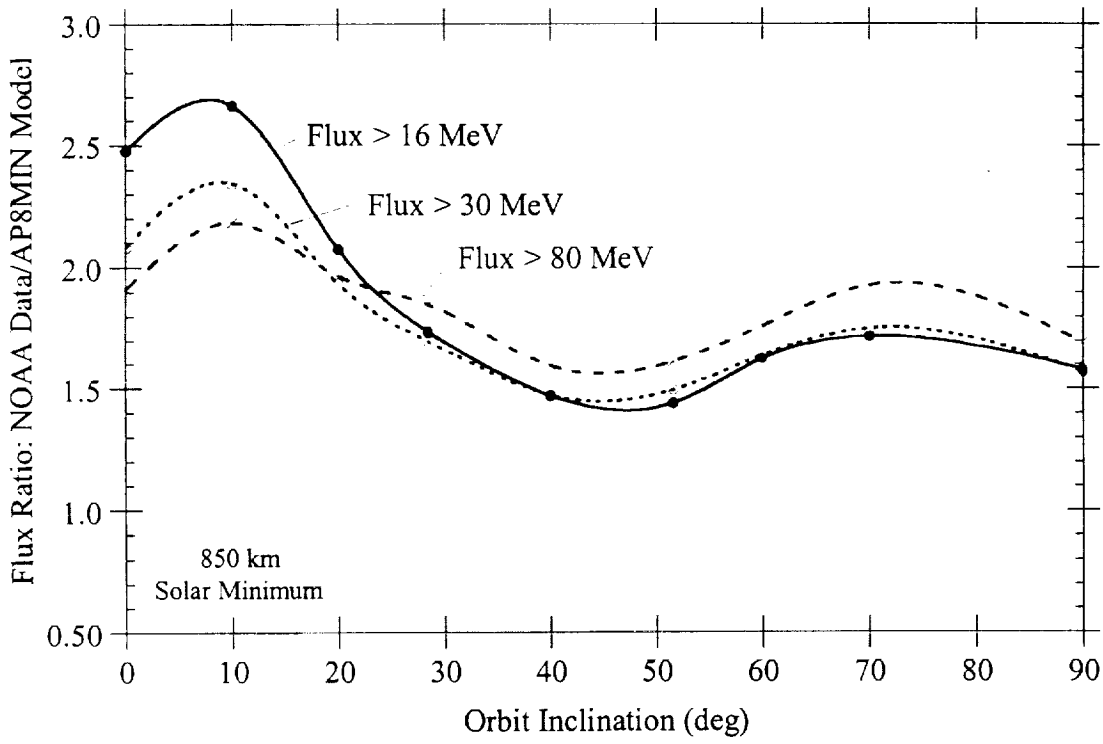

Fig. 6-1. Ratio of integral proton fluxes based on NOAA satellite data to AP8MIN trapped proton model predictions for circular, 850 km orbits at solar minimum.

7. Model – Model Comparisons

7-1. Introduction

In addition to comparing model predictions with flight data as described in previous sections and in [7-1], we have also compared trapped radiation predictions for several different models: the NASA AP8 (proton) and AE8 (electron) models (used almost exclusively for predictions in the U. S.), models used by the European Space Agency (ESA), and the SINP and LOWALT Russian models from Moscow State University. The comparisons are made in terms of orbit-average integral flux spectra for a range of altitudes (350, 500, and 1000 km) and orbit inclinations (28.5°, 51.6°, and 90°).

7-2. Model Descriptions

7-2.1. AP8 and AE8 Models

The particular implementation of the Vette, et al. AP8 and AE8 models [7-2, 7-3, 7-4] used here for model comparisons is the same as incorporated in software packages used routinely for predictions at NASA/MSFC, the same as used in comparisons with flight data here and in [7-1], and the same as incorporated in the TRAP/SEE code [7-5]. The magnetic field models used are the 80-term International Geomagnetic Reference Field for 1965.0 [7-6] projected to 1964 for solar minimum calculations and the U.S. Coast and Geodetic Survey 168-term geomagnetic field model for 1970 [7-7] for solar maximum calculations. The magnetic moment is calculated from the field model expansion coefficients for the epoch of the field.

The B and L calculations are made using the ALLMAG code and associated programs developed by Stassinopoulos and Mead [7-8]. These models are coupled with the MSFC orbit code written by Burrell and Wrifht [7-9] to obtain orbit-average flux spectra.

7-2.2. ESA Versions of the AP8 and AE8 Models

The AP8 and AE8 model data bases consist of integral flux values stored as a function of E, B/B_o, and L, where E is the particle energy, B is the magnetic field intensity, $B_o = M_o/L^3$ is (approximately) the minimum magnetic field intensity where the field line crosses the magnetic

equator, M_o is the magnetic moment, and the McIlwain L parameter is a measure of the radial extent of the field line. A shortcoming of the AP8 model is that the flux data base grid is coarse at low altitudes where protons are being removed by atmospheric interactions and the flux vs. altitude gradient is very steep. Daly and Evans [7-10] of the European Space Agency have devised an improved data base interpolation method for such low altitudes. They define a new variable for interpolation purposes, $\phi = \sin^{-1} [(B - B_o)/(B_{max} - B_o)]$, where B_{max} is the field strength at the atmospheric cutoff. Then ϕ and L are used for flux data interpolation rather than B/B_o and L. This modified interpolation method is used for both AP8 and AE8 calculations.

Comparisons between the standard AP8 and AE8 models and the "ESA versions" using the improved interpolation method were made by incorporating those subroutines containing the extrapolation modifications, provided by Evans and Daly [7-11], into the standard versions. This has the advantage that the model comparison differences can be attributed to the different interpolation methods – i.e., the magnetic field models, orbit code calculation, etc. are the same. However, the ESA versions of AP8 and AE8 normally used at ESA (as contained in the UNIRAD trapped radiation software package [7-12], which is part of the ESA Space Environment Information System) are implemented somewhat differently – they use different magnetic field models and a fixed magnetic moment, as described in [7-13], as well as other software differences [7-12].

7-2.3. Russian Models

Two Russian models have been used: SINP (1991 version) and LOWALT. The SINP (Skobeltsyn Institute of Nuclear Physics) model [7-14, 7-15] developed at Moscow State University (MSU) contains much of the same data as in AP8 and AE8 but augmented with Russian satellite data, mainly measurements made on the GORISINT, COSMOS, and INTERCOSMOS satellites. The AP8/AE8 and SINP models also differ in some of the numerical computation procedures incorporated [7-16], such as E-L grid values and data base interpolation algorithms.

We have also made some calculations using a second MSU model [7-17], called LOWALT, applicable for electrons (at solar maximum or solar minimum) with integral fluxes in

the range from 0.04 to 2.0 MeV in the altitude range 300 - 1000 km. LOWALT is based on measurements made by the Russian satellites INTERCOSMOS-19 and COSMOS-1686.

For the SINP calculations we have used the same magnetic field models and orbit code coupling as described above for AP8 and AE8. A magnetic field model is not needed in running the LOWALT model – this model data base is organized in geographic coordinates (10 deg. x 10 deg. longitude-latitude grid).

7-3. Model Comparisons

The models are compared in terms of orbit-average, integral fluxes for protons and electrons. The proton energy range considered is 0.1 to 398 MeV for protons and 0.04 to 6 MeV for electrons.

Figures 7-1 and 7-2 compare predicted flux spectra for protons and electrons, respectively, for the case of a 500 km circular orbit at 51.6 deg. inclination and solar maximum conditions. For the proton spectra, the overall agreement is good, with the ESA model fluxes somewhat higher than AP8 and the SINP model predicting the highest flux. For the electron spectra, the ESA and AE8 spectra are essentially the same, with the SINP predictions substantially higher in the 0.5 – 2 MeV range and the LOWALT spectrum substantially lower. The energy-dependent ratios of the ESA and SINP spectra to AP8 and AE8 spectra for this orbit are shown in Fig. 7-3.

Figures 7-4 and 7-5 compare flux ratios for the maximum ratio over the applicable energy range and the minimum ratio over the energy range for different orbit altitudes, inclinations, and for solar minimum and solar maximum. These plots are from the spectra ratio values tabulated in Tables 7-1 through 7-4.

7-4. Conclusions

From the model comparisons shown in Figs. 7-1 through 7-5 we conclude the following:

ESA vs. AP8 For the orbit parameters considered, the ESA model predicts proton fluxes about 30% higher than AP8 over most of the energy range, with the exception that for the highest altitude (1000 km) the agreement is within about 10%. The extreme ESA/AP8 ratios over all orbits and over the complete proton energy range is +30% and -13%.

ESA vs. AE8 In general, the ESA model predicts somewhat higher fluxes than AE8 at low electron energies (typically about 20% higher at 0.04 MeV) and usually tends to underestimate the flux slightly at the highest energies. The largest difference was found at the lowest altitude (350 km) where at the high-end of the energy range the ESA prediction is about 40% and 30% lower than AE8 for solar minimum and solar maximum, respectively (see Table 7-3).

SINP vs. AP8 The SINP model generally predicts higher fluxes than AP8 over most of the energy range, typically by 30 to 50%; for the 350 km, 28.5°, solar max case, SINP fluxes are about a factor of two higher.

SINP vs. AE8 The SINP model for electrons predicts higher fluxes than AE8 by a nominal average of about 70%; for particular orbits, the SINP/AE8 difference can vary from a few tens of % to a factor of 2.5 (Fig. 7-5).

LOWALT vs AE8 While we have not extensively checked the LOWALT model, the comparison in Fig. 7-2 indicates that this model substantially underpredicts the others for low electron energies.

Overall, the model predictions for orbit-average spectra are in general agreement – almost always within a factor of two and usually much less difference. The somewhat higher proton flux predictions by the ESA and SINP models compared to AP8 are, as indicated by the flight data comparisons in previous sections and in [7-1], in the direction needed for model–data improvement.

While the ESA interpolation method gives somewhat better agreement with flight data at low altitudes than AP8, the difference becomes smaller with increasing altitude, and the two models give the essentially same results above about 1000 km. Since flight data indicate that AP8 underestimates the proton flux at not just low altitudes but up to the peak of the proton belt (Section 5), the ESA interpolation improvement does not provide a general "fix" for the standard AP8 model.

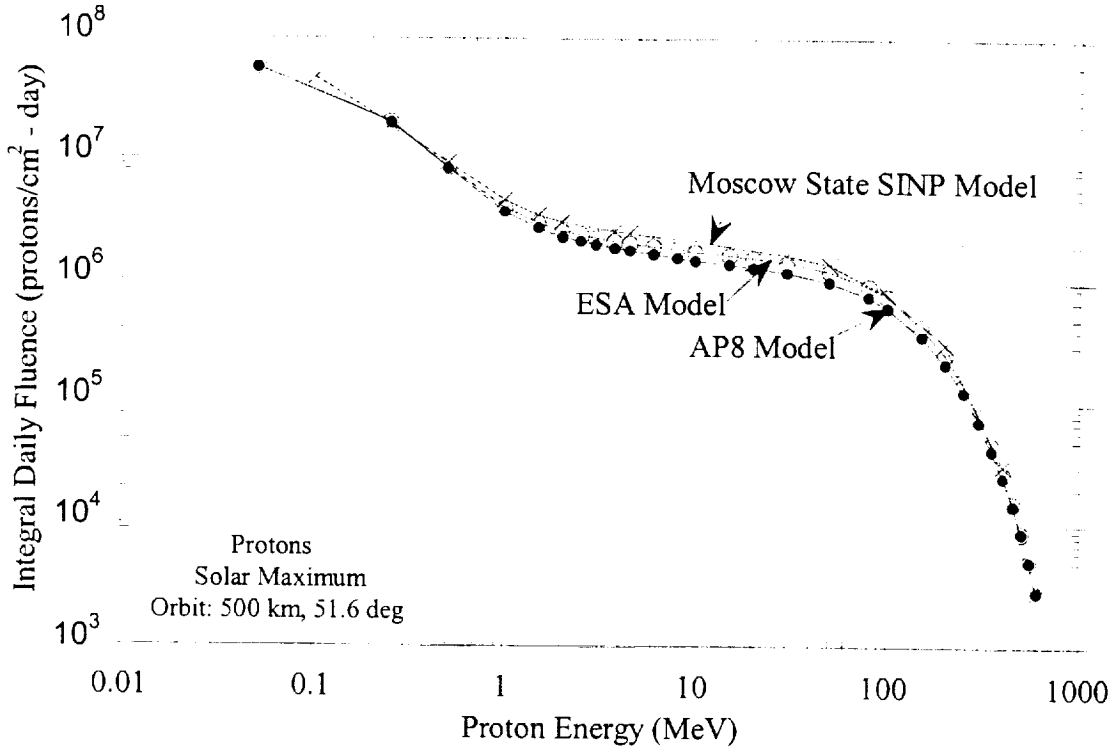

Fig. 7-1. Comparison of trapped proton models for 500 km, 51.6 deg inclination orbit.

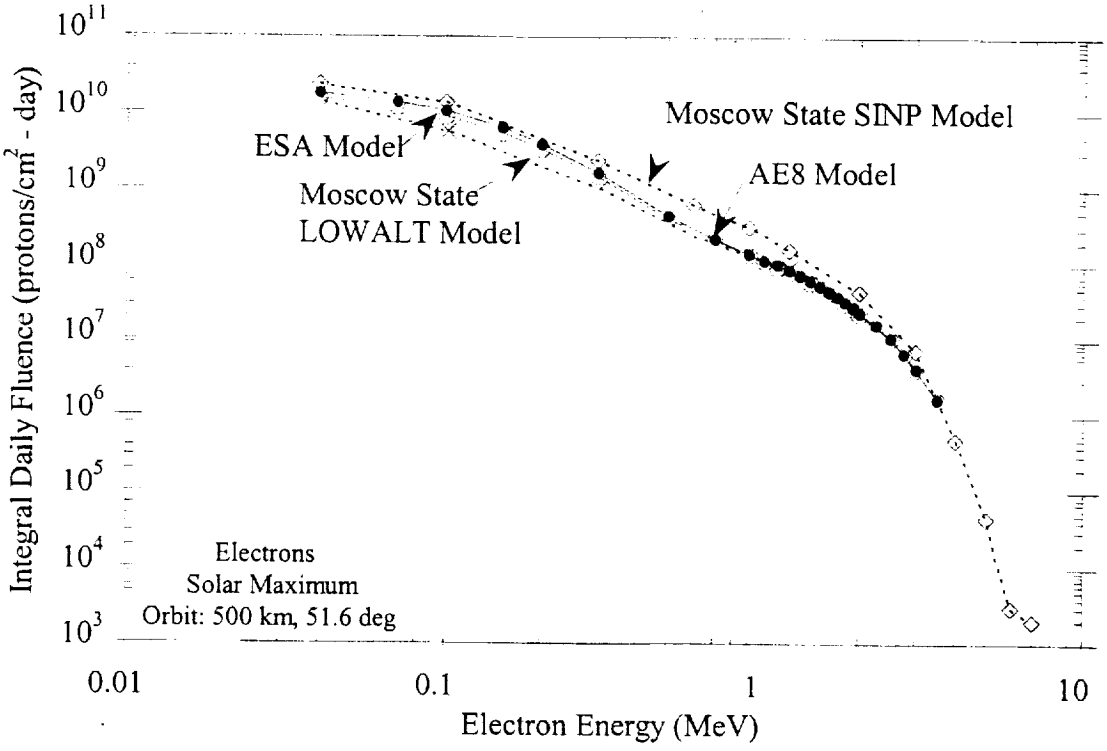

Fig. 7-2. Comparison of trapped electron models for 500 km, 51.6 deg inclination orbit.

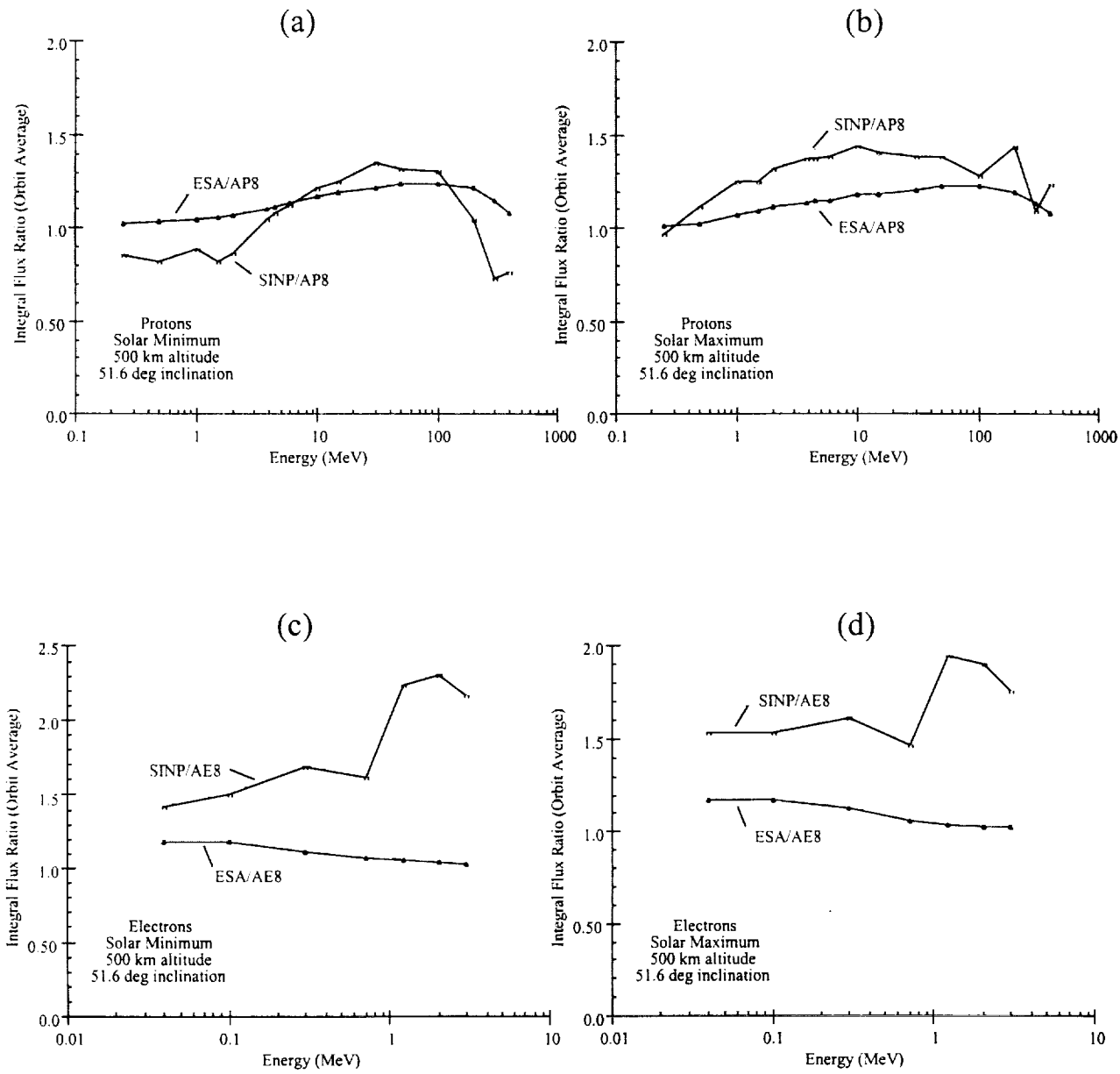

Fig. 7-3. Ratio of integral fluxes for circular, 500km altitude, 51.6° inclination orbit predicted using different trapped radiation models: (a) protons at solar minimum, (b) protons at solar maximum, (c) electrons at solar minimum, and (d) electrons at solar maximum.

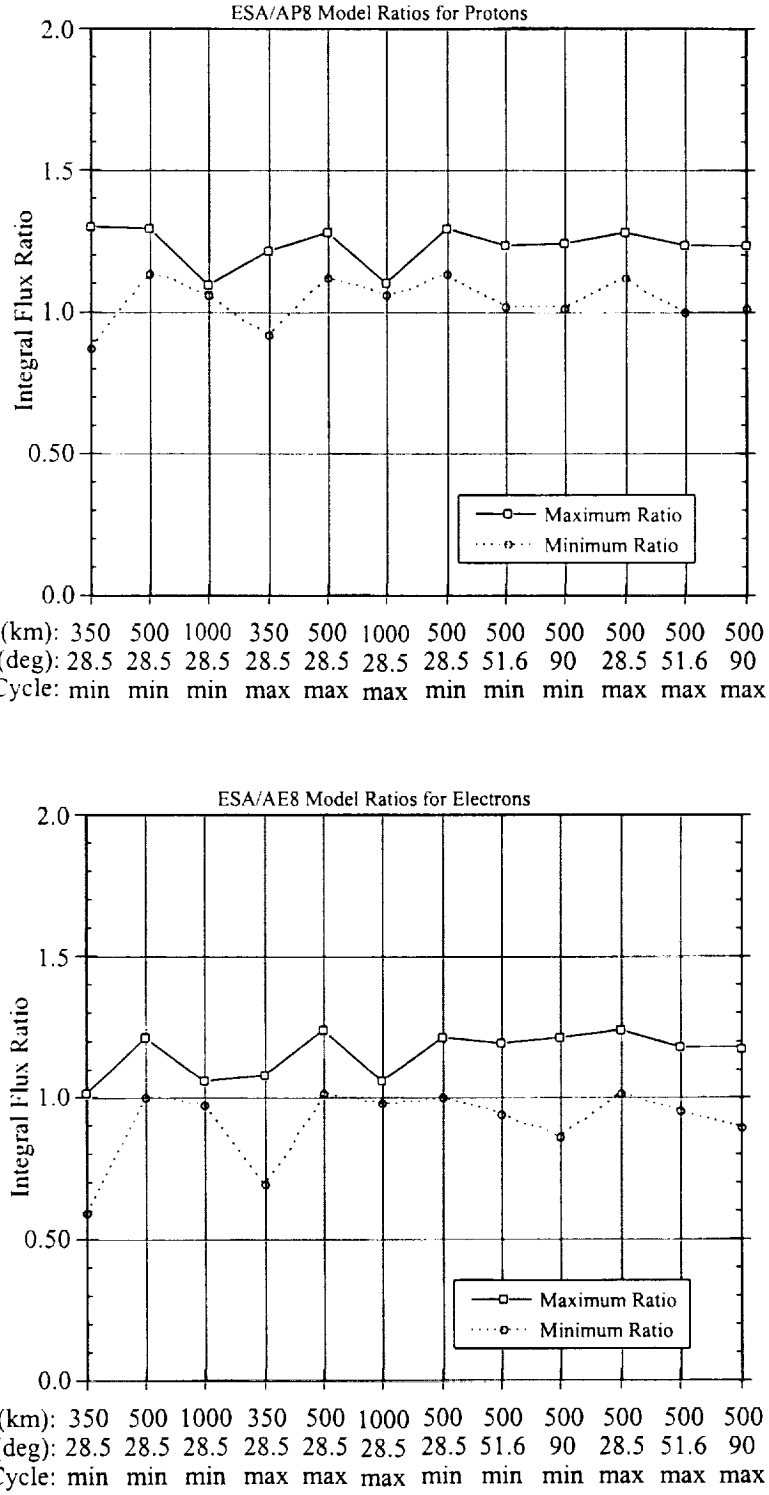

Fig. 7-4. Comparison of ESA trapped radiation models with AP8 and AE8 models. Top graph for ESA/AP8 maximum and minimum integral flux ratios in the proton energy range from 0.1 to 398 MeV; bottom graph for ESA/AE8 ratios in the electron energy range from 0.04 to 6 MeV.

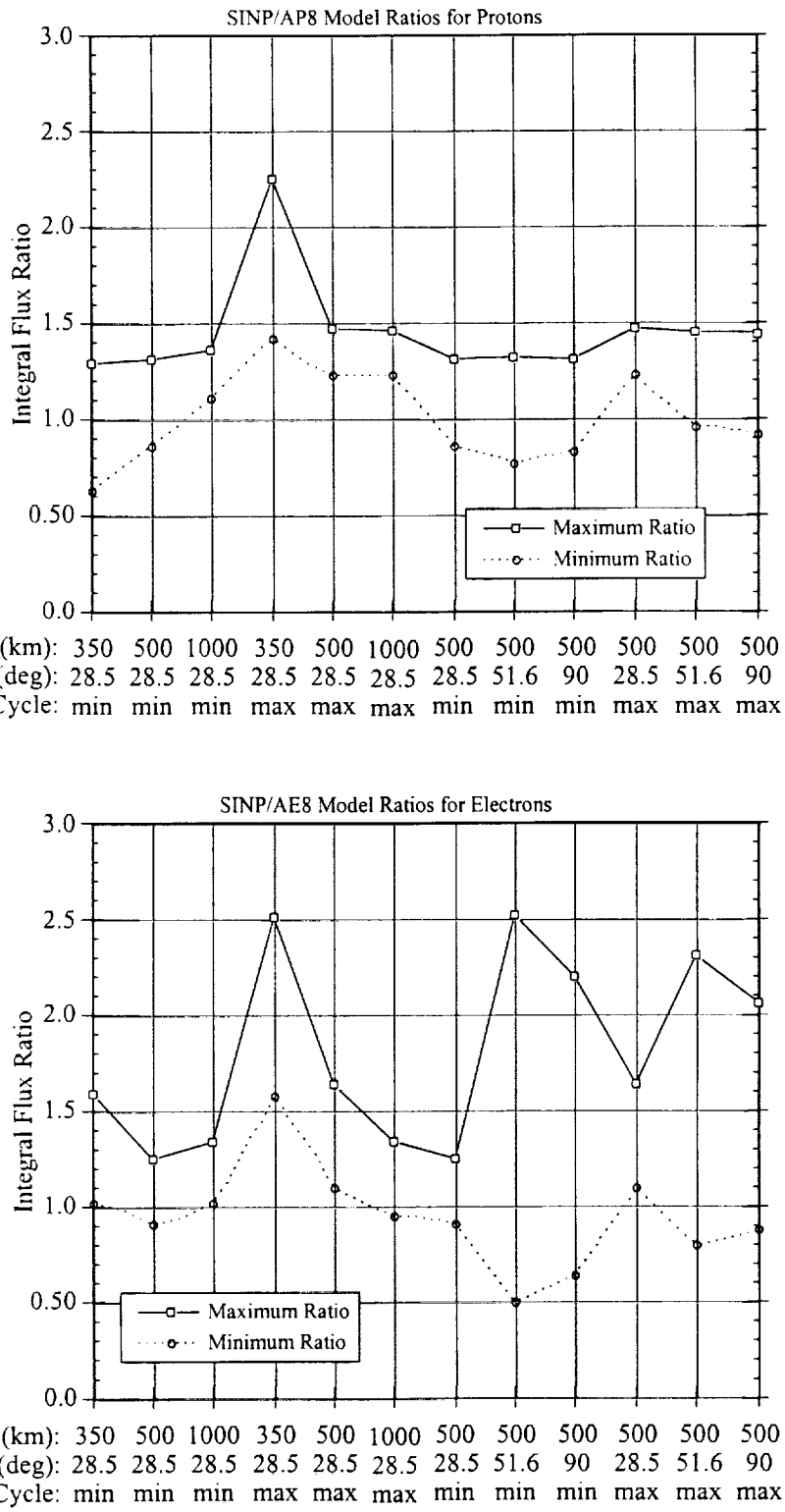

Fig. 7-5. Comparison of Russian SINP trapped radiation models with AP8 and AE8 models. Top graph for SINP/AP8 maximum and minimum integral flux ratios in the proton energy range from 0.1 to 398 MeV; bottom graph for SINP/AE8 ratios in the electron energy range from 0.04 to 6 MeV.

Table 7-1. Proton integral flux ratios vs. altitude for 28.5° inclination orbits.

Altitude (km):	350		350		500		500		1000		1000	
Inclination (deg):	28.5		28.5		28.5		28.5		28.5		28.5	
Solar Cycle:	min		max		min		max		min		max	
Energy (MeV)	ESA/AP8	SINP/AP8	ESA/AP8	SINP/AP8	ESA/AP8	SINP/AP8	ESA/AP8	SINP/AP8	ESA/AP8	SINP/AP8	ESA/AP8	SINP/AP8
0.1	1.27	1.13	1.16	2.17	1.23	1.24	1.22	1.41	1.06	1.36	1.06	1.46
0.16	1.27	1.13	1.15	2.14	1.24	1.25	1.22	1.41	1.06	1.35	1.06	1.46
0.25	1.27	1.13	1.15	2.11	1.23	1.25	1.22	1.42	1.06	1.34	1.06	1.45
0.4	1.27	1.15	1.15	2.08	1.24	1.26	1.22	1.42	1.06	1.33	1.06	1.45
0.63	1.27	1.14	1.15	2.14	1.23	1.24	1.22	1.43	1.06	1.33	1.06	1.45
1	1.26	1.15	1.15	2.25	1.23	1.22	1.22	1.47	1.06	1.33	1.06	1.46
1.58	1.26	1.17	1.15	2.22	1.23	1.22	1.22	1.43	1.06	1.31	1.06	1.44
2.51	1.27	1.19	1.15	2.21	1.24	1.21	1.22	1.41	1.06	1.31	1.06	1.42
3.98	1.26	1.21	1.15	2.22	1.24	1.21	1.23	1.39	1.06	1.32	1.07	1.43
6.31	1.26	1.23	1.14	2.16	1.25	1.21	1.24	1.40	1.07	1.30	1.07	1.41
10	1.26	1.26	1.14	2.16	1.25	1.22	1.25	1.45	1.08	1.32	1.08	1.45
15.8	1.27	1.26	1.13	2.09	1.27	1.25	1.25	1.41	1.08	1.30	1.09	1.42
25.1	1.27	1.29	1.15	2.06	1.27	1.30	1.26	1.39	1.09	1.28	1.10	1.41
39.8	1.29	1.26	1.16	1.99	1.28	1.31	1.26	1.38	1.09	1.29	1.10	1.40
63.1	1.30	1.09	1.18	1.89	1.29	1.25	1.28	1.34	1.09	1.25	1.10	1.36
100	1.26	0.95	1.21	1.78	1.27	1.27	1.28	1.35	1.09	1.28	1.09	1.38
158	1.22	0.71	1.18	1.62	1.27	1.04	1.25	1.33	1.09	1.17	1.09	1.29
251	1.09	0.63	1.09	1.42	1.22	0.86	1.21	1.23	1.08	1.11	1.08	1.23
398	0.87	0.89	0.92	1.58	1.13	0.86	1.12	1.31	1.08	1.30	1.07	1.43
Average Ratio:	1.24	1.10	1.14	2.02	1.24	1.19	1.23	1.39	1.07	1.29	1.08	1.41
Maximum Ratio:	1.30	1.29	1.21	2.25	1.29	1.31	1.28	1.47	1.09	1.36	1.10	1.46
Minimum Ratio:	0.87	0.63	0.92	1.42	1.13	0.86	1.12	1.23	1.06	1.11	1.06	1.23

Table 7-2. Proton integral flux ratios vs. inclination for 500 km altitude orbits.

Altitude (km):	500		500		500		500		500		500	
Inclination (deg):	28.5		28.5		51.6		51.6		90		90	
Solar Cycle:	min		max		min		max		min		max	
Energy (MeV)	ESA/AP8	SINP/AP8	ESA/AP8	SINP/AP8	ESA/AP8	SINP/AP8	ESA/AP8	SINP/AP8	ESA/AP8	SINP/AP8	ESA/AP8	SINP/AP8
0.1	1.23	1.24	1.22	1.41	1.02	1.17	1.00	1.11	1.01	1.14	1.01	1.10
0.16	1.24	1.25	1.22	1.41	1.02	0.94	1.00	0.96	1.01	0.94	1.01	0.92
0.25	1.23	1.25	1.22	1.42	1.02	0.85	1.01	0.97	1.02	0.88	1.01	0.93
0.4	1.24	1.26	1.22	1.42	1.03	0.88	1.03	1.19	1.03	0.94	1.03	1.16
0.63	1.23	1.24	1.22	1.43	1.04	0.81	1.04	1.13	1.05	0.86	1.04	1.08
1	1.23	1.22	1.22	1.47	1.05	0.89	1.07	1.26	1.06	0.93	1.07	1.22
1.58	1.23	1.22	1.22	1.43	1.06	0.83	1.10	1.26	1.08	0.88	1.10	1.25
2.51	1.24	1.21	1.22	1.41	1.08	0.91	1.13	1.33	1.10	0.96	1.14	1.33
3.98	1.24	1.21	1.23	1.39	1.11	1.08	1.15	1.38	1.13	1.11	1.15	1.37
6.31	1.25	1.21	1.24	1.40	1.14	1.13	1.16	1.39	1.16	1.15	1.17	1.39
10	1.25	1.22	1.25	1.45	1.18	1.22	1.18	1.45	1.19	1.22	1.19	1.44
15.8	1.27	1.25	1.25	1.41	1.20	1.25	1.19	1.39	1.20	1.25	1.19	1.39
25.1	1.27	1.30	1.26	1.39	1.21	1.32	1.21	1.39	1.21	1.30	1.21	1.39
39.8	1.28	1.31	1.26	1.38	1.23	1.31	1.22	1.38	1.23	1.31	1.22	1.37
63.1	1.29	1.25	1.28	1.34	1.23	1.25	1.22	1.28	1.24	1.24	1.23	1.30
100	1.27	1.27	1.28	1.35	1.23	1.31	1.23	1.29	1.24	1.30	1.23	1.31
158	1.27	1.04	1.25	1.33	1.23	1.03	1.21	1.27	1.24	1.05	1.22	1.29
251	1.22	0.86	1.21	1.23	1.19	0.81	1.17	1.16	1.20	0.84	1.17	1.18
398	1.13	0.86	1.12	1.31	1.08	0.77	1.08	1.23	1.11	0.83	1.09	1.27
Average Ratio:	1.24	1.19	1.23	1.39	1.12	1.04	1.13	1.25	1.13	1.06	1.13	1.25
Maximum Ratio:	1.29	1.31	1.28	1.47	1.23	1.32	1.23	1.45	1.24	1.31	1.23	1.44
Minimum Ratio:	1.13	0.86	1.12	1.23	1.02	0.77	1.00	0.96	1.01	0.83	1.01	0.92

Table 7-3. Electron integral flux ratios vs. altitude for 28.5° inclination orbits.

Altitude (km):	350		350		500		500		1000		1000	
Inclination (deg):	28.5		28.5		28.5		28.5		28.5		28.5	
Solar Cycle:	min		max		min		max		min		max	
Energy (MeV)	ESA/AE8	SINP/AE8	ESA/AE8	SINP/AE8	ESA/AE8	SINP/AE8	ESA/AE8	SINP/AE8	ESA/AE8	SINP/AE8	ESA/AE8	SINP/AE8
0.04	1.01	1.59	1.08	2.51	1.20	1.24	1.24	1.64	1.06	1.17	1.06	1.16
0.06	1.00	1.38	1.08	2.34	1.21	1.19	1.24	1.53	1.06	1.14	1.05	1.12
0.1	1.00	1.32	1.08	2.35	1.19	1.24	1.23	1.57	1.05	1.22	1.06	1.17
0.16	0.98	1.10	1.06	1.87	1.17	1.03	1.21	1.33	1.05	1.02	1.05	1.01
0.25	0.96	1.30	1.04	1.95	1.14	1.25	1.18	1.50	1.05	1.21	1.05	1.14
0.4	0.93	1.23	1.00	1.76	1.13	1.11	1.14	1.22	1.04	1.08	1.05	0.95
0.63	0.90	1.33	0.95	1.81	1.12	1.13	1.12	1.30	1.04	1.17	1.04	1.09
1	0.88	1.28	0.93	1.80	1.10	1.10	1.10	1.30	1.04	1.09	1.04	1.15
1.5	0.84	1.25	0.90	1.73	1.09	1.00	1.09	1.17	1.04	1.02	1.04	1.07
2	0.80	1.32	0.87	1.84	1.07	1.06	1.08	1.22	1.04	1.07	1.04	1.11
3	0.59	1.02	0.69	1.58	1.00	0.91	1.01	1.10	1.02	1.03	1.02	1.12
4									0.97	1.34	0.98	1.34
Average Ratio:	0.90	1.28	0.97	1.96	1.13	1.11	1.15	1.35	1.04	1.13	1.04	1.12
Maximum Ratio:	1.01	1.59	1.08	2.51	1.21	1.25	1.24	1.64	1.06	1.34	1.06	1.34
Minimum Ratio:	0.59	1.02	0.69	1.58	1.00	0.91	1.01	1.10	0.97	1.02	0.98	0.95

Table 7-4. Electron integral flux ratios vs. inclination for 500 km altitude orbits.

Altitude (km):	500		500		500		500		500		500	
Inclination (deg):	28.5		28.5		51.6		51.6		90		90	
Solar Cycle:	min		max		min		max		min		max	
Energy (MeV)	ESA/AE8	SINP/AE8	ESA/AE8	SINP/AE8	ESA/AE8	SINP/AE8	ESA/AE8	SINP/AE8	ESA/AE8	SINP/AE8	ESA/AE8	SINP/AE8
0.04	1.20	1.24	1.24	1.64	1.19	1.42	1.18	1.54	1.21	1.45	1.17	1.50
0.06	1.21	1.19	1.24	1.53	1.19	1.37	1.18	1.45	1.16	1.39	1.16	1.42
0.1	1.19	1.24	1.23	1.57	1.18	1.51	1.17	1.53	1.14	1.51	1.14	1.50
0.16	1.17	1.03	1.21	1.33	1.16	1.33	1.16	1.35	1.11	1.39	1.13	1.40
0.25	1.14	1.25	1.18	1.50	1.12	1.73	1.13	1.71	1.09	1.66	1.11	1.74
0.4	1.13	1.11	1.14	1.22	1.10	1.84	1.09	1.74	1.08	1.71	1.07	1.72
0.63	1.12	1.13	1.12	1.30	1.08	2.26	1.06	2.19	1.06	1.98	1.05	2.01
1	1.10	1.10	1.10	1.30	1.06	2.52	1.05	2.31	1.06	2.20	1.04	2.06
1.5	1.09	1.00	1.09	1.17	1.05	2.14	1.04	1.76	1.05	1.84	1.04	1.58
2	1.07	1.06	1.08	1.22	1.04	2.31	1.03	1.90	1.04	1.99	1.03	1.74
3	1.00	0.91	1.01	1.10	1.02	2.17	1.02	1.75	1.03	1.93	1.03	1.63
4					1.02	0.50	1.02	0.80	1.02	0.64	1.02	0.88
6					0.94	1.36	0.95	1.50	0.86	1.88	0.89	1.97
Average Ratio:	1.13	1.11	1.15	1.35	1.09	1.73	1.08	1.66	1.07	1.66	1.07	1.63
Maximum Ratio:	1.21	1.25	1.24	1.64	1.19	2.52	1.18	2.31	1.21	2.20	1.17	2.06
Minimum Ratio:	1.00	0.91	1.01	1.10	0.94	0.50	0.95	0.80	0.86	0.64	0.89	0.88

7-5. References

[7-1] T. W. Armstrong and B. L. Colborn, "Evaluation of Trapped Radiation Model Uncertainties for Spacecraft Design", Science Applications International Corporation, Contractor Report for NASA/MSFC, SAIC-TN-99020, September 1999.

[7-2] Donald W. Sawyer and James I. Vette, "AP-8 Trapped Proton Environment for Solar Maximum and Solar Minimum", National Space Science Data Center, NASA Goddard Space Flight Center, NSSDC/WDC-A-R&S 76-06, 1976.

[7-3] M. J. Teague and J. I. Vette, "A Model of the Trapped Electron Population for Solar Minimum", National Space Science Data Center, NASA Goddard Space Flight Center, NSSDC 03-74, 1974.

[7-4] James I. Vette, "The AE-8 Trapped Electron Model Environment", National Space Science Data Center, Goddard Space Flight Center, NSSDC/WDC-A-R&S 91-24, Nov. 1991.

[7-5] T. W. Armstrong and B. L. Colborn, "TRAP/SEE Code Users Manual for Predicting Trapped Radiation Environments", Science Applications International Corporation, Contractor Report for NASA/MSFC, SAIC-TN-99010, November 1999.

[7-6] IAGA Commission 2 Working Group 4, "Analysis of the Geomagnetic Field, International Geomagnetic Reference Field 1965.0", J. Geophys. Res. 74, 4407 (1969).

[7-7] Louis Hurwitz, "Mathematical Model of the 1970 Geomagnetic Field", ESSA Coast and Geodetic Survey, preprint, 4 May 1970.

[7-8] E. G. Stassinopoulos and G. D. Mead, "ALLMAG, GDALMG, LINTRA: Computer Programs for Geomagnetic Field and Field-line Calculations", National Space Science Data Center, NASA Goddard Space Flight Center, NSSDC 72-12, 1972.

[7-9] M. O. Burrell and J. J. Wright, "Orbital Calculations and Trapped Radiation Mapping", NASA TM X-53406, March 8, 1966.

[7-10] E. J. Daly and H. D. R. Evans, "Problems in Radiation Environment Models at Low Altitudes", Radiat. Meas. 26(3), 363 (1996).

[7-11] E. J. Daly and H. D. R. Evans, European Space Agency (ESTEC), pri. comm.

[7-12] D. Heynderickx, M. Kruglanski, J. Lemaire, E. J. Daly, and H. D. R. Evans, "The Trapped Radiation Software Package UNIRAD", in Radiation Belts: Models and Standards (J. F. Lemaire, D. Heynderickx, and D. N. Baker, Eds.), American Geophysical Union Geophysical Monograph 97, 1996.

[7-13] E. J. Daly, J. Lemaire, D, Heynderickx, and D. J. Rodgers, "Problems with Models of the Radiation Belts", IEEE Trans. Nucl. Sci. 43(2), 403 (1996).

[7-14] M. I. Panasyuk, "Model Presentations of Radiation Fluxes in Space", Skobeltsyn Institute of Nuclear Physics, Moscow State University, Moscow, Russia - preprint, to be published in Nucl. Meas.

[7-15] Mikhail I. Panasyuk, "Empirical and Theoretical Models of Terrestrial Radiation", in: Workshop on the Earth's Trapped Particle Environment, Geoffrey D. Reeves (Ed.), American Inst. Physics Conf. Proc. 383, AIP Press, Woodbury NY, 1996.

[7-16] M. I. Panasyuk and K. Tolstaya, Skobeltsyn Institute of Nuclear Physics, Moscow State University, pri. comm.

[7-17] M. I. Panasyuk, Yu. V. Mineev, E. D. Tolstaya, and G. I. Pugacheva, "Electron Component of the Trapped Radiation Environment at Altitudes below 1000 km, According to Recent Satellite Data", Skobeltsyn Institute of Nuclear Physics, Moscow State University, Moscow, Russia - preprint, to be published in Nucl. Meas.

REPORT DOCUMENTATION PAGE

Form Approved
OMB No. 0704-0188

1. AGENCY USE ONLY (Leave blank)	2. REPORT DATE	3. REPORT TYPE AND DATES COVERED
	September 1999	Final Technical (partial), 4/95- 9/99

4. TITLE AND SUBTITLE
Trapped Radiation Model Uncertainties:
Model – Data and Model – Model Uncertainties

5. FUNDING NUMBERS
Contract No.
NAS8-40294

6. AUTHOR(S)
T. W. Armstrong and B. L. Colborn

7. PERFORMING ORGANIZATION NAME(S) AND ADDRESS(ES)
Science Applications International Corporation (SAIC)
1706 Prospect–Elkton Road
Prospect, TN 38477

8. PERFORMING ORGANIZATION REPORT NUMBER
SAIC-TN-99030

9. SPONSORING / MONITORING AGENCY NAME(S) AND ADDRESS(ES)
Space Environments and Effects (SEE) Program Office
NASA Marshall Space Flight Center
Huntsville, AL 35812

10. SPONSORING / MONITORING AGENCY REPORT NUMBER

11. SUPPLEMENTARY NOTES

12a. DISTRIBUTION / AVAILABILITY STATEMENT

12b. DISTRIBUTION CODE

13. ABSTRACT (Maximum 200 words)

The standard AP8 and AE8 models for predicting trapped proton and electron environments have been compared with several sets of flight data to evaluate model uncertainties. Model comparisons are made with flux and dose measurements made on various U.S. low-Earth orbit satellites (APEX, CRRES, DMSP. LDEF, NOAA) and Space Shuttle flights, on Russian satellites (Photon-8, Cosmos-1887, Cosmos-2044), and on the Russian Mir space station. This report gives the details of the model–data comparisons — summary results in terms of empirical model uncertainty factors that can be applied for spacecraft design applications are given in a companion report. The results of model–model comparisons are also presented from standard AP8 and AE8 model predictions compared with the European Space Agency versions of AP8 and AE8 and with Russian trapped radiation models.

14. SUBJECT TERMS
Trapped Radiation Model Uncertainties, AP8, AE8, Space Radiation, Space Ionizing Radiation Environments

15. NUMBER OF PAGES
80

16. PRICE CODE

17. SECURITY CLASSIFICATION OF REPORT	18. SECURITY CLASSIFICATION OF THIS PAGE	19. SECURITY CLASSIFICATION OF ABSTRACT	20. LIMITATION OF ABSTRACT
Unclassified	Unclassified	Unclassified	